1-6-2004

Inflow and Loadings from Ground Water to the Great Bay Estuary, New Hampshire

Thomas P. Ballestero
University of New Hampshire, tom.ballestero@unh.edu

Robert Roseen
Geosyntec Consultants

Larry K. Brannaka
University of New Hampshire, Durham

Inflow and Loadings from Ground Water to the Great Bay Estuary, New Hampshire

A Final Report Submitted to
The NOAA/UNH Cooperative Institute for Coastal and Estuarine Environmental Technology (CICEET)

Submitted by

Dr. Thomas P. Ballestero
Dr. Robert M. Roseen
Dr. Larry K. Brannaka
Department of Civil Engineering
University of New Hampshire
Durham, NH

January 6, 2004

This project was funded by a grant from NOAA/UNH Cooperative Institute for Coastal and Estuarine Environmental Technology, NOAA Grant Number(s) NA87OR512 and NA07OR0351

TABLE OF CONTENTS

LIST OF TABLES

LIST OF FIGURES

ABSTRACT

This final report presents the results of a study to evaluate groundwater inflow and nutrient loadings to the Great Bay Estuary, New Hampshire. The evaluation of inflow was accomplished independently by two methods: one, used thermal imagery, and the other, piezometric mapping. The thermal imagery method assessed groundwater that was observed to discharge within the intertidal zone of an inland estuary. The groundwater piezometric mapping method used bedrock wells around the bay to create an overall piezometric map of the near-bay area. Groundwater discharge was evaluated with respect to flow, concentration, and ultimately nitrogen loading to coastal waters. The results represent a snapshot for these variables, examined by a thermal infrared aerial survey in the spring of 2000, and water quality, specific discharge, and piezometric surface maps in the summer of 2001. Monitoring wells upgradient of the Great Bay were analyzed for nitrogen as an indicator of potential discharge source waters. Total groundwater discharge to the estuary was calculated as 24.2 cubic feet per second (cfs) with an average of 0.81± 0.89 mg dissolved inorganic nitrogen (DIN)/L, with a maximum value of 2.7 mg DIN/L (n=20). Nutrient concentrations, averaging 0.83± 1.34 mg DIN/L, with a maximum value of 10.2 mg DIN/L, were observed in upgradient bedrock groundwater analyzed from 192 wells. Nutrient loading was calculated to be 19.3±21.2 tons of N per year for the total Great Bay Estuary, covering nearly 144 miles of shoreline. The groundwater derived nutrient loading accounts for approximately 5% of the total non-point source load to the estuary. The thermal imagery method was found to be an effective and affordable alternative to conventional groundwater exploration approaches.

Keywords: Thermal Imagery, GIS, Groundwater Discharge, Contaminant Loading, Coastal Waters, Nutrient, Pollution, Coastal Management, Piezometric

INTRODUCTION

OBJECTIVES

The objective of this study was to evaluate the groundwater inflow and groundwater derived loadings to the Great Bay Estuary, New Hampshire. This evaluation entailed three major components: 1) the quantification of groundwater discharge to coastal waters via the construction of a groundwater surface map; 2) the quantification of groundwater discharge to coastal waters via thermal imagery; and 3) the calculation of annual estuarine nitrogen loading from groundwater. This research provided a first step in the methodology verification for the use of thermal imagery (TIR) and GIS analysis for quantifying groundwater discharge.

The importance of this research is made evident in that the amount of groundwater discharge and subsequent contaminant loading to coastal waters generally represents a significant unknown for regulators and resource managers. Current regulatory guidelines require states to develop Total Maximum Daily Loads (TMDLs) by 2015 for contaminants of all impaired waters. This research demonstrates that the groundwater component is a significant portion of the overall contaminant load. The ability to quantify this component will better enable regulators and resource managers to optimize the health, productivity, and ecological diversity of estuarine and coastal waters.

RESEARCH SUMMARY

There are three major components of this study: 1) the quantification of groundwater discharge to coastal waters via the construction of a groundwater surface map; 2) the quantification of groundwater discharge to coastal waters via thermal imagery; and 3) the calculation of annual nitrogen loading from groundwater to the coastal waters of the Great Bay Estuary.

The first component of the study involved quantification of flow via groundwater mapping and entailed two years of field work to locate, survey, and monitor wells in the study area. Location of the wells began with determining the extent of municipal water supplies, beyond which homeowners would be on private wells. Public involvement was solicited and the resulting support was overwhelming, without which the mapping could not have been accomplished. Private wells were then located and evaluated for use. Spatial location of over 200 wells was accomplished by a combination of GPS and surveying. GPS was used to locate the X and Y coordinates. To determine elevation required greater accuracy. This required the use of mapping grade GPS, or Real Time Kinematic (RTK) GPS. Two depth-to-water monitoring events were performed: one during 2000 and one during 2001. Data from about 30 additional wells was used from Pease International Tradeport for the Newington area. Aquifer characterization was accomplished by the use of pump test data from multiple studies in the area. The piezometric map was then constructed and evaluated for regions of uniform piezometric gradient. Application of Darcy's Law was used to estimate flow.

The second component of this study was the quantification of flow via thermal imagery and GIS analysis. This was further subdivided into the following tasks: 1) identification and cataloguing of discharge zones by thermal imagery, 2) field investigations of groundwater discharge zones, 3) GIS analysis of thermal imagery, and 4) large-scale flow estimation.

The study area was surveyed from an elevation of 10,000 feet, during winter, at low tide, on a cool calm night. The thermal images were studied for thermal anomalies indicated by groundwater discharge. The winter survey maximized temperature differentials between surface features and groundwater. Suspected discharge zones were compiled and mapped to identify specific areas of interest. Field investigations were then performed to verify the presences of suspected discharge zones. Characterization included assessment of specific discharge, measurement of piezometric gradient, characterization of hydrogeology, surface area determination, and water quality sampling and analysis. Analysis of the thermal imagery was accomplished by a combination of GIS analysis and graphical analysis of pixel data. The analysis determined the seepage face surface area for groundwater discharge zones. Finally, the results of the field characterization and GIS analysis were applied to calculate flow for individual discharge zones. These same results were applied by factorial design to calculate groundwater discharge, on a larger scale, throughout the estuary.

The third component, calculation of annual nitrogen loading from groundwater to the Great Bay Estuary, was determined based on the results from sampling 20 groundwater discharge zones throughout the study area. The water quality data was combined with flow estimation from thermal imagery to determine loading. Additionally, water quality analyses were performed for the monitoring wells used in the construction of the groundwater map, to determine upgradient source water quality. Water quality and loading data were then reviewed and compared with published loading data for point, non-point, and atmospheric sources.

FLOW ESTIMATION FROM THE PIEZOMETRIC MAPPING METHOD AND THE THERMAL IMAGERY METHOD

This report examines and compares two methodologies for assessing groundwater discharge to coastal waters. Specifically, it reports and compares the flow estimation by piezometric mapping and aquifer characterization compared with the innovative use of thermal imagery (TIR), Geographic Information System (GIS) based analyses, and limited field characterization. The piezometric mapping approach is presented first. The use of TIR, coupled with field characterization to assess groundwater discharge for individual zones is reported second, followed by the same approach applied to a regional scale with the use of a flow expression matrix.

Recent developments in thermal imagery have improved its accessibility and affordability for use in management of coastal resources. In April 2000, a series of TIR aerial surveys were flown over the Great Bay Estuary in coastal New Hampshire. This study delineated groundwater discharge throughout the ecosystem on a large scale. The aerial survey included nearly 50 miles of the Great Bay shoreline and four of the major contributing rivers. Each survey was completed in one night and the images were available shortly thereafter, with no need for corrective post-processing. The images were then studied for thermal anomalies that indicated a potential upwelling of groundwater.

TIR-identified discharge zones were catalogued and characterized as to size, type and intensity. A subset of suspected groundwater discharge zones were located in the field, characterized for hydrologic parameters, and sampled for water quality. The surface area of each individual groundwater discharge zone was computed by GIS analysis of the TIR. Finally, the GIS-derived surface area, combined with field-derived flow estimates, was used to determine the total groundwater flux and nutrient loading to the estuary.

The issue of groundwater discharge to coastal waters is of particular interest to scientists and resource regulators in the performance of a detailed accounting of significant contaminant sources. A body of emerging research has investigated and reported quantities of groundwater discharge that have the potential to represent a significant component of contaminant loading to coastal waters (Bokuniewicz, 1980; Johannes and Hearn, 1985; Giblin and Gaines, 1990; Reay et al., 1992; Moore, 1996; Burnett, 1999). Consequently, methodologies that can be used to assess the extent of groundwater flux and the resulting contaminant loading are of great interest. As detailed by Banks et al. (1996), "Airborne thermal-infrared imaging is an effective method to quickly assess large areas and acquire information about specific locations of groundwater discharge." The results of this study using GIS-based analyses of thermal imagery, combined with field characterization, increases the utility of thermal imagery beyond delineation capabilities and into the realm of quantitative assessments of groundwater discharge.

Groundwater is a uniquely difficult non-point source to assess and is commonly overlooked, as is evident by the lack of available data. TIR combined with field characterization is a powerful alternative to conventional approaches such as the use of piezometric surface maps to assess groundwater discharge and contaminant loading. TIR is ideal for locating specific concentrated discharge areas symptomatic of complex hydrogeology. Banks and others used TIR to determine the presence or absence of discharge as well as the manifestation of discharge zones as either concentrated or diffuse. However, TIR alone cannot be used to quantitatively assess flow, as can piezometric surface maps combined with aquifer characterization. Yet the coupling of GIS analyses and TIR can be used to determine the surface area of the seepage face of a discharge zone. The surface area of the seepage face combined with field measurements of specific discharge (such as those commonly obtained with seepage meters) can be used to estimate individual discharge zones.

Combined with water quality data, GIS-derived surface areas, and the field-derived flow estimates, it is possible to estimate the total groundwater flux and nutrient loading from individual zones, or over an entire study area. The method can be applied to a large-scale investigation in which a representative subset of TIR-identified discharge zones are field investigated, and the results of which could be applied to the data set as a whole. Thus was the approach followed in this study.

Advances in thermal imaging in the past 10 years have improved temporal and spatial resolution as well as increases in camera affordability (Davis, 2001). Historically, access to thermal imaging capabilities was limited to large projects that could afford expensive thermal scanners. Private sector access was typically limited as most scanners were owned and maintained by federal agencies, some defense related. This research used modern staring array thermal imagers, also known as digital thermal cameras

(DTCs), for identifying groundwater discharge zones. DTCs have a distinct advantage over digital scanners in that they do not require expensive and time-consuming image correction. Aerial thermal image surveys can be flown for a little as $6,000 with DTCs. As such, thermal imagery is becoming increasingly widespread and accessible by coastal regulators and scientists.

The temperature resolution of typical thermal imagers is 0.08 degrees Celsius. The cameras can be mounted on either fixed wing or non-fixed wing aircraft and can survey at elevations from just above tree line to roughly 10,000 feet, with a range of ground resolution from 16 square feet per pixel down to 0.2 square feet per pixel. The resolution is determined for a particular camera by flight altitude and field of view of the imaging device. Flight altitude and corresponding resolution can be adjusted based on the needs of the survey. For large areas encompassing many miles of shoreline, low altitude surveys provide high resolution, but also significantly more data to process and analyze. Affordability is expected to increase as the usage of the thermal image cameras increases. DTCs have been used in law enforcement, fire fighting, animal migration studies, industrial applications, resource management, and now increasingly with groundwater research. The present limitation to the latter application is in the GIS-based analyses applications of the thermal imagery.

The data of the thermal signature is based on a pronounced thermal gradient between the groundwater and the ambient surface conditions. For a typical winter survey in North America, there is a range of grayscale values from warmer subsurface groundwater to cooler ambient conditions at or near freezing (the opposite would be the case during warm summer months).The digital thermal imagery data is recorded in grayscale pixels. The pixel data can be analyzed by use of a query through GIS for determining the size of individual thermal signatures. A GIS query is a logically constructed search of a spatially organized dataset. However, the difficulty arises in obtaining a reliable and repeatable criterion on which to base the query.

Much of the use of thermal imagery for groundwater research began in the 1990's. A thermal scanner was used by Baskin (1990) for locating groundwater discharge zones, in the non-mixed quiescent environment of the Great Salt Lake. Baskin's study illustrated the utility of the thermal imagery for identifying the density stratification of freshwater over saltwater similar to what occurs in coastal systems. Delineation of groundwater discharge zones using thermal imagery was shown to be effective by Banks (1996) in coastal waters at the Aberdeen Proving Ground, Maryland. Banks found that the thermal signatures in the surrounding waters influenced by groundwater could be interpreted to determine the extent of groundwater discharge. Similarly, Mustard et al (1999) used thermal imagery to quantitatively assess thermal effluent impacts in the waters of Narragansett Bay. Recently, Campbell and Keith (2001) used thermal imaging scanners combined with computer modeling using CORMIX to estimate groundwater flow rates from discharge zones. Their study had no field verification but represents an important transition of TIR from delineation to quantitative flow measurements. Satellite borne thermal imagery has been used to detect coastal storm water and sewage run-off (Svejkovsky and Jones, 2002). The present study has developed a GIS method for assessing seepage face surface area. This parameter is critical to estimating groundwater flow. Surface area estimates were combined with field-derived flow rate measurements to calculate the total flow from groundwater discharge zones.

GROUNDWATER-DERIVED NITROGEN LOADING TO COASTAL WATERS

Water quality sampling and analyses for nutrient concentrations were also performed. The nitrogen concentrations, combined with the groundwater discharge rates from either the piezometric or thermal method, provided an estimate of nitrogen loading.

The groundwater loading results can be compared with nutrient loading from nearby waste water treatment facilities (WWTF), surface water, and atmospheric inputs; all components required for Total Maximum Daily Loads (TMDLs).

Effective development of TMDLs is predicated upon an accurate assessment of all significant sources of contamination for a particular water body. Typically, this would involve monitoring of surface waters, point sources (such as municipal and industrial waste water treatment facilities), atmospheric contribution, and groundwater. However, the loading from groundwater often remains unknown, due largely to the difficulty in measuring groundwater discharge. A body of research using a variety of approaches supports the contention that groundwater is a significant component of the total freshwater discharge and is capable of carrying a substantial contaminant load (Bokuniewicz, 1980; Johannes and Hearn, 1985; Simmons Jr., 1992; Moore, 1996; Burnett, 2002). In the coastal ecosystem of the Atlantic Bight located in the southeastern United States, Moore (1996) has estimated that 40% of the river water/freshwater resulted from groundwater discharge. In some cases, such as in the Perth Region of Australia, it has been demonstrated that nitrate loading from groundwater discharge is several times that of surface waters (Johannes, 1980). Our research in the Great Bay of coastal New Hampshire indicates that groundwater is a significant source of nitrogen. The loading from groundwater is nearly double that from a WWTF with primary and secondary treatment from a town with over 12,000 people. Loading from groundwater is roughly one third that of the major tributaries. The estimated total groundwater influx for the entire Great Bay Estuary (144 miles of shoreline) is nearly 24.2 cubic feet per second (cfs) with concurrent loading of around 20 tons of dissolved inorganic nitrogen per year. TIR has the potential to be a powerful and affordable tool for coastal regulators and scientists for evaluation of pollution from groundwater.

STUDY AREA

The study was performed in the Great Bay Estuary, a drowned river valley, in coastal New Hampshire. The entire estuary is composed of seven contributing rivers, approximately 144 miles of shoreline, with tidal waters covering about 10,900 acres (Jones, 2002). The study area was limited to a more easily defined portion of the estuary, the Great Bay and the Little Bay, which includes 4 rivers and over 50 miles of shoreline. The study site includes portions of the Towns of Dover, Durham, Newmarket, Newfields, Stratham, Greenland, and Newington, NH next to the Pease International Development Tradeport (Figure 1), the former site of Pease Air Force Base. The mouth of the estuary is the Piscataqua River, which is the border of Maine and New Hampshire with an active port, and the Portsmouth Naval Shipyard. The daily tidal exchange is approximately 8 feet. At low tide, in the upper portions of the estuary, significant fringing salt marsh, large mudflats, and eelgrass beds are exposed. Tidal mixing due to strong currents

generally prevents vertical stratification and presumably obscures submerged groundwater signals.

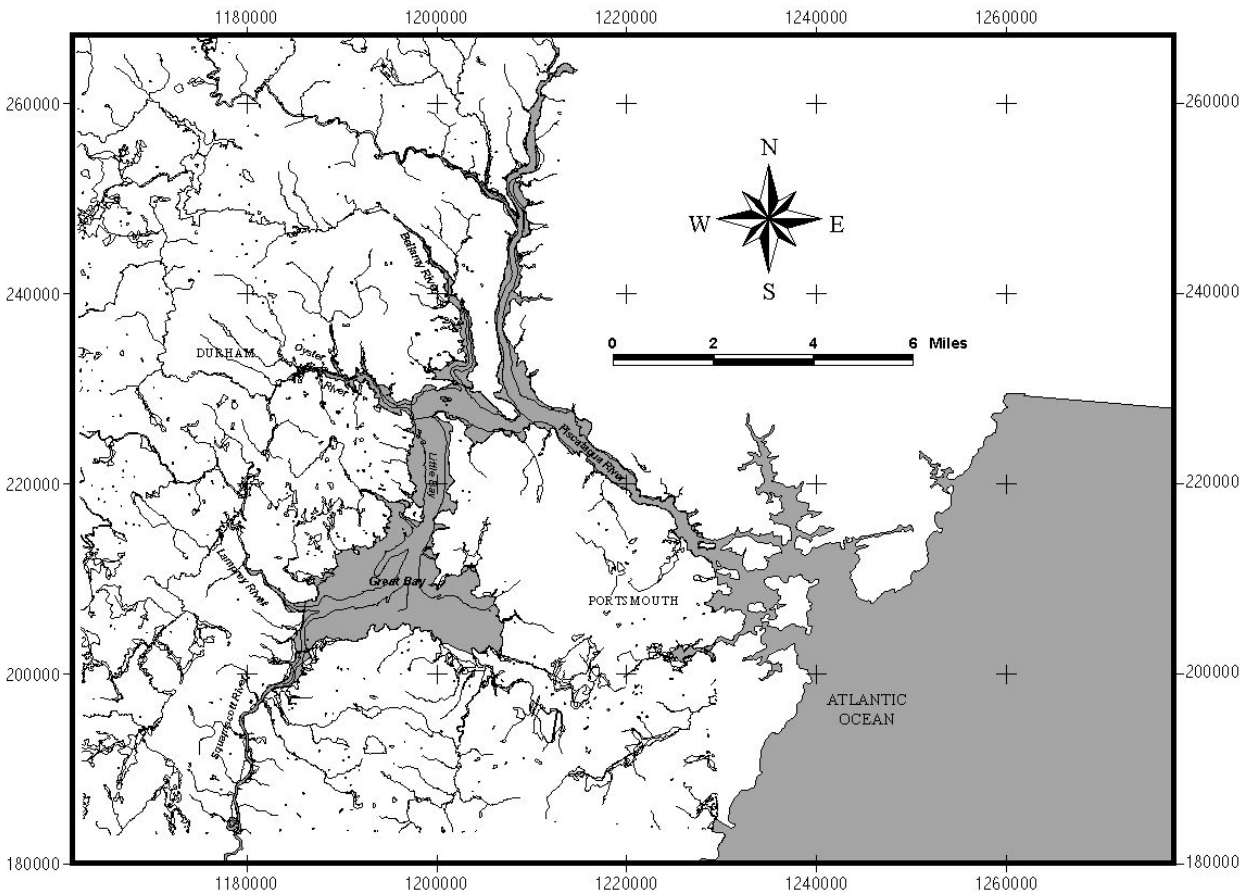

Figure 1: Map of Great Bay Study Area

The health and effective long-term management of the estuary is a major interest for New Hampshire as the estuary represents the majority of its marine shoreline. There are 11 cities and towns bordering the tidal portions of the estuary comprised of nearly 100,000 people. Within the estuary, 38% of the abutting lands are undeveloped (Rubin and Merriam, 1998). The estuary is used extensively for its natural resources, particularly commercial fishing and shellfish harvesting. Furthermore, a wide variety of research is conducted there due to the proximity to the University of New Hampshire and the location of a National Estuarine Research Reserve (NERR) within the Great Bay Estuary.

The study area was chosen because of a broad interest in coastal research in the Great Bay estuary. The area has US Environmental Protection Agency (EPA) designation as a medium priority for assessment of TMDLs (USEPA, 1998). Coastal New Hampshire was uniquely suitable for such a study in that the majority of homeowners use private wells for water. As such, these private wells are all potential monitoring points for the construction of a piezometric groundwater map. In total, over 200 private wells were

surveyed and monitored and additional data from over 30 monitoring wells from Pease International Tradeport were used for the groundwater map produced in this report.

Hydrogeology

The geology of the Great Bay area is quite complicated and includes both unconsolidated surficial geology and occasional bedrock outcrops. The area is faulted and folded with a syncline extending from the northeast to the southwest (Novotony 1969).

Tightly folded metasedimentary rocks of the Merrimack group underlie the Great Bay area. The bedrock geology consists of Ordovian-Silurian metasedimentary rocks, Devonian intrusive igneous rocks, and Triassic or Jurassic aged dikes (Lyons et al. 1997). Two formations dominate the region: the Kittery and the Eliot. The centerline of the Great Bay is the contact zone between the Kittery (to the west) and the Elliot (to the East) and closely follows what some believe to be either a syncline (Novotony, 1969), or a fault line. The bedrock is typically highly fractured at the surface, with the depth of the fractured zone extending to greater than 10 feet in some areas (Weston, 1993). The two bedrock formations are very similar hydrogeologically, with low primary porosity and higher secondary porosity. The depth to bedrock varies from exposed outcrops to nearly 60 feet, and in most cases 20 feet. Exposure of bedrock is more prevalent along the northern shore of the Great Bay, on smaller headlands on the south shore, and along the narrower reaches of the rivers.

In a shallow bedrock system, it is likely that subsurface flow patterns are controlled by the bedrock topography. The shape and form of the bedrock topography was influenced by the preceding glaciations. The subsurface bedrock control and the subsequent varying depths of surficial materials may account for the observations of a large number of concentrated groundwater discharge zones within the study area. In an environment in which a transmissive surficial geology is the dominant factor (e.g. Cape Cod, MA), one might expect to see more diffuse discharge zones.

The surficial deposits in the Great Bay area are of glacial origin, which includes lodgment and ablation tills and stratified drift. Historic ocean basins, which flooded the region due to the depression of the land surface by the glacier, left a marine clay and silt deposit over much of the region. The stratified drift deposits are widely used and productive aquifers, composed of coarse grained materials (sands and gravels), which were sorted during the glacial retreat. This sorting resulted in the size-based layering of materials. In contrast, the till deposits are generally low transmissivity materials composed of unsorted clay, silt, sand and gravel (Moore, 1990). On a microscopic level, the mixture of stratified drift and tills suggest that the hydrogeology is complex and most likely indicative of discrete concentrated discharge zones. On a macroscopic level, the region can be generalized as a mixture of drift and tills with accompanying characteristics.

Geophysical surveys performed during the study support the presence of three distinct surficial hydrogeologic units. From top to bottom, these include a sand and gravel unit, a marine clay layer, and beneath the clay a glacial till layer. Investigations at the Pease International Tradeport show the presence of up to four surficial units, adding a lower sand layer immediately beneath the marine clay. Groundwater discharge zones have been identified in the tidal zone and in deposits of coarse sands and gravels. Below the tidal zone, significant accumulation of marine clays occurs acting as a confining unit.

Various hydrogeologic investigations have been, and are ongoing, at the previous site of Pease International Tradeport. An extensive network of monitoring wells exists for this site. The wells are monitored regularly. Data from some of the wells was used for the groundwater map of the Great Bay created for this report. The Town of Newington, NH (to the west) and the City of Portsmouth (to the east) rely upon a public reservoir, thereby limiting potential private monitoring wells.

GROUNDWATER DISCHARGE STUDIES

Studies on groundwater discharge in coastal waters tend to use the following approaches: piezometric mapping (often associated with modeling efforts), seepage meters, tracers, and thermal imagery. Seepage meters, thermal imagery, and piezometric mapping are especially relevant to this research.

Johannes (1980) published a thorough review assembling a somewhat scattered body of research on the discharge of groundwater to coastal waters. The review tied together literature focusing on freshwater environments, brackish waters, and coastal waters. The review included the observations from multiple researchers, that in brackish waters (the freshwater and saltwater interface), groundwater discharge appeared limited to a narrow horizon at the perimeter of the water body. This was explained by the occurrence of a zone of diffusion at the interface between a seaward saltwater wedge and upgradient freshwater discharge. This phenomenon forces the exit of groundwater, called submarine groundwater discharge (SGD), below the high tide line and at the contact with saltwater wedge. Perhaps most importantly, Johannes reported that SGD has been shown to contribute many times the amount of nitrate to coastal waters as does river water. Burnett (2002) reviewed a large study by a working group of scientists established by the Scientific Committee on Oceanic Research (SCOR) and co-sponsored by the Land-Ocean Interaction in the Coastal Zone (LOICZ). The SCOR/LOICZ working group examined a variety of approaches for assessing groundwater discharges, including seepage meters, tracer studies, modeling, and seepage meters.

Groundwater Mapping and Flow Estimation

Piezometric mapping coupled with aquifer characterization can be used to estimate flow through homogenous isotropic flow tubes (Freeze and Cherry, 1979). This form of mapping is the basis for numerical groundwater modeling packages such as MODFLOW that are commonly used to estimate flow, flow paths, and residence time. It is important to recognize that groundwater models are driven by the imposed boundary conditions such as intertidal groundwater discharge. In areas that are neither homogenous or isotropic, useful approximations can be made by identifying relatively uniform regions within the flow domain. Uniform regions can then be treated as “flow tubes” for flow calculations. Hydrogeologically, the two primary bedrock units are very similar, with low primary porosity, and higher secondary porosity through fractures. The stratified drift aquifers are distributed throughout the study area. Aquifer characterization using pumping tests can evaluate the connectivity between an unconfined surface formation and an underlying bedrock formation (Kruseman and deRidder, 1994). A pump test run for 4-8 days typically entails a large radius of influence, in some cases nearly up to a

mile, over which the aquifer properties measured by the test are averaged. The pump test is useful for calculating large-scale formation transmissivity and storage coefficient for large regions with a mix of heterogeneous materials.

Seepage Meters and Nutrient Studies

Many studies have been performed using seepage meters (Lee, 1977) to estimate groundwater flux, particularly with respect to nutrient loading from areas below the high tide line to significant depths. Table 1 illustrates ranges of nutrient concentrations and Table 2 illustrates ranges of specific discharge reported from related studies.

Table 1: Groundwater Nitrate Concentrations Reported from Various SGD Studies

Source	Land Use	NO3-N (mg/L)		
		low	high	ave
Sewell '82	urban, septic	1.0	55.0	12.3
Sewell '82	non-urban	0.3	20.0	0.0
Giblin and Gaines '90	w/in 1 km of town center	0.0	10.5	2.9
Simmons '92	offshore marine sanctuary			0.1
Reay et al '92	agricultural			8.2
Reay et al '92	forested			0.4
Valiela '78		0.3	1.1	0.7
Marsh '77				2.5
Kay '77		0.4	1.3	0.8
Webb '80		1.2	3.5	2.4
Johannes '80		1.6	5.3	3.5

Table 2: Specific Discharge Values Reported from Various SGD Studies

Source	Specific Discharge (GPD/ft2)	
	low	high
Sewell '82	0.005	0.028
Giblin and Gaines '90	0.589	1.767
Simmons '92	0.147	0.491
Reay et al '92	0.012	2.173

Seepage meters function best when submerged and the majority of studies use that approach. Sewell (1982) and Giblin and Gaines (1990) documented elevated nitrate groundwater concentrations and subsequent SGD, in an area dominated by septic systems. Simmons (1992) reported discharge measurements for zones at depths of up to 130 feet and observed discharge variances in response to tidal action. Reay et al (1992) concluded that significant nutrient fluxes were increasing surface water nitrate concentrations in a coastal inlet by 20 times and summer rates of specific discharge 15

times ≥ rates in winter. Staver and Brinsfield (1996) reported variations in response to tidal and recharge events with discharge rates being as much as 5 times greater in winter than summer. Research on seepage meters by Shaw and Prepas (1989) indicated that short-term anomalous influx of water was observed using seepage meters and could be corrected by pre-filling of the sampling bags. Significant advances in seepage meter technology were reported by Taniguchi and Fukuo (1993) with the development of an automated heat-pulse seepage meter. Recently, Burnett (2002) reported good agreement between manual, automated heat-pulse, and automated ultrasonic seepage meters. Ultrasonic seepage meters have the advantage that they function exposed in intertidal areas and submerged (Paulsen et al., 1997).

Thermal Imagery

The use of thermal imagery for groundwater research was reported in the 1990's. A thermal scanner was used by Baskin (1990) for locating groundwater discharge zones, in the non-mixed quiescent environment of the Great Salt Lake. This study illustrated the utility of the thermal imagery for identifying the density stratification of freshwater over saltwater much like what occurs in coastal systems. Delineation of groundwater discharge zones using thermal imagery was shown to be effective by Banks (1996) in coastal waters at the Aberdeen Proving Ground, Maryland. Banks found that the thermal signatures in the surrounding coastal waters influenced by groundwater could be interpreted to determine the extent of groundwater discharge. Mustard et al. (1999) used thermal imagery to quantitatively assess thermal effluent impacts in the waters of Narragansett Bay. Recently, Campbell and Keith (2001) used thermal imaging scanners combined with computer modeling using CORMIX to estimate flow rates from discharge zones. Their study had no field verification but represents an important transition of TIR from delineation to quantitative flow measurements. Satellite-borne thermal imagery has also been used to detect coastal storm water and sewage run-off (Svejkovsky and Jones, 2002).

Our study examined groundwater flow estimates from thermal imagery and field-derived flow measurements into the tidal waters of the Great Bay Estuary, New Hampshire. Estimates were also derived from piezometric mapping of the groundwater table surrounding the Great Bay Estuary. The conventional piezometric approach was used to compare and verify the thermal imagery procedures

Tracer Studies

Tracer studies are an exceptionally useful approach, especially for large-scale quantification and method inter-comparisons. One notable study included an evaluation of enrichment of coastal waters by ^{226}Ra (Moore, 1996). Moore concluded that groundwater flux constituted approximately 40% of the river water flux along the South Atlantic Bight, South Carolina. Moore et al (2000) also examined radioisotopes ^{223}Ra and ^{224}Ra to determine mixing rates of estuarine and near-coastal waters with the open ocean. In another study, Burnett et al (2001) used another conservative tracer, ^{222}Rn, enriched in coastal waters by higher concentration groundwater for estimating submarine groundwater discharge.

TMDL Regulation and Implementation

The evolution of regulatory practices associated with the 1972 Clean Water Act (CWA) has led to the realization that non-point source (NPS) contamination is now the leading concern for protection of water resources (EPA, 2000). With the implementation of the CWA, point source (PS) contamination from industry and municipalities was the primary focus and regulated through the National Pollutant Discharge Elimination System (NPDES). Effective regulation of point sources produced a marked improvement in water quality in many respects, however, much of the nations waters remain impaired, so non-point sources became the current focus. According to Saltman (2001) TMDLs are all inclusive such that impacts omitted by point source regulation will be considered in total loading. TMDLs, as described in section 303d of the CWA, are a pollutant budget intended to regulate based on the health and ecological function of a water body by determining a sustainable pollution load. The actual contaminant load from point, non-point, and atmospheric sources for an impaired water body is then to be regulated to meet the sustainable load.

Currently, the regulation of non-point sources rests with the state, primarily through the use of best management practices targeted for specific water quality impairments. The states have the responsibility to develop TMDLs through listing and assessment of impaired waters. It is up to the states to decide how to regulate the various sources. The US Environmental Protection Agency subsequently certifies that the TMDL will meet the necessary water quality and the regulation occurs for all sources. As of July 2000, states have up to 15 years to develop TMDLs for each impaired water body, with a requirement to update their list of impaired waters every 4 years, and no deadline for implementation (Saltman, 2001).

One of the leaders in the development of TMDLs in the Northeastern US is the Buzzards Bay Program (BBP) of Massachusetts. In 1999, the BBP proposed to use standards based on three factors: bay volume, flushing time, and depth. With these factors, unique standards can be developed for each water body that represents a sustainable level of pollution. The USEPA water classification scheme used by the BBP is based on a three tiered system (from high quality to low): Outstanding Resource Waters (ORW), resource waters with outstanding recreational or ecological significance; Shellfish Class A Waters (SA), waters used primarily for market shellfishing; Shellfish Class B Waters (SB), waters used primarily for recreation. Additionally, waters are further classified as shallow if they have an average mean low water depth of less than 6 feet, or have $\geq$ 40% of the bottom less than 6 feet deep (BBP, 1999).

Great Bay, NH Status

The 1998 listing of impaired waters for the Great Bay Estuary, NH included the Great and Little Bays, the tidal portion of all the estuary's major rivers (Salmon Falls River, Cocheco River, Lamprey River, Squamscott River, Bellamy River, Oyster River), and Hampton Harbor. All are listed as a medium priority for water quality impairments for pathogens and PCBs (EPA, 1998). Studies in 1976 and 1996 indicated a general decrease in the nutrient concentrations for most of the estuary, with the exception of the two largest surface water sources, the Cocheco and Salmon Falls Rivers, which have increased significantly (Loder et al, 1976; Jones and Langan, 1996; Langan, 2002). These reports identify seasonal nitrogen trends of highest dissolved inorganic nitrogen in the

late fall through early spring and longitudinal trends in which nitrogen concentration varied inversely with salinity and was highest at the upper reaches of the estuary.

METHODS

FLOW ESTIMATION VIA PIEZOMETRIC MAPPING METHOD

The piezometric mapping and analysis yielded flow estimates for the areas immediately adjacent to the Great Bay. Nearly 200 wells were used to develop the piezometric map, most from private homes with an additional 34 wells at the Pease International Tradeport.

The piezometric map was based on measurements of water levels from all wells measured within a 3 day period. The resulting data was plotted and contoured. Aquifer characterization involved the geophysical analyses of suspected target areas, slug testing of monitoring wells, and analysis of historic pumping test data on some bedrock wells. Interpretation of slug tests and pumping tests provided aquifer parameters for comparison with the results of the geophysics analyses. Directions and estimates of total groundwater flow were derived from the piezometric maps.

The possible temporary drawdown of private wells was considered when developing the groundwater map. Based on calculations assuming standard minimum demand on domestic wells in these formations, drawdown was not a problem. The slowest wells would recharge nearly 40 feet of drawdown in 30 minutes. Prior to taking depth to water measurements, the homeowners were requested to limit major usage of water during the monitoring. Typically, houses were sampled in about 45 minutes (ample recovery time). During the synoptic monitoring events, most homeowners were not at home, therefore their wells were at or close to static water levels. This was also indicated by water level readings when the wells were originally surveyed at a different time.

In the summer of 2000, two synoptic data collection events occurred on all private wells: a monitoring well survey event, and a water level monitoring event. The first component of the monitoring well survey event took place over a single week using Real Time Kinematics (RTK) GPS. RTK is a mapping grade GPS system with vertical accuracy to within 2-3 cm.. Limitations with RTK (associated with satellite positions) required event planning. This involved selection of base stations, obtaining the necessary access for points around the bay, and scheduling teams of two to three people to survey throughout the day and night when satellite availability was optimal. The NH Geodetic Survey Office provided us with survey benchmarks from which to base the surveying efforts. The station at Cedar Point, Dover was used (43º07'39.69"N, 70º51'27.05"W{NAD 83/96}, 10.26 ft { NGVD29 & NAVD 88}), which is part of the national High Accuracy Reference Network (HARN) and has geodetic accuracy control with latitude, longitude and elevation of several millimeters. Base stations were selected at Cedar Point, Wagon Hill, the Durham Waste Water Treatment Plant, Stratham Hill, and Woodman Point in the Great Bay National Wildlife Refuge in Newington, NH. The base station located at Woodman Point proved to be the most effective location. The biggest problem encountered with this technique was the interference from tree cover, which blocked direct access to satellite signals. Woodman Point was the most effective base station, as much of the study area was directly across open water from Woodman Point. Signal range was nearly 6 miles from Woodman Point in some cases, whereas through dense trees, the range at Wagon Hill was limited to a mile and a half. RTK achieved an elevation accuracy of 2-3 cm, and greatly reduced well survey efforts. Following RTK, some “clean-up” survey activities were required to close survey loops not completed by

the RTK. This effort required only a few additional weeks. The RTK technology saved several months of conventional survey efforts.

The second Phase 2 task completed in early summer was a synoptic or measurement of the groundwater elevations. The depth-to-water measurement event took place in a single week. The results of the RTK survey were used to convert measured groundwater depth to elevations.

Aquifer characterization used several pumping tests to determine hydraulic characteristics of the bedrock aquifer. There is probably interconnectivity between the surficial aquifer and the bedrock, so multi-day pumping tests were used to account for interconnectivity. To obtain flow estimates from the piezometric map using Darcy's Law, it is necessary to have uniform isotropic flow tubes for piezometric gradients. The piezometric surface was analyzed and divided into regions of uniform piezometric gradient (Figure 5), and the flow was then calculated and summed for the entire study area.

FLOW ESTIMATION VIA THERMAL IMAGERY METHOD

The quantitative use of TIR for individual discharge zones was investigated, followed by its regional scale application using a flow expression matrix. Phase 1 involved four components: 1) delineation of groundwater discharge zones by thermal imagery, 2) GIS analysis of TIR to obtain seepage face surface area estimates, 3) field verification, and 4) development of a flow expression matrix.

Delineation of Groundwater Discharge Zones by Thermal Imagery

To delineate the groundwater discharge zones, a thermal infrared survey was flown over the study area. Delineation involved TIR surveys performed in April and August of 2000. The April survey was performed at 10,000 feet elevation and the August survey at 4,000 feet elevation. The April survey maximized temperature differentials in early spring after the ice had cleared from the Great Bay. Survey conditions were ideal for identifying discharge within the tidal zone: clear skies, low wind, ambient air temperature of 34ºF, and an expected groundwater temperature of 50ºF. The bay temperature was nearly 45ºF, which was less than ideal for locating deeper submarine discharge zones.

In August, a second, less successful survey was flown, despite weather related difficulties, including high winds and low cloud layers (4,500 feet and above). Due to the low cloud cover, the survey flight was forced down to 4,000 ft to obtain acceptable results. As a result, image resolution was improved from 15 to 2.5 square feet per pixel. Weather related difficulties prevent a heavy reliance upon the August survey data. When used in conjunction with the April data, the August data has utility. Warm surface temperatures provided a strong temperature gradient from which to identify discharge zones. Survey conditions for groundwater, surface water, and mudflats were approximately 48, 69, and 80 ◦F, respectively. Since this was the second survey, specific IGD identified from the previous (April) survey were monitored to determine their respective thermal signatures.

Each survey was recorded on digital video. Separate overlapping images are selected from the video to obtain complete ground coverage. Each image was tagged with latitude, longitude (from DGPS), elevation, date, and a time stamp. Each pixel is one of a 256-color gray-scale that is directly defined by temperature. Figure 2 illustrates a sample thermal image displaying groundwater discharge. The circled groundwater discharge zones shown as white (white is cold) are nearly 47^0F. Black represents warm regions. The surrounding mudflats are nearly 70˚F. The white "cloud-like" feature at the bottom of the image is vegetation, and the bay is on the upper half of the image.

The images are useable immediately thereafter with out post-processing. After the images are reviewed, and a subsequent cataloguing of the suspected discharge zones, field investigations were undertaken to assess the reliability of TIR analysis for identifying groundwater discharge zones.

Figure 2: Thermal Imagery for Identifying Groundwater Discharge Zones, Great Bay Estuary, NH.

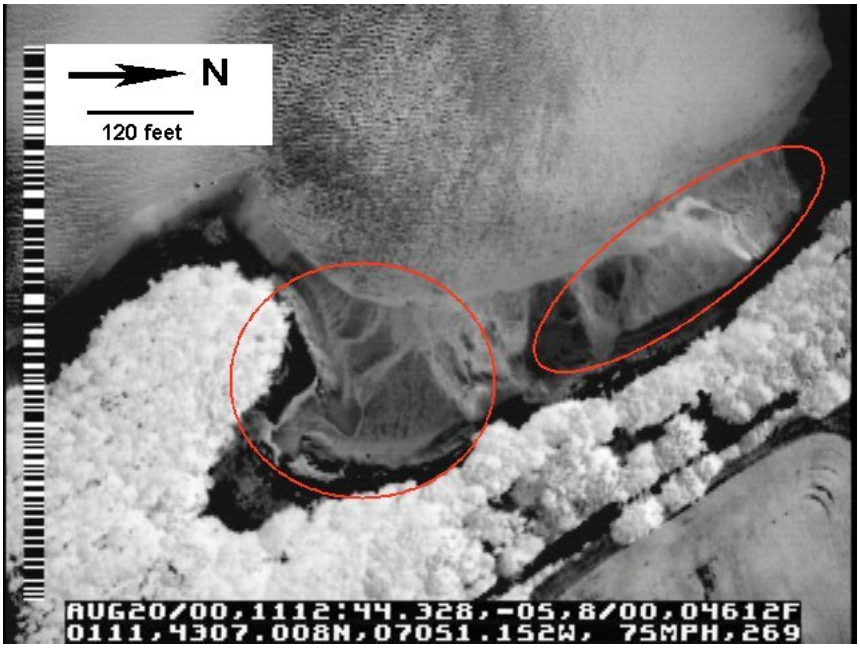

Suspected discharge zones were compiled and mapped. The discharge zones were then characterized by size, shape, location, and intensity.

GIS Analysis Of TIR

Delineation of the thermal signature was accomplished by cropping the suspected discharge zone within the thermal image. The cropped image excluded false positive results, which were the dominant problem interfering with expeditious processing. False positives are anything that might have a thermal signal similar to the suspected groundwater discharge, such as ponded surface water, tree cover, and deep surface waters. Most are predictable and readily apparent to the trained observer, and can therefore be avoided using a cropped image.

Figure 3 illustrates false positives in thermal imagery. The sample thermal imagery is the product of an aerial survey flown in August 2000 over the Great Bay Estuary. The survey elevation was at 4,000 feet, resulting in a pixel resolution of 2.5 square feet. The images are standard polarity: the image grayscale spectrum of black to white represents hot to cold, respectively. Reverse polarity was used for the April winter survey. The results of switching polarity is that the summer and winter surveys are comparable. The darkest (warmest) objects in Figure 3 are the exposed mudflats at low tide, while the lightest (coolest) objects are generally the groundwater discharge areas and the tree canopy. This particular survey was flown at noon to minimize shadows and maximize temperature differentials of land surface features. The greater the temperature gradient between the groundwater and the surrounding landforms the easier it is to resolve the thermal signature.

Figure 3: Thermal Imagery for Displaying False Positives and Groundwater Discharge Zones

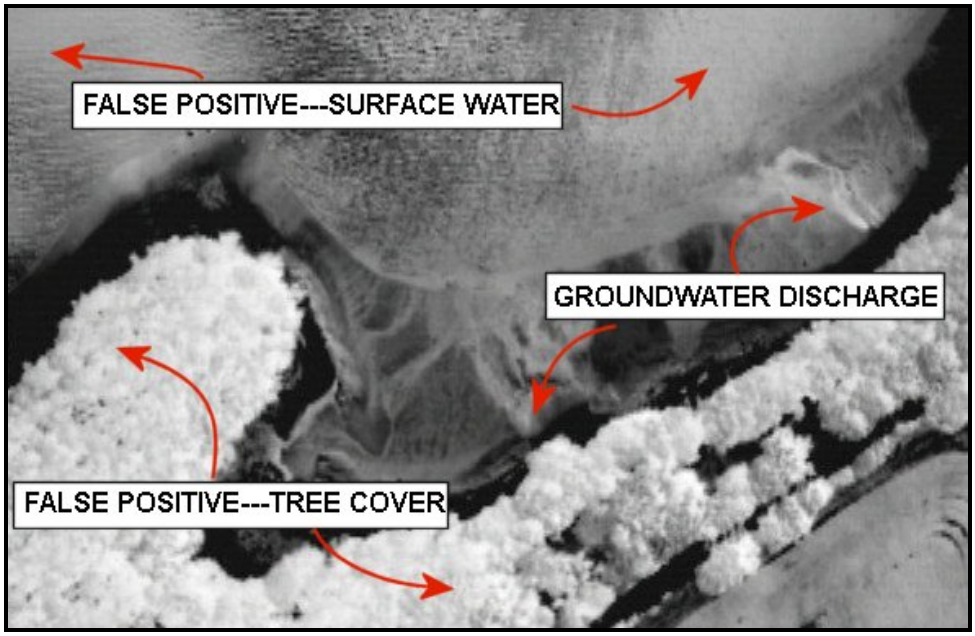

Once the image was cropped around each discharge zone, it was then imported into Arc View and converted to a grid. This format provided temperature/grayscale data for each pixel. With the image in grid format, the pixel data could be directly queried with Arc View. With the known survey altitude and pixel resolution, the query was used to determine the discharge zone flow area. Yet a reliable criterion had to be developed from which to base the query. To accomplish this, the query criteria was developed from a graphical analysis of the grayscale data.

Field Verification of the Thermal Imagery Method

Field verifications of TIR-identified groundwater discharge zones were performed using the thermal images and topographic maps. Field investigations typically involved

characterizing the size of the discharge area, confirming an upward groundwater gradient, and quantifying the flow per unit area (specific discharge). The discharge water salinity was monitored to verify presence of groundwater rather than saltwater. Typical measured salinity was less than 16 parts per thousand. Seepage meters were used to measure specific discharge. Surface area of the seepage face was derived from TIR analysis by GIS. The two combined could calculate total flow per discharge zone.

Large seepage meters, with diameters of nearly 15 feet, were used to assess SGD. Standard seepage meters (Lee, 1977) were ineffective in these intermittently submerged conditions. These variations in seepage meter design were necessary to obtain specific discharge measurements in highly porous, intermittently submerged discharge zones. The alterations involved large strips of plastic edging (the kind used for lawn edging), that were depressed into the sediments, forming a circle. A V-notch weir was cut into the down-gradient side from which volumetric flow was measured. Seepage meters were deployed for the duration of the low tide.

Three sites were characterized for surface area. The limitation on the number sites verified was due primarily to the enormous amount of time required to field map the discharge zones, some in excess of 5,000 square feet. This entailed mapping a grid, and taking surface temperature measurements cell by cell (typically in 10 foot by 10 foot cells). Field assessment of the thermal signature area was through the use of a thermal infrared gun, which measured surface temperature in the same fashion as was done by the thermal imagery. Bare feet also worked remarkably well for locating temperature differences. To delineate the seepage face from the discharge zone and surrounding mudflats, the hydrogeology and piezometric gradient were examined. The hydrogeology was identified using a soil auger to depths of 2 feet. Confining units were indicated by the presence of the surface accumulation of marine clays, which increased seaward and with depth. Piezometric gradients were examined by use of mini-piezometers.

Flow Estimation Of Groundwater Discharge Zones

The product of GIS-derived surface area (A) and the field-derived specific discharge (q) was the flow (Q) from an IGD zone: $Q = Aq$. This method was applied to each of the 9 sites visited in the field for which field-derived specific discharge was measured. Flow was calculated for each of the 9 individual sites.

Regional-Scale Flow Estimation For Discharge Zones

A factorial design was used to determine SGD flow on a large scale. Approximately 10 % (n=9) of suspected groundwater discharge zones were field characterized for specific discharge. Approximately 20% (n=22) of these zones were analyzed by GIS for surface area. Based on these results, a classification scheme was developed to apply specific discharge and surface area to the complete set of TIR identified discharge zones. A method similar to Bricker et al. (1999) was tailored to apply sampling data of a subpopulation to produce estimates for large-scale characterization. This entailed use of a *flow expression matrix*, which is a series of *if/and/then* statements that process data based upon multiple classifications, to obtain individual flow estimates for a discharge zone.

Matrix Analyses of Regional-Scale Flow

The method developed was based on one used by Bricker et al. (1999) in which an evaluation of discrete parameters was used to assess water quality over a large-scale. This method used a scoring system, based on numerical ranges, applied to each of the parameters, to integrate a large data set that encompassed the nation's estuaries. A flow expression matrix was constructed to assess flow over large areas based on the classification criteria for the discharge zone (e.g. surface area, specific discharge, and frequency of occurrence). Once the cataloguing of the discharge zones was completed, numerical ranges were applied based on field verification and GIS analysis for a subset of the 165 suspected discharge zones. Specific discharge classes were established for the range of measured values based on 9 sites. Surface area classes were based on GIS analyses of 22 discharge zones. The classes were then applied to the catalogued data set of IGD zones, which were classified into subcategories of size, type, and intensity to "…establish response ranges for each parameter to ensure discrete gradients among responses." (Bricker et al., 1999) This ensures a consistent qualitative data set from which flow measurements can be applied.

Water Quality Sampling and Analysis

Water quality samples were taken from 20 groundwater discharge zones and analyzed for dissolved inorganic nitrogen (DIN = nitrate, nitrite and ammonia). Prior to sampling, salinity was checked to verify the presence of groundwater rather than saltwater storage. Sampling of discharge zones was accomplished using mini-piezometers installed in the near surface (top 6 inches) of the discharge zones. The mini-piezometer was then connected by tubing (Precision Tygon tubing) to a filter flask, which was connected to a vacuum pump. Approximately 500 ml were extracted and filtered using a 0.45 micron filter (GN-6 Metricel) and preserved by freezing for later bulk analysis by the method suggested by Avanzino (1993). The water was filtered for microbes that consume nitrogen and were frozen within 4 hours of sampling. Mini-piezometers were constructed using clear small diameter plastic tubing and screened using a geotextile to wrap small horizontal slots at the base of the piezometer. No adsorption or desorption was observed from flushing with 50 ppb nitrate and ammonia standards. Blind duplicates, duplicates, and certified standards were used for quality control.

Samples were also taken from a network of ~ 200 wells to determine potential upgradient source water quality. Wells were primarily limited to bedrock water because drinking water wells are normally constructed in bedrock. Because the wells were owned by private homeowners, it was assumed that the minimum household usage was conservatively 150 gallons per day for two people. This would imply that an average well of 80 feet deep was flushing at minimum one volume casing per day. Thus, minimal flushing (5 minutes) was performed directly at the outside tap with hose removed. Samples were not filtered but preserved immediately as previously indicated.

RESULTS

FLOW ESTIMATION FROM PIEZOMETRIC METHOD

Estimates of flow based upon the piezometric gradient and aquifer characterization were completed based on the June 2000 water level monitoring. A transmissivity average from several pumping tests was used for aquifer characterization. To obtain flow estimates from Darcy's Law using piezometric gradients, it was necessary to have regions of uniform gradient. The piezometric surface (Figure 4) was analyzed and divided into regions of uniform piezometric gradient (see Figure 5), in which flow was then calculated and summed for the entire study area. Because the source composition (relative percentage surficial and bedrock aquifer) of the SGD is unclear, no attempts were made to distinguish contributions. The multi-day pump-tests in fractured bedrock will draw from a connected surficial aquifer.

Figure 4: Groundwater Map for the Great Bay Region

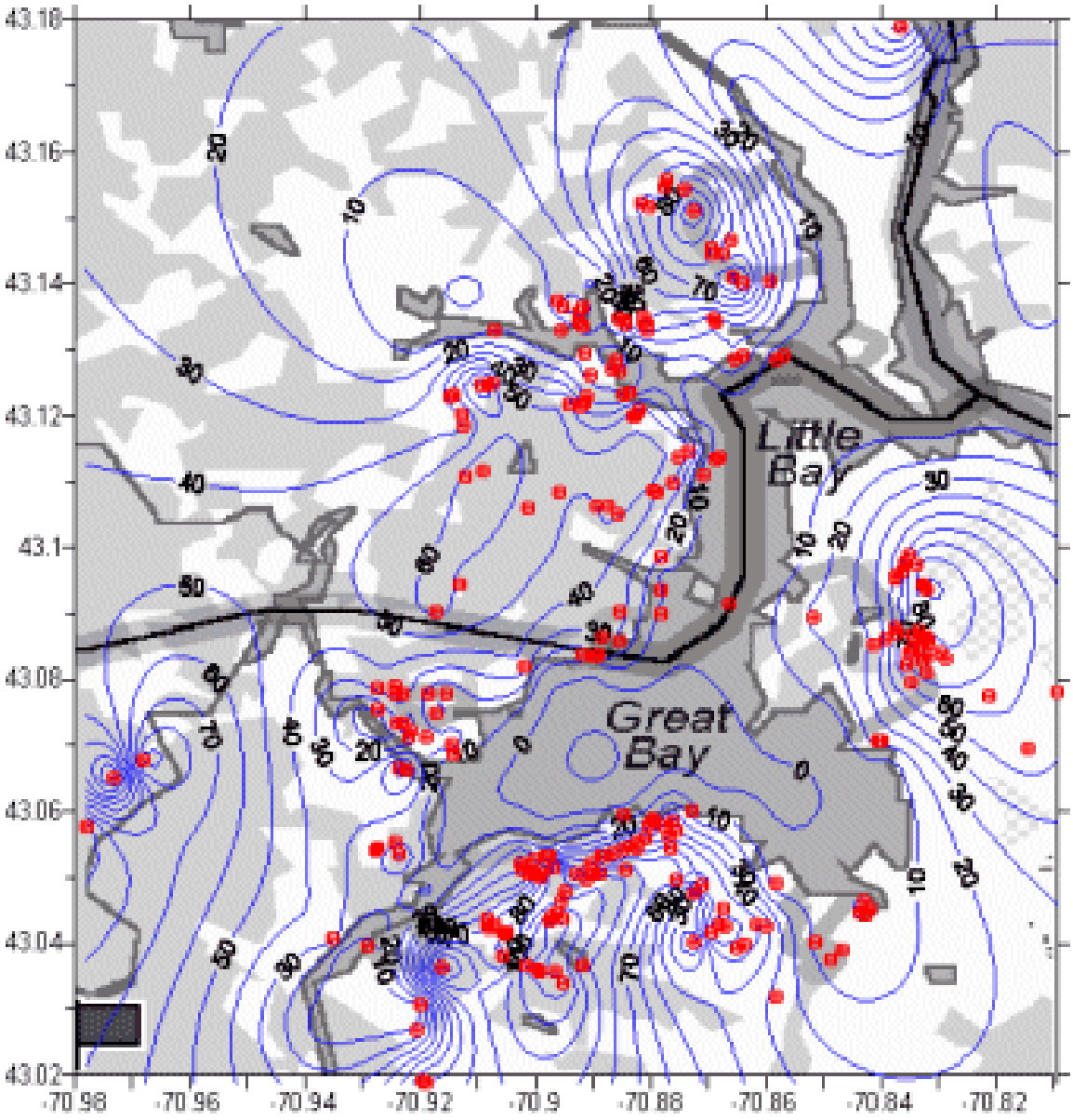

Figure 5: Regions of Uniform Piezometric Gradient

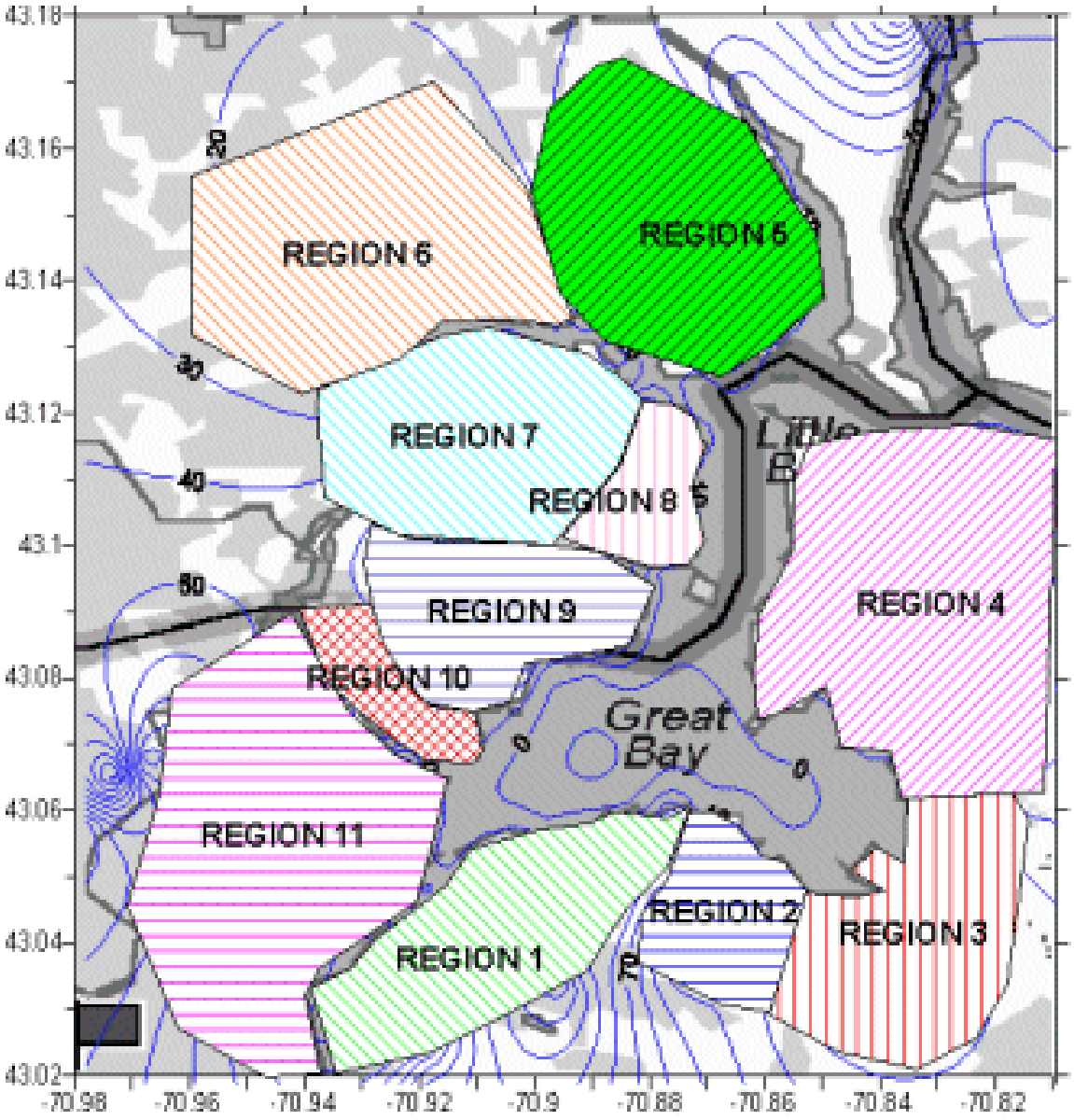

FLOW ESTIMATION VIA THERMAL IMAGERY METHOD

Observations from thermal imagery combined with field investigations showed that the actual seepage face was somewhat indistinguishable from the resulting discharge plume because of similar thermal characteristics. This was a standard problem in determining the surface area of the thermal signature. Thus a reliable methodology for determining the surface area was necessary.

One primary issue was that areas down gradient of a seepage face, which did not contribute to flow, were covered with groundwater discharge running down the surface, and shared a similar thermal signature as areas that contributed to flow. Figure 6 illustrates an idealized cross-section of a typical groundwater seepage face and surface discharge plume. These normally occur at the free surface of the transmissive water bearing unit.

The overlapping seepage face and discharge plume (surface runoff) was more easily detected in the field, based primarily on hydrogeology, as the seepage face was often coincident with a marine clay aquitard. GIS analysis of the TIR imagery was easily performed, but absent of an easily definable seepage face, did not reliably reflect field observations of surface area. Two approaches were used to resolve the differences between seepage face and surface runoff plume: the use of a qualitative visual cue provided by the type curve, and a direct measurement obtained in the field.

Figure 6:Idealized Cross-Section Displaying Groundwater Seepage Face and Concurrent Discharge Plume

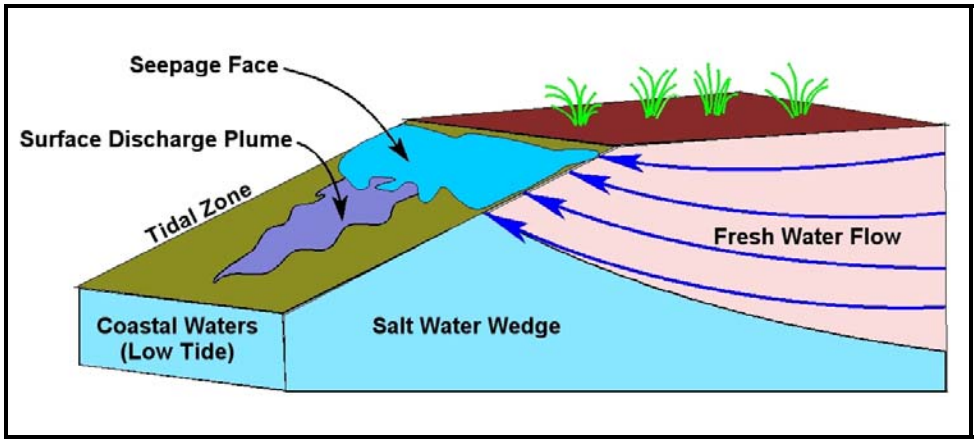

Figure 7 illustrates a TIR image in which the seepage face and the discharge plume are indistinguishable. The sample thermal imagery is the product of an aerial survey flown August 2000 over the Great Bay Estuary, New Hampshire. The survey elevation was 4,000 feet, resulting in a pixel resolution of 2.5 square feet. The images are standard polarity: the image spectrum of black to white is hot to cold, respectively.

Figure 7: Thermal Infrared Image of Groundwater Seepage Face and Discharge Plume

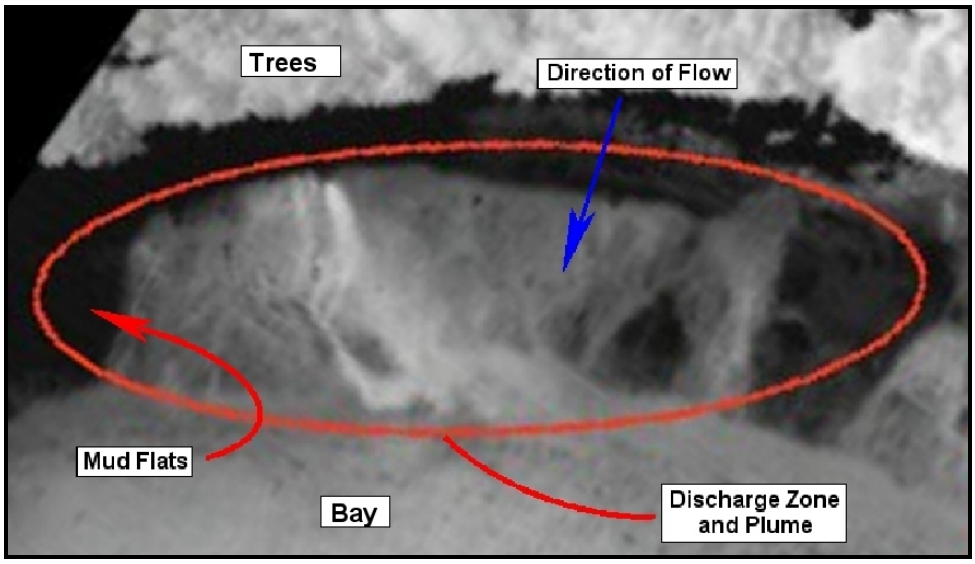

GIS analyses of the imagery enabled the development of the characteristic type curve for each seepage face. Type curves for > 15 discharge zones were examined and were found to have consistent and predictable characteristics. Comparisons of the type curve with field observations and subsequent GIS analyses revealed a plot with three significant slopes that could be used to distinguish the seepage face from the discharge plume. The many components of the type curve represent the features on the ground and captured by the TIR image (Figure 8). This curve was predictable and was the key to determining a repeatable area of the seepage face. The curve had two inflection points with three predominant slope components to it: the upper slope (slightly negative and bounded above by a horizontal asymptote); the middle slope (steeply negative); and a bottom slope (slightly negative, bounded below by a horizontal asymptote). The lower inflection point proved an indicator of the seepage face area.

Figure 8: Thermal Image Features as Components of Type Curve

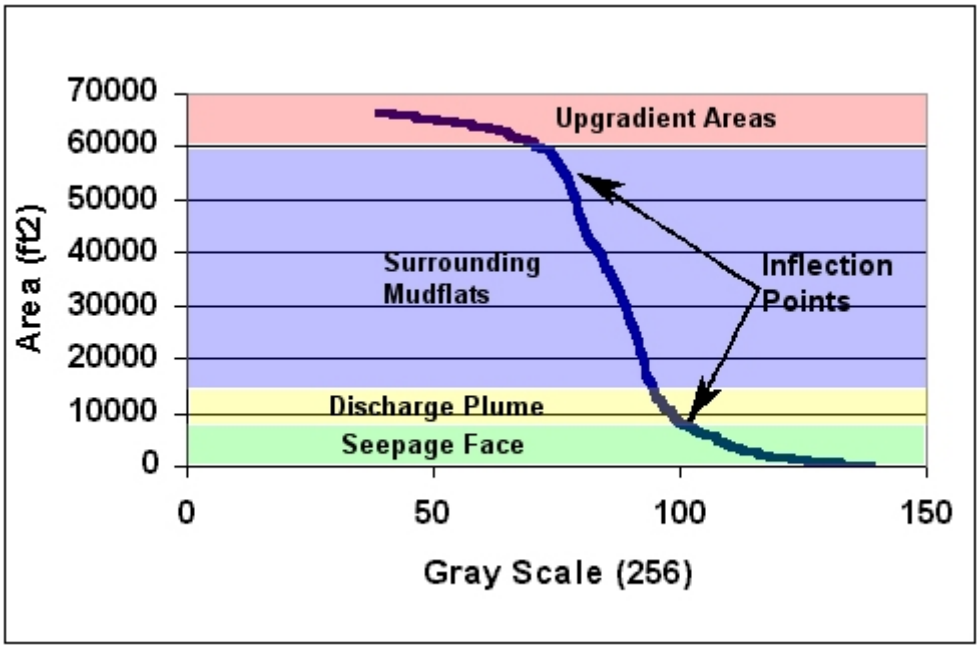

Procedure for Analysis of TIR

By GIS analysis, the imagery was converted to a grid, a format in which the pixel data could be queried. The query function in GIS applications is one of the strengths of this technology in that it enables geospatial analysis (Figure 9). Unfortunately, the pixel data did not have a consistent temperature equivalent from which to construct the query (e.g., based on the temperature of groundwater). The imaging device continually adjusts the intensity of the grayscale to maximize the effectiveness of the imagery to resolve temperature gradients. If this were not the case, and the imagery could be normalized, a universal query (a query applied uniformly to all the imagery) could be applied. Analysis of the field observations and the pixel data revealed a standard type curve from which to base the criterion.

The type curve was constructed by plotting the surface area of the discharge zone as a function of grayscale. The reasoning for this was to establish a relationship between the size of the discharge zone as it related to the intensity of subsurface discharge. The selection of the query criterion was based on the graphical analysis of the type curve produced. The results of the selected discharge area, for one such query, are highlighted in yellow in Figure 9. Field verification showed strong agreement between the field and GIS analysis of surface area. In future work, these limited results should be more rigorously tested by increasing the number of field verified sites.

Figure 9: Query and Location of Groundwater Discharge Zones by GIS Analysis

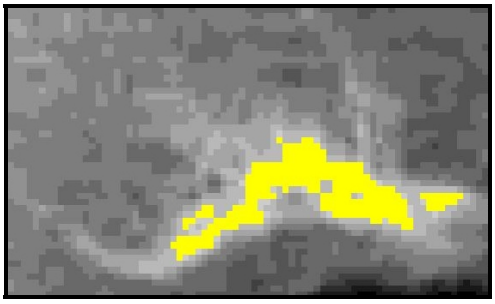

Figure 10 illustrates the use of the type curve for estimating the middle and lower slopes and interpolating the lower inflection point. The lower slope was determined by first anchoring the line at the highest values of the grayscale corresponding with the lowest area values. This line had a slightly negative slope and ran fairly close to the x-axis. In some cases the tail of the lower slope is very short and the x-axis was a good approximation of the lower slope. The middle slope was determined by estimating the slope between the two inflection points. The two lines were extended, and at their intersection a line was drawn perpendicular to the curve. The intersection of this line and the curve is the criterion for determining seepage face surface area.

Figure 10: Interpolation of Inflection Point Using Standard Type Curve

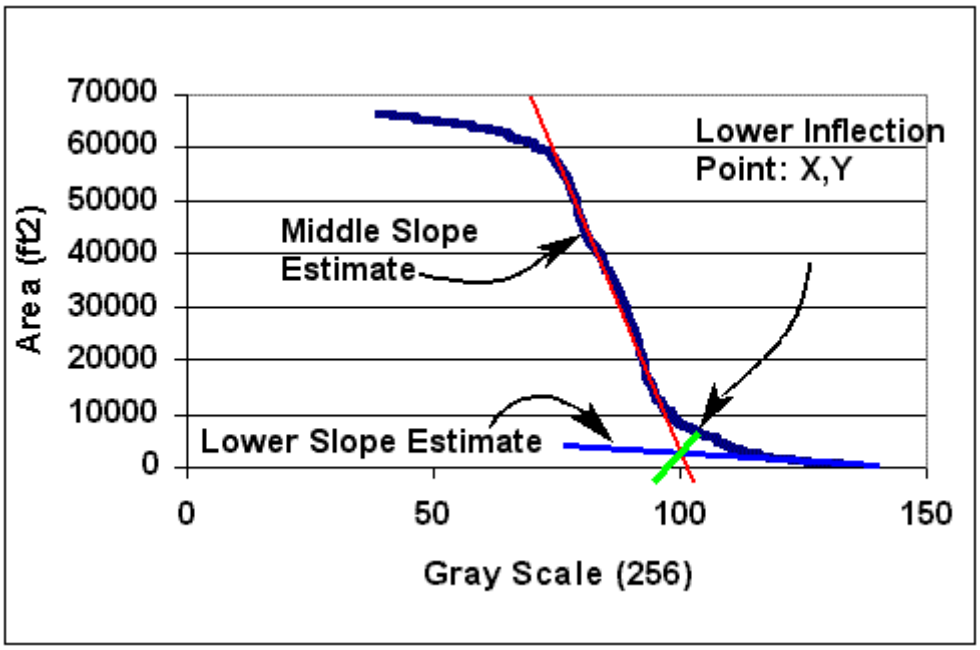

The plot of the type curve was developed from tabulation of the pixel data: the number of occurrences (or count) and grayscale value. This was accomplished by exporting the tabular data associated with grid. The data was exported and opened in a spreadsheet. The cumulative area was then calculated for the sum of all pixels greater than or equal to each grayscale value. Table 3 depicts the tabular data used to develop Figure 6. The key to establishing the surface area of the plume was setting a cutoff point for the query of the grayscale value and the resulting cumulative area. The greater the temperature gradient between the groundwater and the surrounding landforms, the easier it was to resolve the thermal signature. The construction of the query depended on whether the groundwater was warmer or cooler than the surrounding landforms (winter to summer, respectively), and whether the image was reverse or standard polarity.

Table 3: Tabular Data for Plot of Standard Type Curve

GRAYSCALE VALUE	PIXEL COUNT	CUMULATIVE COUNT SUM	CUMULATIVE AREA SUM (FT2)
116	15	1043	5124
117	15	1058	4899
118	22	1080	4673
119	7	1087	4343
120	13	1100	4237
121	12	1112	4042
122	16	1128	3862
123	14	1142	3621
124	13	1155	3411
125	14	1169	3216

Sample GIS Analysis

An example analysis of a large well-defined groundwater discharge zone was performed for Fox Point, Newington, New Hampshire.

The images were analyzed for thermal anomalies which located suspected groundwater discharge zones. The image was cropped to avoid effects of false positives, as indicated in Figure 11.

Figure 11: Thermal Infrared Image of Groundwater Discharge Zones Indicating Cropped Area

The cropped image was analyzed by GIS to produce the associated pixel data. The pixel data was then transformed into the type curve of surface area as a function of grayscale. The middle and lower slopes were estimated for the type curve, and the resulting inflection point was interpolated (Figure 12). A seepage face surface area of 5,409 square feet was determined from the inflection point.

Figure 12: Type Curve Analysis Determining Seepage Face Surface Area

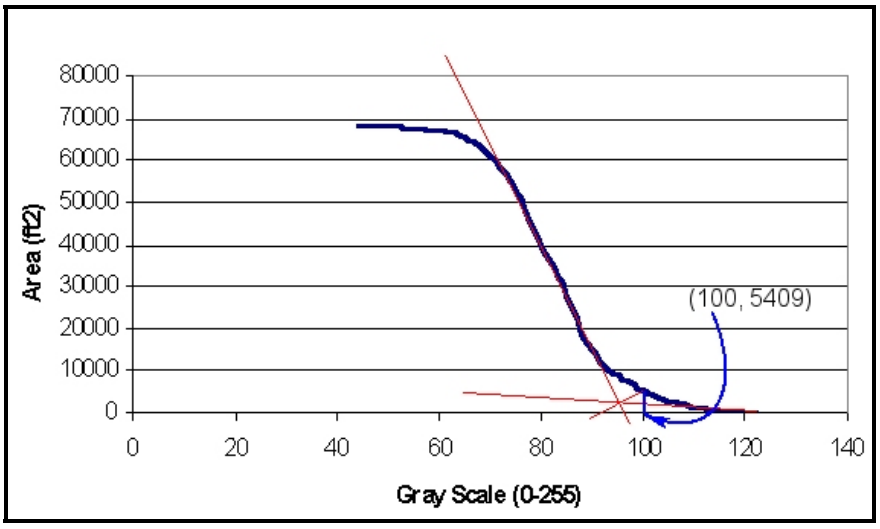

The resulting surface area was used to query the thermal image to observe the seepage face (Figure 13).

Figure 13: GIS Query of Cropped Thermal Image Indicating Seepage Face of Groundwater Discharge Zone

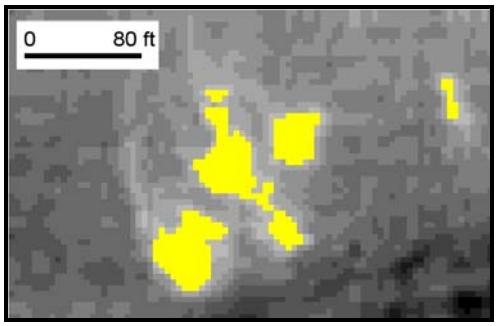

Based on the type curve analysis, the resulting groundwater discharge zone was delineated within the discharge plume. These results, combined with specific discharge estimates made in the field, were used to calculate flow from the entire discharge zone.

Delineation of Groundwater Discharge Zones by TIR

Analyses of the TIR imagery produced a catalogue of suspected groundwater discharge zones characterized by size, type, intensity, and coordinates. For the April survey, a total of 165 groundwater discharge zones were identified along the 51 miles of shoreline surveyed. Table 4 lists some of the groundwater discharge zones and their classification characteristics and Figure 14 illustrates the locations.

Table 4: Sample Catalogue of Groundwater Discharge Zones

NAME	SIZE	TYPE	INTENSITY
4.1.1	Medium	linear	Medium/low
7.1.1	Small	linear	Medium/low
8.1.1	Small	diffuse	low
8.2.1	Small	diffuse	low
9.1.1	Small	diffuse	low
9.2.1	Small	point	Medium/high
16.1.1	Small	point	high
17.1.1	Medium	linear	Medium
17.3.1	Medium/Large	dendritic	Medium/high
18.1.1	Medium/Large	dendritic	Medium/low
18.2.1	Medium/Large	dendritic	Medium/low
19.2.1	Small	point	low

Previous research has shown that the bulk of the SGD is expected within several meters of shore and within the tidal zone (Bokuniewicz, 1980; Johannes and Hearn,

1985; Giblin and Gaines, 1990). Because of this and intense tidal flushing, the aerial survey was performed at low tide to prevent obscuring of the groundwater thermal signatures at the seepage faces. Because of underlying saltwater and thickening clay below the low water elevation, the tidal zone represented the path of least resistance for upwelling groundwater, so the TIR should have recorded the majority of groundwater discharge in the bay, but would not have located deeper SGD correlated with bedrock fractures. Side scanning sonar was used to detect deeper SGD, but without success. Side scanning sonar has been used to effectively to locate riffles and pools in the sediments that are due to upwelling groundwater in quiescent lentic environments (Hay, 1984). This is due to the heavily mixed tidal environment in which upwelling features (e.g. riffles and pools) are washed away.

Field Verification

Groundwater discharge zones were characterized and classified over 2000 and 2001 through significant field efforts over two summers. These efforts, while instrumental for large-scale characterization of groundwater discharge zones, were insufficient for the verification of the type curve. The level of field effort required for type curve verification increased the field time at each site significantly. Thus, due to time and financial constraints, limited field verification were performed to test the use of the type curve. Future research should be performed to more rigorously substantiate the field verification of the type curve procedure by using a greater number of sites. Logistical difficulties were encountered simply due to the location of the discharge zones within the tidal zone, which limited the window of opportunity for investigating the exposed discharge zones. Additional constraints were posed by the need to access these locations by boat during the hours of operation of the University's Jackson Estuarine Laboratory, Durham, NH.

Three sites were verified successfully and are summarized in . A strong correlation, albeit for a limited number, was observed. Many of the sites were tested repeatedly to develop proper field procedures for ascertaining the surface area of the thermal signature. Field assessment using hand-held thermometers inserted in the soils was less successful than use of the handheld TIR gun, and as a result additional site data was not usable. This was attributed to the need for measuring precisely the surface temperature (the top millimeter) to correlate with the imagery. Temperature changed drastically with depth.

Other confounding factors were surface temperatures affected by shadows, wind, and time exposed by the tides. The hydrogeology of the seepage faces was coarse sand and gravels, highly transmissive materials. Lower limits of the discharge zone were often evident by the occurrence of seaward-thickening marine clays.

Mini-piezometers installed in the upper foot of surficial materials indicated strong piezometric gradients. Gradients ranged from over 12 inches in the center of the discharge zone to zero at the perimeter. The exception was at the seaward limit of the discharge zone, when limited by a marine clay confining unit, where the piezometric gradient persisted. This is consistent with the belief that discharge zones are occurring within only the tidal zone due to a confining unit and a saltwater wedge.

Table 5: Correlation of Surface Areas Derived from Field Measurements Versus GIS Analysis of Thermal Imagery

Site	Field Derived Area (ft2)	GIS Derived Area (ft2)	Correlation Ratio
Fox Point 1	3,600	3,772	1.048
Fox Point 4	4,300	4,237	0.985
Wagon Hill 2	2,500	2,675	1.070

Field verification of TIR-identified discharge zones resulted in about an 85% success rate (total field verified n=34), with 15% of the failures attributed to false positives. 11% percent of the zones could not be located, perhaps because they were ephemeral and there was a long time delay between surveying and field sampling in which they might have diminished or disappeared. The false positives included were pipe discharge, ponded waters within a salt marsh, or unique features similar in appearance to discharge zones. Some of these features include unique sandbars formed by tidal waters. The success rate increased with increasing familiarity with the characteristics of discharge zones therefore some false positives, such as ponded water, could be avoided.

Figure 14: Locations of TIR Indicated Groundwater Discharge Zones in the Great Bay Estuary

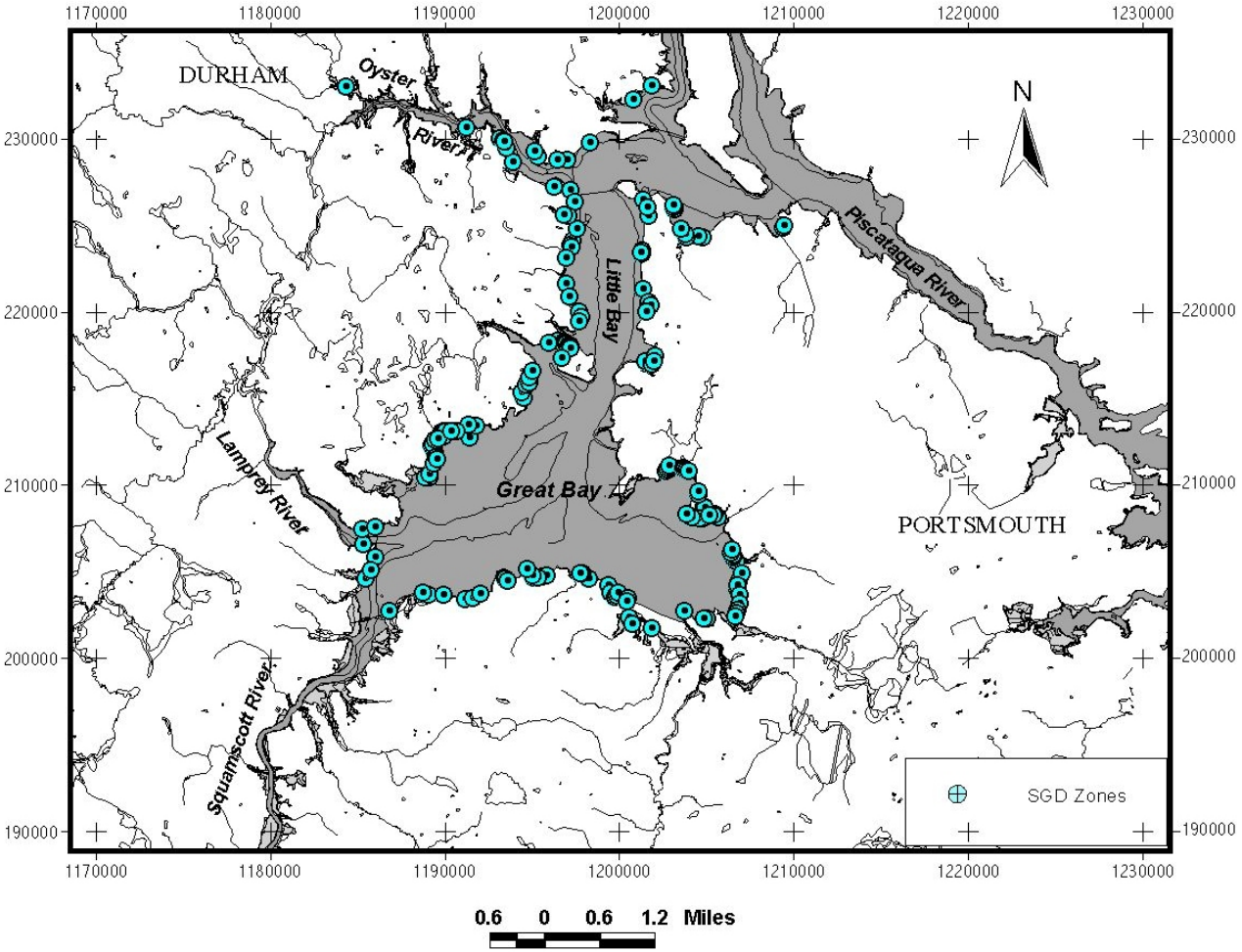

Most of the groundwater discharge zones identified during the investigation originated from sand and gravel layers. In most cases, groundwater flowrate occurred inversely with increasing depth (or distance from shoreline) and incidence of marine clays. Marine clays are greatest at depth (low elevations) and pinch out at the high tide mark.

Significant field efforts over two summers characterized and classified groundwater discharge zones. These efforts, while instrumental for large-scale characterization of groundwater discharge zones, allowed insufficient time for many verifications of the type curve. The need to resolve the seepage face from the discharge plume was not recognized until late in the research and after the bulk of the field efforts were completed. Logistical difficulties were posed because the discharge zones were located within the tidal zone, which limited the window of opportunity during which the exposed discharge zones could be investigated. Additional constraints were posed by boat access and availability.

Analysis of the type curve and field investigations showed that the seepage face could be readily and reliably determined. Field verification showed strong agreement between the field and GIS analysis of surface area (Table 6). Three sites were verified successfully with surface areas of 2,675, 3,772, 4,237 square feet respectively. Table 6 illustrates the strong correlation, albeit for a limited number of sites, between surface areas derived from field observations and the type curve. Many of the sites were tested repeatedly to develop proper field procedures for ascertaining the surface area of the thermal signature. Field assessment used thermal infrared temperature guns, which measure temperature by the same means as the aerial surveys. Field assessment using hand-held thermometers inserted in the sediments was less successful, and as a result additional site data was not useable. This was attributed to the need for precisely measuring the surface temperature (the top millimeter) to correlate with the TIR. Temperature changed drastically with depth. Other confounding factors were surface temperatures affected by shadows, wind, and time exposed by the tides. Because field measurements used similar means as did the surveys, adequate field characterization was needed to distinguish the seepage face from the discharge plume. The seepage face commonly occurred at the interface of the marine clay and the coarse sands and gravels.

Table 6: Correlation of Surface Areas Derived from Field Measurements Versus GIS Analysis of TIR

Site	Field Derived Area (ft2)	GIS Derived Area (ft2)	Correlation Ratio
Fox Point 1	3,600	3,772	1.048
Fox Point 4	4,300	4,237	0.985
Wagon Hill 2	2,500	2,675	1.070

Lower limits of the discharge zone were often evident by the occurrence of seaward-thickening marine clays. Mini-piezometers installed in the upper foot of surficial materials indicated strong piezometric gradients. Piezometric head ranged from over 12 inches above the ground surface in the center of the discharge zone to zero at the perimeter. When limited by a marine clay confining unit, the piezometric gradient persisted at the seaward limit of the discharge zone. This is consistent with the belief that

discharge zones occur due to a confining unit. Salinity was monitored during sampling of discharge zones, to assure presence of freshwater SGD rather than saltwater storage, and averaged 6.1 ±6.5 ppt (n=19), which assured the assumption.

Matrix Analyses of Regional-Scale Flow

A subset of SGD zones were characterized and the results applied by matrix analyses to estimate regional-scale flow by use of a flow expression matrix. The population subset was about 5% of the total for specific discharge, and 3% for surface area. Surface area classes were calculated based on TIR analysis of 22 sites (Table 7). The specific discharge classifications were calculated from field measurements at nine sites (Table 8).

Table 7: Groundwater Discharge Zone Surface Area Classifications

Rank	Class	Interval (ft2)	Average Interval Area (ft2)
1	s	766-3366	2066
2	s/m	3366-5966	4666
3	m	5966-8565	7265.5
4	m/l	8565-11165	9865
5	l	11165-13765	12465
6	xl	13765-16365	15065

The flow regimes were divided into the following categories:

Table 8:Groundwater Discharge Zone Specific Discharge Classifications

Rank	Type	Avg. Flow (GPD/ft2)
1	Low	13
2	Medium/Low	22
3	Medium	30
4	Medium/High	39
5	High	48

A *flow expression matrix* is a series of *if/and/then* statements that process data based upon multiple classifications, to obtain individual flow estimates for a discharge zone. Table 9 illustrates the full *flow expression matrix*. The application of the flow expression matrix in a GIS framework is used to estimate flow over a large scale. While extreme flow ranges are possible within this matrix, from 3,252 to 393,329 gallons per day, not all expressions are necessarily observed. Flow was calibrated by multiplying the Table 7 values by the Table 8 values, then multiplying by an intensity coefficient (1.0-intense, 0.3-diffuse) and the correlated correction factor (0.6). The factor was based on the comparison of matrix flow estimates which showed a 40% overestimation. Figure 16 illustrates the fit as described with calibration coefficient. A diffuse coefficient (0.3) was applied to account for the large size and the low flow typically observed with a diffuse

zone. The final 0.6 coefficient was a calibration factor based on a comparison of flows derived by the flow expression matrix. Flows derived from analysis individually by TIR and field data, are discussed in the following sections.

Table 9: Flow Expression Matrix

If	*And*	*And*	*Then*
Size	**Intensity**	**Type**	**Value (GPD)**
Small	Low	Diffuse	3252
	Low	Other	10841
	Medium/Low	Diffuse	6485
	Medium/Low	Other	21616
	Medium	Diffuse	9717
	Medium	Other	32390
	Medium/High	Diffuse	12949
	Medium/High	Other	43164
	High	Diffuse	16182
	High	Other	53939
Size	**Intensity**	**Type**	**Value (GPD)**
Small / Medium	Low	Diffuse	7345
	Low	Other	24484
	Medium/Low	Diffuse	14645
	Medium/Low	Other	48817
	Medium	Diffuse	21945
	Medium	Other	73150
	Medium/High	Diffuse	29245
	Medium/High	Other	97484
	High	Diffuse	36545
	High	Other	121817
Size	**Intensity**	**Type**	**Value (GPD)**
Medium	Low	Diffuse	11438
	Low	Other	38127
	Medium/Low	Diffuse	22806
	Medium/Low	Other	76019
	Medium	Diffuse	34173
	Medium	Other	113911
	Medium/High	Diffuse	45541
	Medium/High	Other	151803
	High	Diffuse	56908
	High	Other	189695
Medium/ Large	Low	Diffuse	15531
	Low	Other	51769
	Medium/Low	Diffuse	30966
	Medium/Low	Other	103220
	Medium	Diffuse	46401
	Medium	Other	154671
	Medium/High	Diffuse	61837
	Medium/High	Other	206122
	High	Diffuse	77272
	High	Other	257573
Size	**Intensity**	**Type**	**Value (GPD)**
Large	Low	Diffuse	19624
	Low	Other	65412
	Medium/Low	Diffuse	39127
	Medium/Low	Other	130422
	Medium	Diffuse	58629
	Medium	Other	195431
	Medium/High	Diffuse	78132
	Medium/High	Other	260441
	High	Diffuse	97635
	High	Other	325451
Size	**Intensity**	**Type**	**Value (GPD)**
Extra Large	Low	Diffuse	23716
	Low	Other	79055
	Medium/Low	Diffuse	47287
	Medium/Low	Other	157623
	Medium	Diffuse	70858
	Medium	Other	236192
	Medium/High	Diffuse	94428
	Medium/High	Other	314760
	High	Diffuse	117999
	High	Other	393329

If	*And*	*And*	*Then*
Size	**Intensity**	**Type**	**Value (GPD)**

A sample of the discharge flow estimates (Table 10) is the fulfillment of the *flow expression matrix* (Table 9) using the catalogue (Table 4), the classification schemes for surface area (Table 7) and specific discharge(Table 8).

Table 10: Discharge Zone Flow Estimates

NAME	SIZE	TYPE	INTENSITY	SGWD Flow (GPD)
4.1.1	Medium	linear	Medium/low	50,680
7.1.1	Small	linear	Medium/low	14,411
8.1.1	Small	diffuse	low	2,168
8.2.1	Small	diffuse	low	2,168
9.1.1	Small	diffuse	low	2,168
9.2.1	Small	point	Medium/high	28,778
16.1.1	Small	point	high	35,961
17.1.1	Medium	linear	Medium	75,942
17.3.1	Medium/ Large	dendritic	Medium/high	137,413

The largest flow observed was medium/large (size), medium/high (intensity), at 257,570 gallons per day, and the lowest is small (size), low (intensity), diffuse (type) at 3,253 gallons per day.

Comparison of TIR Methods: Individual Discharge Zones Vs. Matrix Analyses

Comparisons of the area determination methods (flow matrix versus TIR) resulted in a reasonable correlation of slopes (not significantly different at 95%, Figure 15). Limitations to this approach were likely from human bias that occurs when analyzing TIR. Classification of the discharge zones is by the judgment of the analyst. The analyst reviews the entire set of images and sorts them into classes based on size, type, and intensity. Because of the difficulty of the GIS analysis of the TIR imagery, only a subset of the images is processed.

Figure 15: Correlation of Seepage Face Surface Area Estimates Made for Individual Discharge Zones Using GIS Analysis of TIR Versus TIR and Flow Expression Matrix

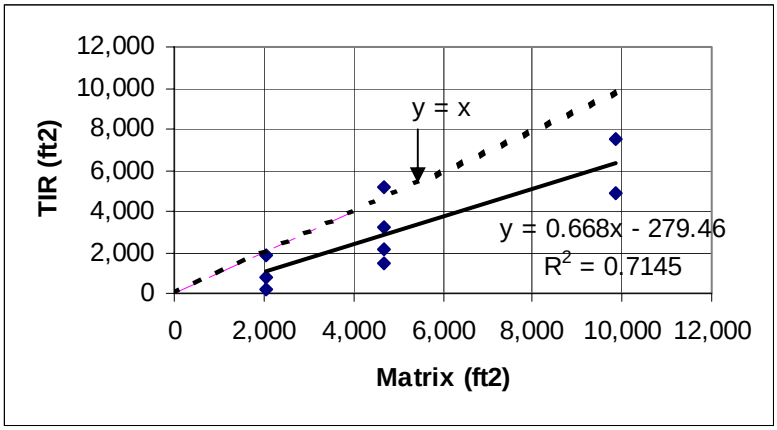

This section discusses a comparison of the use of TIR and field-based measurements to assess flow for individual groundwater discharge zones in comparison with the estimates from the flow expression matrix (not to be confused with piezometric mapping). Both methods use TIR, however, use by the flow matrix is indirect. To calibrate the matrix method, field-verified values of groundwater discharge are needed. An initial comparison of the two methods showed a close correlation with slope (not significantly different at 95%), but a matrix overestimation of flow by about 40%. As a result, a calibration coefficient of 0.6 was included in the matrix calculations, which resulted in a reasonable correlation. (Figure 16). The flow expression matrix overestimated the discharge when compared with field characterization, however the fit is favorable. This correlation could be improved by increasing the number of sites examined (n=9), in the refinement of categorization/classification schemes of groundwater discharge zones, and performing field characterizations shortly after the TIR surveys are flown. This last point is a major issue which has not been adequately addressed. It may affect all of the comparisons as effects of seasonality are not currently well understood. This issue is currently under examination as long-term variations (over multiple seasons) of discharge zones are being monitored (Brannaka et al., 2001). Staver and Brinsfield (1996) reported that the size of the groundwater discharge zone varied with lateral distance from the shoreline, with winter discharge being as much as five times that during the dry summer months.

Figure 16: Correlation of Groundwater Discharge Estimates Made for Individual Discharge Zones Using GIS Analysis of TIR and Field Techniques Versus TIR and A Flow Expression Matrix

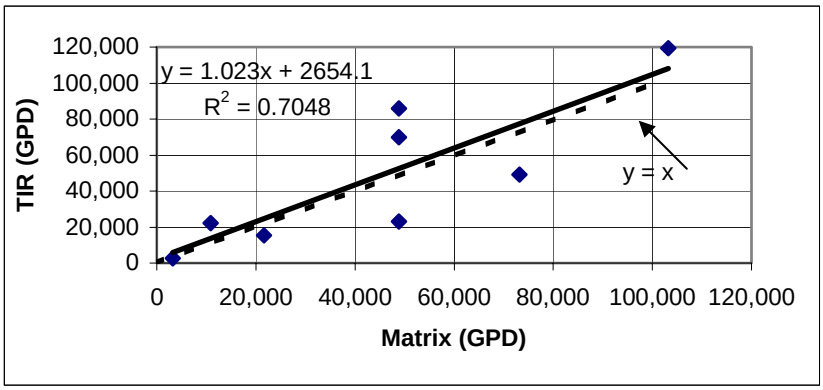

Comparisons of specific discharge measurement made in the field with those predicted by the matrix analyses showed a poor correlation (slopes significantly different at 95%). These results were not a problem with the flow expression matrix, but rather with the large amount of time elapsed between the thermal imagery survey and the field characterizations. For example, no correlation was observed between two adjacent discharge zones, one with an intense thermal signal, the other with a minor signal. The actual field measured specific discharge was the opposite of what was expected based on the signal intensity. For an intense signal, a large flux is expected, and for a diminished signal one would expect a smaller flux. The opposite was observed in some instances. A few possible explanations are possible. The first is that 18 months elapsed between survey and field characterization. Varying climate, precipitation, and evapo-transpiration no doubt cause seasonal variations in groundwater discharge zones. Another important influence is the effect of soil temperatures upon the temperature of groundwater discharge. In April, groundwater and soil temperatures to a depth of 12 feet may be as much as 3ºF colder, than deeper sourced waters (Hillel, 1982; Marshall and Holmes, 1988; Wu and Nofziger, 1999). The TIR imager can resolve temperature differences up to 0.15ºF. In the case of mixed or varying sources of groundwater, with contributions from surficial materials and bedrock materials, variations in thermal signals might parallel variations in composition. This may significantly confound the use of TIR for estimating flux based on signal intensity and should be explored in greater detail. Campbell and Keith (2001) used thermal signals to estimate flow from a modeling approach, which assume consistent thermal signals from waters with consistent source composition.

Figure 17: Correlation of Specific Discharge Estimates Made for Individual Discharge Zones Using Field Techniques Versus TIR and A Flow Expression Matrix

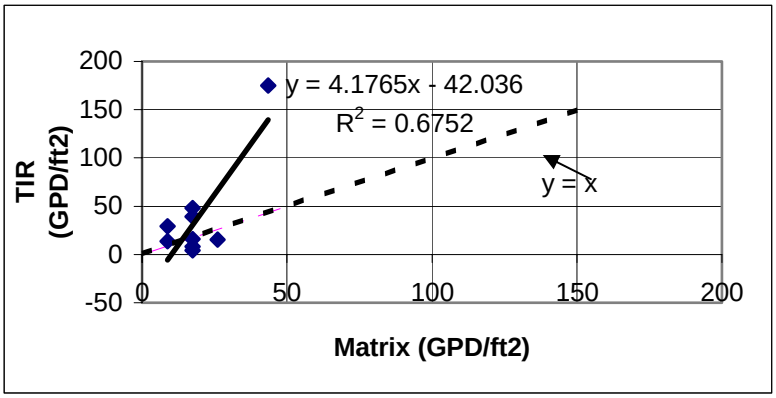

Comparison Of Methods: TIR and Piezometric Mapping

Total flow estimates for the bay were developed for both TIR and piezometric mapping. The discharge estimates were 8.6 and 6.2 cubic feet per second per 51 miles of shoreline for the TIR and piezometric estimates, respectively. That is 0.17 and 0.12 cubic feet per second per mile of shoreline. For the total Great Bay estuary covering nearly 144 miles, thermal imagery and piezometric estimates are 24.2 and 17.4 cubic feet per second, respectively. These values represent substantial flow and are of particular interest when compared with flows from other known sources including surface waters, and waste water treatment plants (Figure 18).

Figure 18:Comparison of Annual Median Flows for Ground Water, Surface Water, and Waste Water Treatment Plants of the Great Bay Estuary

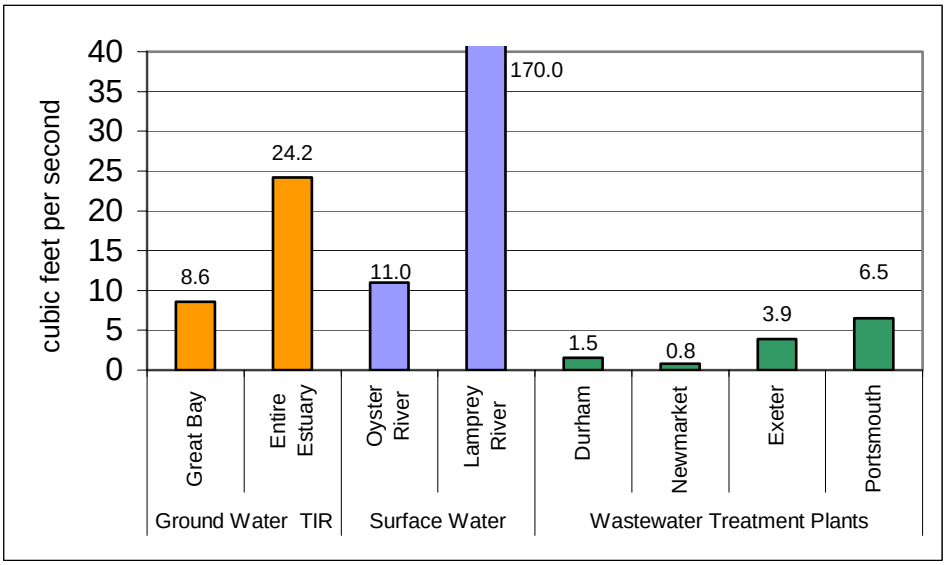

GROUNDWATER-DERIVED NITROGEN LOADING TO COASTAL WATERS

Characteristics of Groundwater Discharge Zones

Based on GIS analysis of TIR for 22 groundwater discharge zones, calculated surface areas ranged from 2,066 to 15,065 square feet. The larger discharge zones were typically diffuse discharge zones.

There was an incidence of widespread elevated DIN concentrations in the groundwater discharge throughout the Great Bay Estuary (Figure 19). Nearly 99% of the DIN was in the form of nitrate and nitrite for both the monitoring wells and SGD. Ammonium was usually absent. Groundwater dissolved inorganic nitrogen concentrations averaged 0.81± 0.89 mg DIN/L, with a maximum value of 2.7 mg DIN/L (n=20). Nutrient contamination was observed in upgradient bedrock groundwater analyzed from 192 monitoring wells averaging 0.83± 1.34 mg DIN/L, with a maximum value of 10.2 mg DIN/L. This data indicates that groundwater discharge is a substantial source of nutrient loading. Figure 19 illustrates the distribution of water quality data throughout the study area. Sampling of upgradient wells was more thorough than SGD zones. Major variations were observed spatially and often within short proximity. In two cases, within less than 20 feet, variations in discharge were seen from 0.55 to 1.51 and 0.28 to 2.59 mg N/L. There is no simple explanation for this other than to say subsurface flow is complex and correlated with hydrogeology.

The water quality results indicate the groundwater influx had elevated nitrate levels. This study did not include a thorough review of upgradient land use, however a cursory review was performed. The elevated DIN concentrations were found

downgradient of low-density residential areas where residences were predominantly on private septic systems, and farms where there were livestock and crop production.

Loading Estimates

The total calculated loading for the study area was 6.8 ± 7.5 tons of N per year per 51 miles of shoreline. That is 0.13 tons of N per year per mile of shoreline. For the total Great Bay estuary, covering nearly 144 miles, the estimate is 19.3 ± 21.2 tons of N per year. This was accomplished by scaling up the results from 51 miles of shoreline (from the Great Bay proper) to 144 miles of shoreline (for the entire estuary).

Comparison of Flow and Loading Data for Groundwater, Surface Water, and Wastewater Treatment Facilities

The groundwater discharge to coastal waters was about 2.5% (24 cfs of a total 931 cfs) of the total average riverine freshwater flow to the bay. This number is significantly smaller than some reports using isotope geochemistry techniques. This difference is affected by the classification of water as surface water or groundwater. The total freshwater flows in the study area are based on tributary flows measured at gauging stations at the tidal extent of the estuary. As a result, groundwaters contributing to the hundreds of non-tidal river and stream miles would be considered surface waters. From a TMDL and nutrient budget standpoint, this is inconsequential because it is just the accounting that differs, and either way the sum of the nutrient sources are all considered. However, this accounting difference is biasing to a very large extent the true groundwater loading, which could potentially be 4 or 5 times what was measured in this study if one were to consider groundwater influx above the tidal extent within the estuary.

Flow estimates from groundwater discharge compared with flows from other known sources including surface waters (USGS, 2002), and wastewater treatment facilities (Jones and Langan, 1994; Mitnick, 1994) are illustrated in Figure 18. The Oyster River drains one of the smallest watersheds in the estuary at 30 square miles, and the Lamprey River drains the largest at 210 square miles (Brown and Arrelano, 1979) and represents the extremes of surface water flow in the estuary. The Cocheco River watershed is 180 square miles. The flows from the WWTFs are from the towns of Durham (pop. 12,664), Newmarket (pop. 8,027), Exeter (pop. 14,058), and Portsmouth (pop. 20,784). Groundwater discharge is double that of the annual median flow of the smaller watershed and about 13% of the largest (Figure 20). SGD exceeds all of the individual WWTFs and more than half of the total 39 cfs discharging from all WWTFs combined into the estuary.

Figure 19: DIN (mg/L) Distribution for Groundwater Discharge Zones and Monitoring Wells

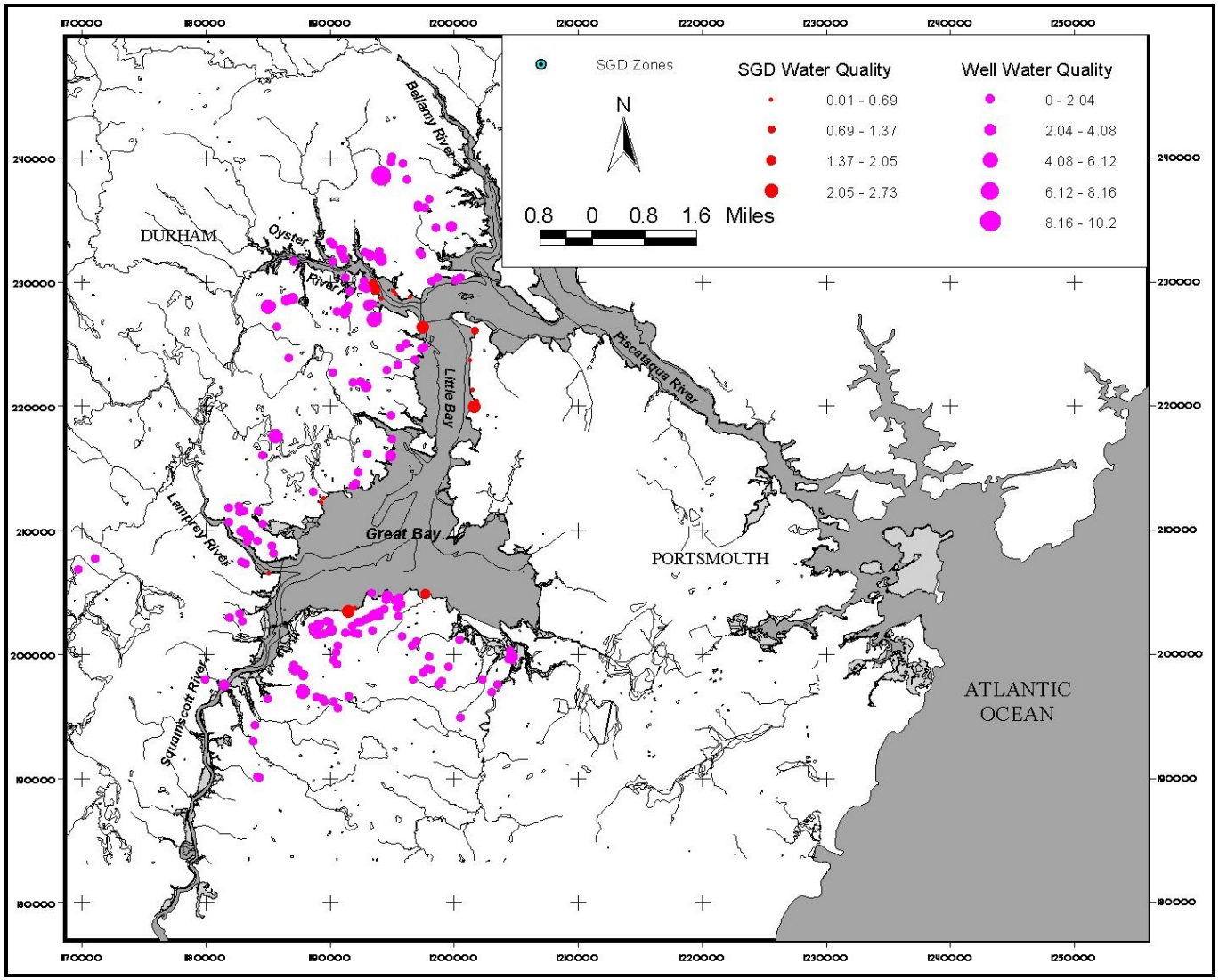

Figure 20: Annual Median Flows for Ground Water, Surface Water, and Wastewater Treatment Plants Entering the Great Bay Estuary

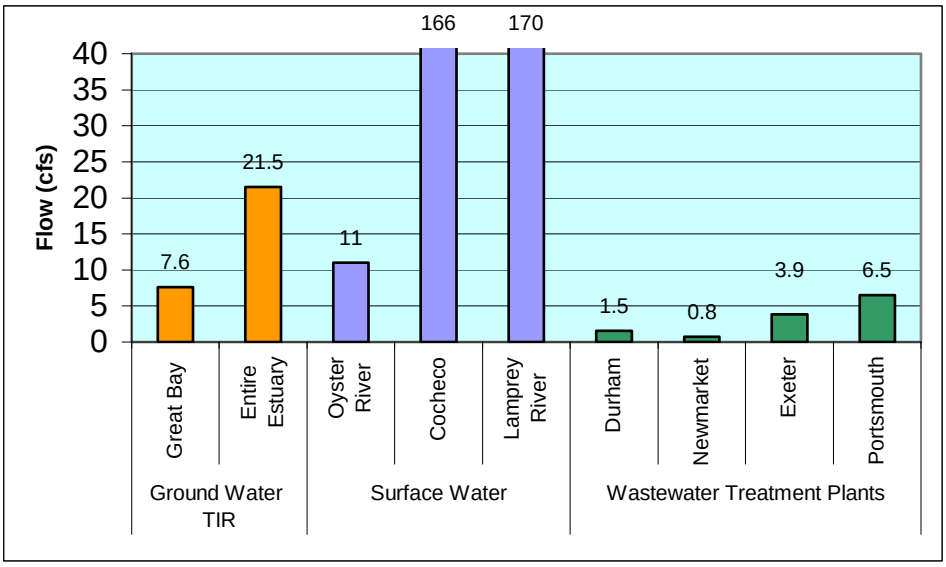

Of particular interest are the loading estimates for groundwater compared with loading from surface water and WWTFs. However, comparison of these results is possibly underestimating total nitrogen from groundwater. The data from the surface waters and WWTFs is reported as total nitrogen. The water quality analyses for groundwater were for DIN (nitrate, nitrite, and ammonia), but did not include dissolved organic nitrogen (DON) or particulate nitrogen (PN). As a result, total nitrogen loading from groundwater may be underestimated. In estuarine waters DIN accounts for nearly 80% of the total nitrogen and DON and PON the remaining 20% (Sharp, 1983). This may apply for SGD. Ongoing research is examining DON and PN concentrations in SGD for Hampton Harbor, New Hampshire (Ballestero and Roseen, 2002).

The Oyster and Lamprey River sources are sampled at the limit of the freshwater extent (at dams) prior to mixing with the estuary and do not include large wastewater inputs. The Cocheco River is also sampled at a dam and point source contribution from upstream WWTFs has been deducted from fluvial loading (Langan, 2000). Loading from SGD is more than double that from the town of Newmarket (pop. 8,027) with primary and secondary wastewater treatment, and about 60% of the town of Exeter (pop. 14,058) with primary treatment and one combined sewer overflow and an emergency overflow lagoon system (Figure 21). SGD is nearly double the loading from the Oyster River (smallest watershed), 25% of the Lamprey River (largest watershed), and 14% of the single largest surface water source (Cocheco River).

Figure 21: Nitrogen Loading Values for Groundwater, Surface Water, and WWTFs

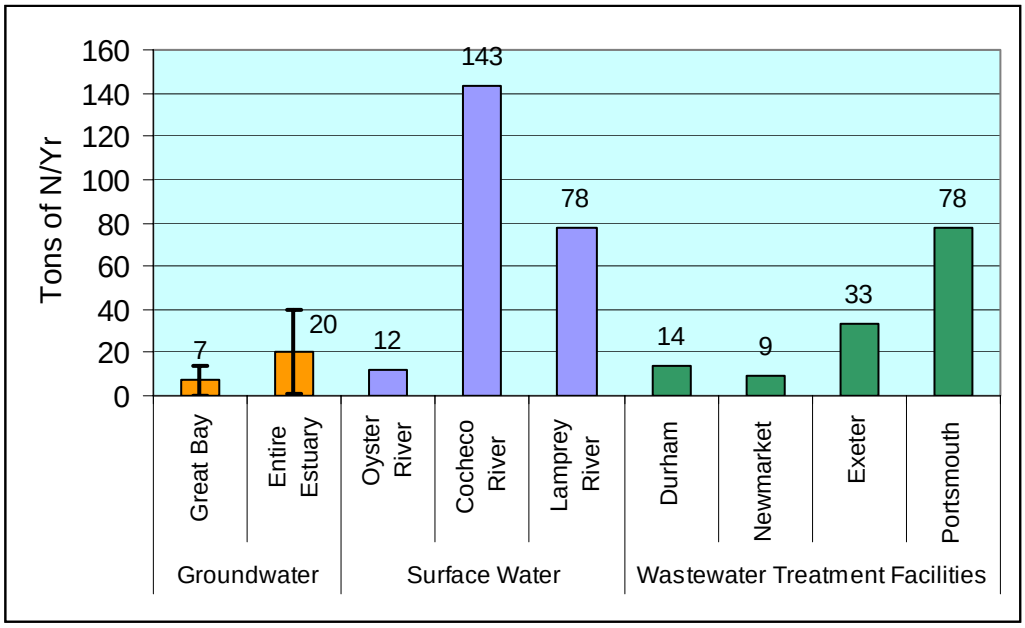

A review of the total loading of all nutrient sources to the estuary, as is needed for TMDLs, includes point sources, non-point sources, and atmospheric contribution (Figure 22). Groundwater is classified as a non-point source but is reported distinctly for comparative purposes. The point source contribution is the sum of the aforementioned WWTFs. The non-point sources (NPS) are measured as surface water concentrations at the limit of the freshwater extent (dams). Surface waters, at this point in the hydrologic cycle, harbor mobile non-point source contaminants within the watershed and thus represent a good measurement of NPS. Any point source contribution above the dams was subtracted from fluvial loading. Further clarification would be useful to resolve the component of surface water that is groundwater in the freshwater reaches. This would provide a clearer understanding of the role of groundwater in nutrient loading to all waters, freshwater and saltwater. Atmospheric contribution is in the form of NOx deposition on the water surface (Mosher, 1995). Including groundwater, non-point sources represent 49% of the total estuarine nitrogen loading. Groundwater is 3% of the total loading and 5% (19 tons N/yr) of the total non-point sources (365 tons N/yr) (data revised from Langan, 2002).

Figure 22: Nitrogen Loading To The Great Bay Estuary; * Data revised from Langan 2002

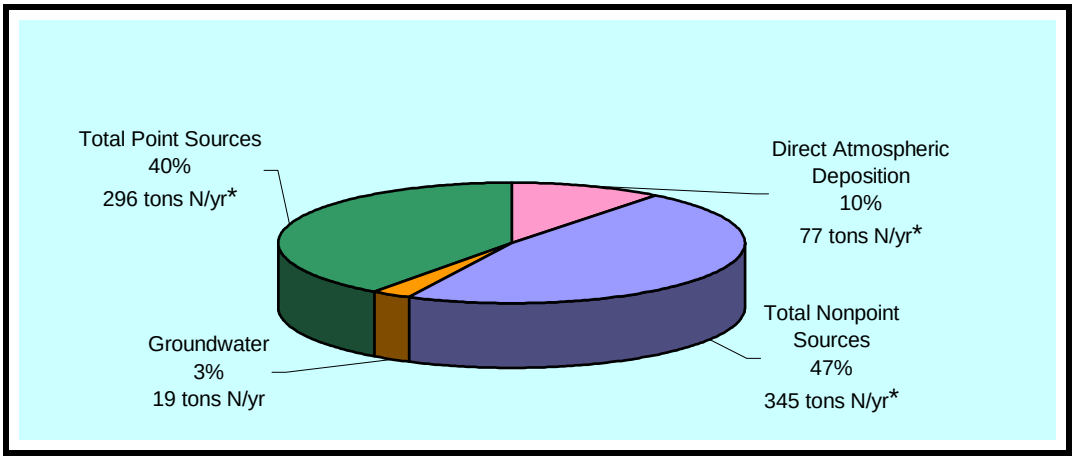

DISCUSSION

Quantification of groundwater discharge by the two methods (TIR and piezometric mapping) proved successful. The two methods used entirely different approaches yet resulted in similar flows. The TIR method is a direct measurement that is in contrast with the more common approach to predict groundwater flow rates using piezometric mapping and aquifer characterization. Remote sensing enabled a large-scale evaluation of discharge zones over a short period of time. The entire survey was performed in a few hours. Months of preparation and monitoring of environmental conditions ensured optimal survey conditions. The primary difficulties to obtaining accurate flow measurements via the TIR method were: 1) the complicated and slow GIS-based analysis of seepage face surface area, and 2) the nonuniformity within the discharge zones.

The use of TIR combined with GIS analysis and field techniques allowed for an expansion of capabilities for assessment of groundwater discharge in coastal waters. TIR is shown to be a powerful tool for delineation of groundwater discharge zones (Banks et al., 1996) however, it has not been used previously to quantify groundwater flow. GIS-based analysis of TIR enabled the assessment of the seepage face surface area which, when combined with specific discharge measurements, can be used quantitatively to assess flow. The primary difficulty preventing the use of GIS was distinguishing the seepage face from the resulting discharge plume, without which there is an overestimation of flow. The characteristic type curve provided a reliable method to estimate seepage face surface area.

While the type curve has been observed for 22 discharge zones, the determination of the seepage face has limited field verification (n=3). Preliminary results suggested that there is a high correlation between GIS-derived and field-derived surface areas (Table 6).

These conclusions will need to be rigorously tested with increased numbers of field observations.

One source of variability was due to the time lag between survey and field verification. These field verifications occurred around 18 months after the survey. Future efforts would ideally focus on examining the thermal signature either during the survey time or shortly thereafter. Logistically, this presents difficulties addressed either by multiple surveys or having some previous knowledge of a groundwater discharge zone. Multiple surveys can be difficult to coordinate within a short time frame because prime survey windows are limited by the need to coordinate maximum temperature gradient, low tide, clear sky, low wind, no (or low) moon, and darkness or high noon to minimize shadows. Performing field verifications within a short time after the surveys would rule out any seasonality or other influences that might cause variations in size or intensity of the SGDs. The importance of concurrent surveys and field verification presents logistical difficulties as surveys are ideally performed in the winter and fieldwork in the summer, as well as the additional time required for cataloguing SGD.

GIS Analysis Of TIR

The enormous efforts required for field characterization of groundwater discharge zones in coastal areas revealed the need for a GIS-based approach to determine the seepage face surface area. GIS analysis of TIR can be performed with relative ease compared to the actual field characterizations. Flow estimates for individual discharge zones were made using a GIS-derived surface area combined with the specific discharge obtained from the field. A standard problem in determining the surface area of the thermal signature was that the seepage face was indistinguishable from the resulting discharge plume because of similar thermal characteristics. The areas downgradient of a seepage face, but did not contribute to flow were covered with groundwater discharge, and shared a similar thermal signature as areas that contributed to flow. The overlapping seepage face and discharge plume were isolated and distinguished in the field, based primarily on hydrogeology and the presence of a piezometric gradient. GIS analysis of the TIR was easily performed, but without a readily definable seepage face may not reliably reflect field observations of surface area. Thus, a reliable methodology (e.g. type curve) for determining the surface area by GIS analysis was needed. The plot of the TIR image pixel data produced a reliable type curve that could be used to determine seepage face surface area. The qualitative visual cue provided by the type curve compared favorably with direct measurements obtained in the field.

One unfortunate deficiency in the use of the DTC was the variation in the grayscale from image to image. This is a characteristic of the imaging device. The imager has a self-adjusting contrast that is designed to account for variations in surface features. Unfortunately, this varying grayscale intensity resulted in an inconsistency from image to image. Because of this inconsistency, a single criterion cannot be used for multiple images, thereby preventing batch analyses. This is a common problem with various types of remote sensing. One advantage of thermal scanners is that they can be used to measure actual surface temperatures and have the potential for large-scale queries. These scanners have a consistent grayscale throughout the image, as the scanner builds it line by line, so the scanned image can be very large. The DTC, instead uses many smaller images, each

of which may vary slightly. DTCs, however, do not require the costly image post-processing to correct for image distortion.

Field Verification

The nonuniformity of the discharge zones presented a difficulty for determining specific discharge in the field. The discharge zones are often several thousand square feet and therefore it is unrealistic to assess flow throughout its entirety. To combat the variations, very large seepage meters (nearly 15 feet in diameter) were used for flow determination. The non-uniformity of piezometric gradient throughout a discharge zone was addressed by the use of a calibration factor for the flow matrix that corrected for the overestimation of flow (Figure 16). Point measurements of piezometric head were taken throughout a discharge zone to verify discharge flow and support the observation of varying intensity. These large-scale operations are perfectly suited for GIS application. The challenge then becomes the verification and calibration of the data.

Comparison of Methods: TIR and Piezometric Mapping

The two methods have shown good agreement. Hydraulic conductivity commonly varies over several orders of magnitude and the two estimates were less than an order of magnitude different. Typically, piezometric derived flow estimates are usually very general. Thermal infrared has the advantage that it can be used to identify exact locations of groundwater discharge, which in some cases behave as point sources. Other flow assessment methods assume uniform diffuse discharge. However areas with a diverse stratigraphy and/or bedrock influence can exhibit a combination of concentrated and diffuse discharge zones. The accuracy of estimates from piezometric mapping suffers with complex subsurface conditions or limited site characterizations. In these locations thermal imagery can be especially useful as a direct assessment of groundwater discharge, and may provide more reliable estimates. With the thermal imagery, groundwater discharge is evaluated directly, without the need to evaluate or address upgradient factors. This is an especially pertinent point as large-scale aquifer characterization is a major endeavor, not to mention installation and monitoring of wells. Direct measurements such as TIR obviate the need for upgradient characterization. Where zones of high nutrient loading or contamination are identified, then a detailed characterization of upgradient conditions or sources of contamination may ensue. The estimation of flow for individual discharge zones was shown to have good agreement (Table 6). The accuracy of flow estimations using the flow expression matrix is largely a function of the detail of study area characterization, as is true for any environmental assessment. The flow expression matrix provides a means to estimate large-scale SGD that can be tailored based upon demands for accuracy. These two methods provide a suite of resources with which to characterize groundwater discharge.

This is only speculation, but since the majority of SGD wass observed in the upper half of the tidal zone, it is likely that variations in flow due to tides are limited. It has been reported that for SGD in nearshore marine environments, the dominant influence is mostly upgradient flow, whereas in deeper marine locations, discharge is affected largely by tide and surge (Simmons Jr., 1992).

FLOW ESTIMATION VIA THERMAL IMAGERY METHOD

The use of thermal infrared imagery combined with GIS analysis and field techniques has expanded our capabilities to assess groundwater discharge to coastal waters. Thermal imagery has been shown to be a powerful tool for delineation of groundwater discharge zones (Banks, Paylor et al., 1996), however it has not been used, to date, in combination with field characterization to quantify groundwater flow. GIS-based analysis of TIR enabled the assessment of the seepage face surface area which, when combined with specific discharge measurements, can be used quantitatively to assess flow. The primary difficulty preventing the use of GIS was distinguishing the seepage face from the resulting discharge plume (Figure 6).

Field verification and GIS analysis of the type curve revealed characteristics of the type curve that were indicative of discharge zone conditions (Figure 8). The cusp at the transition between the two slopes, when bifurcated, the upper portion represented the discharge plume and the lower portion the transition to the perimeter of the discharge zone. The lower portion reflects the variation of piezometric head within the discharge zone. As is evident with the imagery, the greatest intensity is in the center, decreasing to no flow at the perimeter of the discharge plume.

While the existence of the type curve was observed for more than 15 discharge zones, the evaluation procedure of the seepage face area had limited field verification performed. Preliminary results suggest that there is a high correlation between GIS-derived and field-derived surface areas (). These implications will need to be rigorously tested with increased numbers of field observations.

Another weakness is the time lag between survey and field verification. These field verifications occurred approximately 18 months after the survey. The reason for the delay was that the need to separate the seepage face from the discharge zone was not immediately recognized. This need only became apparent after field investigations of GIS analyses. Future investigatory efforts would ideally focus on examining the thermal signature either during the survey time or shortly thereafter. Logistically this presents difficulties addressed either by multiple surveys or having some previous knowledge of a groundwater discharge zone. Multiple TIR surveys can be difficult to coordinate within a short time frame because prime survey windows are limited by the need to coordinate maximum temperature gradient, low tide, clear sky, no (or low) moon, calm wind, and darkness or high noon to minimize shadows. Performing field verifications within a short time after the surveys would rule out any seasonality or other influences that might cause variations in size or intensity.

Ongoing research will address the issue of seasonality in groundwater discharge through long-term monitoring of piezometric gradients (Brannaka et al., 2001). Future research efforts could focus on a laboratory-based analysis of the relationship of the thermal infrared signature, seepage face surface area, temperature gradient, and other factors. The hydrogeology could be controlled in a laboratory environment such that the seepage face surface area would be known and the use of the type curve could be tested.

The use of a combination of remote sensing and field techniques provides a useful and affordable tool for quantitative assessments of groundwater discharge. The use of remote sensing combined with GIS can save large amounts of time that would otherwise be required for field characterization of discharge zones. This was particularly useful for discharge zones over several thousand square feet. This same approach can be used to

assess large numbers of discharge zones over many miles of shoreline and minimize time intensive field characterizations. The crucial function is the determination of surface area for the thermal signature of the groundwater discharge zone. Preliminary results suggest that a standardized approach using a characteristic type curve can be used to generate the necessary criteria to determine the seepage face surface area. Ongoing research to automate the process of interpreting the thermal imagery may simplify this methodology additionally (Rubin and Roseen, 2001).

Groundwater and Water Quality Standards

Development of water quality standards from TMDLs for water bodies are continually evolving. TMDLs are typically based on four factors: bay volume, flushing time, and depth as well as water classification based on use and ecological significance. Waters are further classified as shallow if they have an average mean low water depth of less than 2 meters, or have 40% or more of the bottom less than 2 meters (Buzzards Bay Program, 1999). Much of the Great Bay would be classified as shallow waters by this method.

For comparative purposes, it is instructive to review water quality standards that were produced in 1994 for tidal water bodies by the town of Falmouth, MA. (Langan, 2002) Understanding that concentration based standards are unique and based on bay volume, flushing time, and depth, these standards are useful to compare with surface waters and groundwater for the Great Bay (Figure 23). Standards were intended to balance nutrient concentrations with ecological health, resource use (e.g. shellfishing, ecological significance), and nutrient disposal needs. The standards are (high to low) at 0.75, 0.5, 0.32 mg N/ L. None of the six tributaries of the Great Bay Estuary exceeded the upper limits, including the two largest sources, the Cocheco and Salmon Falls Rivers. Groundwater discharge at 0.81 mg N/L exceeded the highest standard. The distribution of SGD zones throughout the estuary may minimize any localized effects of nutrient contamination. Rather, it is the cumulative loading that need be considered in nutrient budgets. However, in instances where high groundwater concentrations were observed (8.2 mg N/L), increases in surface water nitrate concentrations of up to 20 times have been observed (Reay et al., 1992).

Figure 23: Comparison of Water Quality Standards From Falmouth, MA with Surface Water and Groundwater Concentrations of Nitrogen for the Great Bay Estuary (H=high, M=medium, L=low)

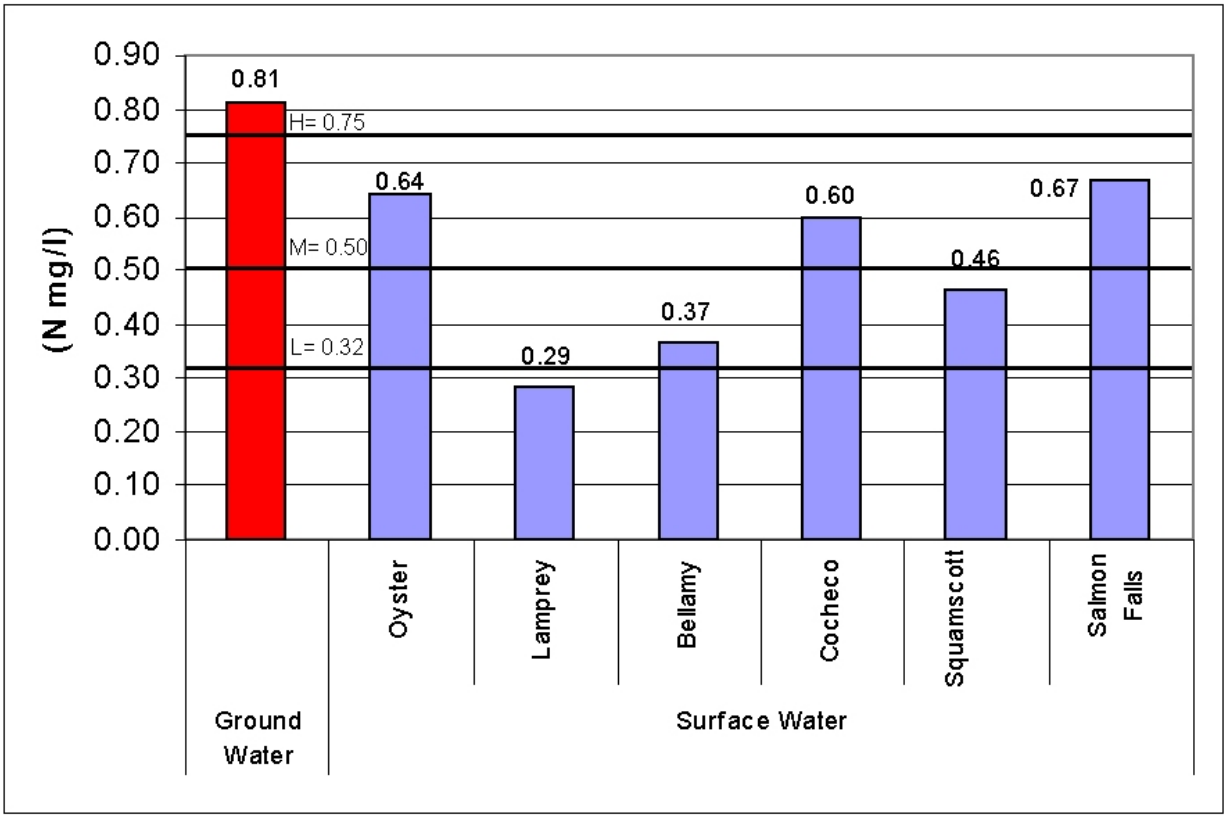

SUMMARY

The total SGD flow observed in the Great Bay, representing 2.5% of the total freshwater input (24.2 cubic feet per second estuary-wide), is lower than some reported values for other areas which showed as much as 40% of the total freshwater may be groundwater derived (Moore, 1996). The difference may be explained by variations in subsurface conditions and seasonal variations in flow.

Extreme seasonal variations in flow have been reported with as much as 5 times more in winter than in summer (Staver and Brinsfield, 1996), and conversely, 15 times greater in the summer than winter (Reay, 1992). In this study it is possible that SGD flow may be underestimated for some of these reasons. Future ongoing research will examine seasonal variations in SGD for the Great Bay and will help clarify flow and loading estimates. SGD loading was calculated to be 3% of the total nitrogen loading to the Great Bay Estuary and 5% of the non-point source load, or 19.3 ± 21.2 tons of N per year.

Perhaps more importantly, changes in land use, as they relate to groundwater nitrogen contamination, have a large potential for increasing the overall groundwater load.

The specific discharge values (4.4-175 GPD/ft^2) measured in this study are high compared to much of the published data for groundwater discharge in coastal environments (0.005-2.2 GPD/ft^2) (Table 2). This is a reflection of different subsurface environments that control whether discharge is concentrated or diffuse. It is also due to the measurement location of the seepage meters. Most of the previous studies examined SGD in shallow waters, rather than this study that analyzed SGD zones that were limited to the intertidal area. The newer ultrasonic seepage meters and the type used in this experiment only function while exposed in the intertidal areas.

The estimated flow and loading data suggested that groundwater is a potential significant source of nitrogen loading to coastal waters, and one that needs to be considered for calculation of TMDLs. Review of current groundwater nitrate concentrations with respect to growth in the seacoast region surrounding the Great Bay estuary is instructive. Rockingham county grew ~13% from 1990 to 2000 with many of the towns around the bay growing 20-25%. Rubin and Merriam (1998) reported that land use with the estuary indicated 38% of the abutting lands are undeveloped. Additional unsewered developments would add to the total loading. Much of the development in these areas is beyond the extent of the WWTFs suggesting that many will be on septic systems. Table 1 reviews groundwater nitrate concentrations from other locations that are in general much higher than what was observed in this study area. An increase in groundwater nitrate concentrations of three times (~3 mg N/L) would result in an annual loading of about 68 tons N to the estuary. This is on par with some of the largest sources. A study in a sewered housing development reported average increases of groundwater nitrate concentrations of 0.22 mg N/ L per year over an 8-year study, with concentrations having increased to an average of 3.3 mg N/L (Flipse et al., 1984). These rates did not include loading from septic systems but rather primarily from the household use of fertilizers. Areas without WWTFs would expect these rates to be even greater. Approximately 3 mg N/L was observed on Cape Cod in the Town of Orleans (Giblin and Gaines, 1990) in an area serviced by septic systems. The town is similar to many small towns in the Seacoast, NH and may be a reasonable indicator of potential development affects.

Another major factor to consider is the groundwater residence time. Currently, the residence time for groundwater is not well understood for the Great Bay. Lengthy residence times (10+ years) would indicate that currently observed contamination reflects historic activities and the current land use impacts are yet to be seen. At this point, we have not linked the groundwater discharge and nitrogen contamination with source waters, either bedrock waters or waters derived from unconfined formations. Detailed characterization of the flow properties and contributing areas, determination of groundwater residence time, and isotope sampling will be necessary to conclusively link groundwater discharge with source waters. This research is ongoing (Brannaka et al., 2001).

Ultimately, this study concludes that assessing groundwater discharge is important when determining a nutrient or contaminant budget. The USEPA has identified nonpoint sources such as underground storage tanks, septic systems, landfills, and agriculture practices as the primary sources of groundwater contamination. In areas were

these sources are prevalent, groundwater represents a potential source for contamination of coastal waters. Thermal infrared used in conjunction with field techniques is an effective tool for assessing groundwater interactions with coastal waters.

This research has shown that thermal imagery is an effective method for assessing groundwater discharge to coastal waters. It has facilitated the advance of thermal infrared imagery from strictly delineation applications to the quantitative assessment of groundwater flow.

The method development for analysis of groundwater discharge zones enabled the powerful application of GIS for spatial analysis. GIS-based analysis of TIR enabled the assessment of the seepage face surface area which, when combined with specific discharge measurements, can be used to quantitatively assess flow. The primary difficulty with the use of GIS was distinguishing the seepage face from the resulting discharge plume, which is necessary to prevent overestimation of the seepage face surface area and subsequent overestimation of flow. Analysis of the seepage face revealed a characteristic type curve that was used to determine surface area. Further investigation is still required to verify these results.

The use of the two concurrent methods has shown good agreement. Typically, flow estimates derived from piezometric mapping do not indicate specific discharge locations and can vary over several orders of magnitude (Freeze and Cherry, 1979). Thermal infrared has the advantage that it can be used to identify exact locations of groundwater discharge, which in some cases behave as point sources. Other flow assessment methods assume uniform diffuse discharge. However, areas with a diverse stratigraphy and/or bedrock influence can exhibit a combination of concentrated and diffuse discharge zones. This is true in inland or shallow estuaries where accumulation of marine clays occurs. The accuracy of estimates from piezometric mapping suffers in complex subsurface conditions or smaller site characterizations with greater spatial resolution. In these locations thermal imagery can be especially useful as a direct assessment of groundwater discharge, and may provide more reliable estimates. Direct measurements such as TIR obviate the need for costly upgradient characterization to determine flow. A detailed characterization of upgradient conditions or sources of contamination may be warranted where zones of high nutrient loading or contamination are identified.

The accuracy of flow estimations by matrix analyses is largely a function of the detail of the study area characterization, as is true for any environmental assessment. The flow expression matrix provides a means to estimate large-scale SGD that can be tailored based upon demands for accuracy.

The development of a detailed piezometric map for the Great Bay area will be useful for future research. This coverage provides a conceptual model which can be the basis for a groundwater model for this region. The location map of groundwater discharge zones will be further utilized by current and future research examining the impacts of land use upon down gradient water quality. Long-term monitoring of discharge zones is being discussed with the Great Bay Coast Watch, a volunteer organization organized to monitor water quality parameters throughout the estuary.

RECOMMENDATIONS FOR FUTURE RESEARCH

The methods reported here would be useful to include in an inter-comparisons study such as performed by the SCOR/LOICZ (Burnett, 2002) studies.

Exploration of the seepage face surface area relationship to the type curve is needed. Limited field verification has been performed. This is important because estimation of seepage face surface area based on the type curve is on a region of the curve (
Figure 10) in which exponential change is occurring. This results in extreme variation based on interpolation.

TIR can read surface temperatures directly (digital thermal cameras and scanners). There have been many studies in which scanners have been used for this purpose (Baskin, 1990, Banks et al, 1996, Mustard et al 1999, Campbell and Keith, 2001, Svejkovsky and Jones, 2002). Scanners, although they require immense corrective post-processing, produce a single large contiguous image that conceivably could be analyzed by the procedures detailed in Chapter 2, on a large scale. Our current approach is on an image-by-image basis. This is because of variations in grayscale from one image to the next. If this variation could be addressed, it would dramatically speed up image analysis. One possible approach would be to apply an algorithm to translate the current grayscale to a reference grayscale. This would apply uniformity to the images enabling batch analysis. Another possible approach would be to prevent grayscale variation altogether. The scanner continuously calibrates line by line to a fixed reference. The DTC calibrates image by image, with one image per 17 milliseconds, but rather DTCs calibrate to optimize sensitivity to the ground features, not a reference. This might be adjustable.

Long-term monitoring of water quality of groundwater discharge around the bay would be useful to identify the significance of land use impacts upon SGD. This needs to be further explored through examination of groundwater residence time. Use of isotope geochemistry and environmental tracers will be used to assess contaminant sources as well as travel time in ongoing research (Brannaka et al, 2001).

Long-term monitoring of SGD would provide useful information with respect to seasonal nutrient and contaminant fluxes. So called “snapshots” of SGD zones do not address this variability. Advances in automated monitoring of discharge zones have been made in recent years (Taniguchi and Fukuo, 1993, Paulsen et al, 1997) that can be used to address some of these issues. However in addition to variations in specific discharge, it is necessary to address variations in size of discharge zone. Regular periodic TIR surveys could address this.

TECHNOLOGY TRANSFER AND MANAGEMENT APPLICATION

There exists some real management potential for the thermal imagery method for estimating groundwater discharge. A current example is of a related research project entitled *Characterization of Groundwater Discharge to Hampton Harbor, New Hampshire,* funded by the New Hampshire Estuaries Project and the USEPA, 1/2002-1/2003. This project used the TIR method to characterize nutrient loading from groundwater. The method found no groundwater discharge in an intertidal environment dominated by salt marsh. The results of this research will be used for strategic planning on nutrient management.

Further efforts are being made for technology transfer through related research entitled *Development of GIS Application Extension for Use in Delineating Groundwater Discharge Zones* where resource managers at the National Estuarine Research Reserves and participants in the Protected Area GIS program will be provided with a package including a related instructional material covering the basic methodology in arranging for an aerial survey, how to analyze the data collected, field characterization procedures, and instructions on calculating contaminant loading. Additionally, the materials will cover event planning and environmental monitoring to optimize survey conditions. Finally, the materials will include lists of the necessary resources, both equipment and labor.

TECHNOLOGY COMMERCIALIZATION

No technology commercialization has come directly from this project. However a related project entitled *Development of GIS Application Extension for Use in Delineating Groundwater Discharge Zones* produced a freely available software extension for use with ArcView for delineating groundwater discharge zones. Discussions regarding commercialization of this product concluded small potential markets did not warrant commercialization.

Another potential product for commercialization is being considered with the development of an automatic seepage meter. Discussions with the Office of Intellectual Property are ongoing, and to date are inconclusive. Some thought is being given to pursuing further product development and commercialization. Like the previous item, market share is thought to be quite small.

SCIENTIFIC AND ACADEMIC ACHIEVEMENT

The products of this research include a doctoral dissertation, multiple publications in review, three related research projects, and numerous presentations at local and regional conferences.

The dissertation entitled *Quantifying Groundwater Discharge Using Thermal Imagery And Conventional Groundwater Exploration Techniques For Estimating The Nitrogen Loading To A Meso-Scale Inland Estuary* was completed by Robert M. Roseen in May of 2002 as part of a Doctorate in Civil Engineering specializing in water resources, at the University of New Hampshire.

Publications:

1. Roseen R.M., J. Degnan, L.K. Brannaka, T.P. Ballestero, T. Mack, *Approximate Potentiometric of the Bedrock Aquifer at Great Bay, Southeastern New Hampshire, 2001*. US Geological Survey Open File Report 03-278.
2. Roseen, R. M., L. K. Brannaka, T. P. Ballestero. *Thermal Imagery for Evaluating Coastal Groundwater Discharge and Its Significance in Nutrient TMDLs* (In review, submitted 5/02 to Biogeochemistry)
3. Roseen, R. M., L. K. Brannaka, T. P. Ballestero. *Thermal Imagery Vs. Piezometric Mapping For Assessing Ground Water Discharge To Coastal Waters* (In review, submitted 6/02 to Ground Water)
4. (In preparation) Roseen, R. M., L. K. Brannaka, T. P. Ballestero. *GIS-Based Analysis of Thermal Imagery for Use in Characterizing Groundwater Discharge Zones in Coastal Waters.* Anticipated submission to Photogrammetric Engineering and Remote Sensing in Winter 2003.

Selected Presentations:

1. (Invited)Roseen, R. M, T.P. Ballestero, G. Bacca-Cortez, L.K. Brannaka, *A Review of Methods and Limitations on the Use of Thermal Infrared Imagery for the Assessment of Inter-Tidal Groundwater Discharge,* presented in 12/2003 at the National Groundwater Association Convention, Orlando, Fl.
2. Roseen, R. M, T.P. Ballestero, G. Bacca-Cortez, W.G. McDowell, *Examination of Inter-Tidal Groundwater Discharge in a Salt Marsh Ecosystem, Hampton Harbor, NH,* presented at the New Hampshire Estuaries Project State of the Estuaries Conference, 10/2003.
3. Roseen, R. M, T.P. Ballestero, G. Bacca-Cortez, L.K. Brannaka, *Limitations of the Use of Thermal Infrared Imagery for the Assessment of Inter-Tidal Groundwater Discharge based on Land Use, Land Cover, and Hydrogeology*, presented at the *Technology Transfer Conference,* Emerging Technologies, Tools, and Techniques, USEPA Office of Water, Office of Wetlands, Oceans, and Watersheds, Oceans and Coastal Protection Division, 2/2002.
4. Roseen, R. M, T.P. Ballestero, L.K. Brannaka. Platform presentation on Methodology Verification for Assessing Groundwater Discharge to Coastal Waters, Geological Society of America, Boston, Massachusetts. Fall 2001Roseen, R. M, T.P. Ballestero, L.K. Brannaka. Poster presentation on Determination Of Nutrient Loading From Groundwater Discharge Into An Inland Estuary Using Airborne Thermal Imagery, Coastal Zone 2001, NOAA, Cleveland Ohio. Summer 2001.
6. Roseen, R. M, T.P. Ballestero, L.K. Brannaka. Platform presentation on *Thermal Imagery and Field Techniques to Evaluate Groundwater Nutrient Loading to an Estuary,* American Geophysical Union, Boston, MA. Spring 2001.

Related Research Projects:

1. *Land Use Influence on the Characteristics of Groundwater Input to the Great Bay Estuary, New Hampshire*, University of New Hampshire, The Cooperative Institute for Coastal and Estuarine Environmental Technology, 8/2001-9/2004.

2. *Characterization of Groundwater Discharge to Hampton Harbor, New Hampshire,* In Cooperation with the New Hampshire Estuaries Project and the USEPA, 1/2002-1/2003.
3. *Development of GIS Application Extension for Use in Delineating Groundwater Discharge Zones,* The Cooperative Institute for Coastal and Estuarine Environmental Technology, 8/2001-9/2002.

ACKNOWLEDGMENTS

Funds for this research were provided by the Cooperative Institute for Coastal and Estuarine Environmental Technology (CICEET), in cooperation with the National Oceanic and Atmospheric Administration (NOAA).

We would like to thank the private homeowners who volunteered the use of their wells for development of the groundwater map. This involved a good deal of trust to allow researchers to use their drinking water wells. Their names are too many to include here and are listed in Appendix A.

This large project is the result of work from many people whose efforts included surveying, field investigating, database design, sampling, data analysis, mapping, imagery analysis, organization and more organization, and last but certainly not least help with taking care of my son Miles. I apologize to those that are not mentioned here.

We would like to thank Fay Rubin, Jen Merriam, Anne Deeley of the Complex Systems Resource Center at the University of New Hampshire for facilitating use of imaging software, and for providing work space and technical assistance. I would especially like to thank Fay for her technical assistance with the use of Arc View; she could turn a day long project into 30 minutes.

We would like to thank Dave Shay and Deborah Lamson of the Jackson Estuarine Lab for their assistance with the use of boats and their insight as to navigation around the Great Bay. They were especially tolerant of our project which had many unusual requirements including taking the boats out off-season and after hours.

We would like to thank Melinda “The Feet” Bubier for her assistance on nearly every aspect of this project including endless hot and cold days on the bay investigating groundwater discharge zones. Also notably, she was instrumental in the early success of the project by managing the well survey efforts and database design, which at many points was very overwhelming. I enjoyed her friendship.

We would like to thank Ryan “Shaggy” McCarthy for his assistance on nearly every aspect of this project. Most notably Shaggy’s efforts in field characterization and familiarity with this large complex project were extremely useful.

We would like to thank Billy McDowell for his assistance in developing the analytical method for seepage face determination. Billy’s assistance and persistence was instrumental in investigating the seepage face type curve. Also notably, Billy was incredibly reliable with the enormous well survey database and required data transcription for hundreds of survey loops.

For the many hours and days of hot and cold field work, which generally did not stop throughout the year, I would like to thank Jason Clark, Chris MacDonald, Britt

Eckstrom, John Richardson, Derek Robinson, Tara Farnsworth, Monica Peters, Kathleen Cairns, Steve Lopez, Ying Shi, and Joel Ballestero and co-conspirator Tory.

We would like to thank Bob Moynihan for his patience and training in the use of surveying and GPS equipment. His assistance was vital in the success of the groundwater mapping project.

We would like to thank Peter Wellenberger at the New Hampshire Department of Fish and Game for his assistance in the use and installation of monitoring wells around the bay.

We would like to thank Jim Degnan and Tom Mack of the US Geological Survey for their efforts in aquifer geophysical analyses. I would especially like to thank Jim for his help with the depth to water monitoring and RTK surveying events.

We would like to thank Dr. William McDowell and Jeff Merriam of The Water Quality Analysis Laboratory at the University of New Hampshire for the sample analyses and their help in QA/QC.

.

REFERENCES

1. Avanzino, R. J. and V. C. Kennedy (1993). "Long-Term Frozen Storage Of Stream Water Samples For Dissolved Orthophosphate, Nitrate Plus Nitrite, And Ammonia Analysis." Water Resources Research 29: 3357-3362.

2. Ballestero, T. P. and R. M. Roseen (2002). *Characterization of Groundwater to Hampton Harbor, New Hampshire,* Funded by The New Hampshire Estuaries Project, Portsmouth, New Hampshire.

3. Banks, W., R. Paylor and W. Hughes (1996). "Using Thermal Infrared Imagery to Delineate Groundwater Discharge." Groundwater 34: 434-444.

4. Baskin, R. L. (1990). Determination Of Ground-Water Inflow Locations In Great Salt Lake, Utah, Using The Thermal Infrared Multispectral Scanner. Masters Thesis, Department of Geography, University of Utah.

5. BBP (1999). New Nitrogen Loading Standards Proposed by the BBP, http://www.buzzardsbay.org/nitrmang/nitrmangfact.htm, Buzzard Bay Project.

6. Bokuniewicz, H. (1980). "Groundwater Seepage into Great South Bay, New York." Estuarine and Coastal Marine Science 10: 437-444.

7. Brannaka, L. K., T. P. Ballestero and R. M. Roseen (2001). *Land Use Influence on the Characteristics of Groundwater Inputs to the Great Bay Estuary, New Hampshire*., Cooperative Institute for Coastal and Estuarine Environmental Technology, Durham, New Hampshire.

8. Bricker, S. B., C. Clement, D. Pirhalla, S. Orlando and D. Farrow (1999). National Estuarine Eutrophication Assessment: Effects Of Nutrient Enrichment In The Nation's Estuaries, Special Projects Office And National Centers For Coastal Ocean Science, National Oceanic And Atmospheric Administration.

9. Brown, W. S. and E. Arrelano (1979). The Application Of A Segmented Tidal Mixing Model To The Great Bay Estuary, N.H., U.N.H. Sea Grant Tech. Rep., UNH-SG-162. University of New Hampshire, Durham.

10. Burnett, W. (1999). Offshore springs and seeps are focus of working group. EOS. **80:** 13-15.

11. Burnett, W. (2002). "SCOR/LOICZ Group Conducts Assessment of Methodologies for Measurement of Groundwater Discharge to the Ocean." Submitted to EOS.

12. Burnett, W. C., G. Kim and D. Lane-Smith (2001). " A continuous radon monitor for use in coastal ocean waters." Jour. Radioanalytical. Nuclear. Chemistry 249: 167-172.

13. Campbell, C. W. and A. G. Keith (2001). "Karst Ground-Water Hydrologic Analyses Based On Aerial Thermography." Hydrological Science and Technology. 17(Special Issue).

14. Flipse, W. J., B. G. Katz, J. B. Linder and R. Markel (1984). "Sources Of Nitrate In Groundwater In A Sewered Housing Development, Central Long Island, New York." Ground Water 22(418-426).

15. Freeze, R. A. and J. A. Cherry (1979). Groundwater, Prentice-Hall, New Jersey.
16. Giblin, A. E. and A. G. Gaines (1990). "Nitrogen Inputs To A Marine Embayment: The Importance Of Groundwater." Biogeochemistry(10): 309-328.

17. Hay, E. A. (1984). "Remote Acoustic Imaging of a Plume from a Submarine Spring in an Artic Fjord." Science **225**: 1154-1156.

18. Hillel, D. (1982). Introduction to Soil Physics, Academic Press, San Diego, CA.Johannes, R. E. (1980). "The Ecological Significance Of The Submarine Discharge Of Groundwater." Marine Ecology Progress Series 3: 365-373.

19. Johannes, R. E. and C. J. Hearn (1985). "The Effect of Submarine Groundwater Discharge on Nutrient and Salinity Regimes in a Coastal Lagoon off Perth, Western Australia." Estuarine, Coastal and Shelf Science 21: 789-800.

20. Jones, S. H., Ed. (2000). A Technical Characterization Of Estuarine And Coastal New Hampshire., New Hampshire Estuaries Project, Portsmouth, NH.

21. Jones, S. H. and R. Langan (1994). Land Use Impacts On Non-Point Source Pollution In Coastal New Hampshire, Final Report. NH Office of State Planning/ Coastal Program, Concord, NH.

22. Kay, A. E., L. S. Lau, E. D. Stroup, S. J. Dollar, D. P. Fellows and R. H. Young (1977). Hydrological and Ecological Inventories of the Coastal Waters of West Hawaii, University of Hawaii, Water Resources Research Center Technical Report 105.

23. Kruseman, G. P. and N. A. deRidder (1994). Analysis and Evalautation of Pumping Test Data, International Institute for Land Reclamation and Improvement.

24. Langan, R. (2002). Inorganic and Organic Nutrients. A Technical Characterization Of Estuarine And Coastal New Hampshire. S. H. Jones, Ed., New Hampshire Estuaries Project, Portsmouth, NH.

25. Lee, R., David (1977). "A device for measuring seepage flux in lakes and estuaries." Limnology and Oceanography 22(1): 140-147.

26. Loder, T.C., J.E. Hislop, J.P. Kim, and G.M. Smith (1976). Nutrient And Hydrographic Data For Rivers Flowing Into The Great Bay Estuary System, New Hampshire. University Of New Hampshire Sea Grant Publication, UNH-SG-161, Durham, 47pp.

27. Lyons, J. B., W. A. Bothner, R. H. Moench and J. B. Thompson. (1997). Bedrock Geologic Map Of New Hampshire, U.S. Geological Survey, Reston, VA.

28. Marsh, J. A. J. (1977). Terrestrial Inputs of Nitrogen and Phosphorous on Fringing Reefs in Guam. Proceedings from 2nd International Coral Reef Symposium, Great Barrier Reef Committee, Brisbane, Australia.

29. Marshall, T. J. and J. W. Holmes (1988). Soil Physics. 2nd ed., Cambridge Univ. Press, New York.Mitnick, P. (1994). Salmon River Waste Load Allocation, Maine DEP, Bureau of Land and Water Quality, Augusta, ME.

30. Moore, R. B. (1990). Geohydrology and water quality of stratified-drift aquifers in the Exeter, Lamprey, and Oyster river basins, southeastern New Hampshire, USGS Open File Report 88-4128.

31. Moore, S. W. (1996). "Large groundwater inputs to coastal waters revealed by Ra enrichments." Nature 380: 612-614.

32. Moore, W. S. (2000). "Determining coastal mixing rates using radium isotopes." Continental and Shelf Resources 20: 1993-2007.

33. Mosher, B. W. (1995). Assessment Of Atmospheric Non-Point Source Nitrogen Input To The Great Bay Watershed And Estuary. Final Report. NH Office of State Planning/Coastal Program,, Concord, NH.

34. Mustard, J. F., M. A. Carney and A. Sen (1999). "The Use of Satellite Data to Quantify Thermal Impacts." Estuarine, Coastal and Shelf Science 9: 509-524.

35. Novotony, R. F. (1969). The Geology of the Seacoast Region, New Hampshire, Department of Resources and Economic Development. Concord, New Hampshire.

36. Paulsen, R. J., C. F. Smith and T. F. Wong (1997). Development And Evaluation Of An Ultrasonic Groundwater Seepage Meter, Geology of Long Island and Metropolitan New York.

37. Reay, W., G., D. Gallagher, L and G. Simmons, M Jr. (1992). "Groundwater Discharge And Its Impacts On Surface Water Quality In A Chesapeake Bay Inlet." Water Resources Bulletin 28(6): 1121-1134.

38. Rubin, F. and J. Merriam (1998). Critical Lands Analysis. Final Report., N.H. Office of State Planning/Estuaries Project, Concord, NH.

39. Rubin, F. and R. M. Roseen (2001). Project entitled *Development of GIS Application Extension for Use in Delineating Groundwater Discharge Zones*, The Cooperative Institute for Coastal and Estuarine Environmental Technology, Durham, New Hampshire.

40. Saltman, T. (2001). "Making TMDLs Work." Environmental Science and Technology 35(11): 248a-254a.

41. Sewell, P. L. (1982). "Urban Groundwater As A Possible Nutrient Source For An Estuarine Benthic Algal Bloom." Estuarine, Coastal And Shelf Science 15: 569-576.

42. Shaw, D. R. and E. E. Prepas (1989). "Anomalous, Short-Term Influx Of Water Into Seepage Meters." Limnol. Oceanogr 34(7): 1343-1351.

43. Simmons Jr., G. M. (1992). "Importance Of Submarine Groundwater Discharge And Seawater Cycling To Material Flux Across Sediment/Water Interfaces In Marine Environments." Marine Ecology Progress Series 84: 173-184.

44. Staver, K. W. and R. B. Brinsfield (1996). "Seepage of Groundwater Nitrate from a Riparian Agroecosystem into the Wye River Estuary." Estuaries 19(2B): 3599-370.

45. Svejkovsky, J. and B. Jones (2002). "Satellite Imagery Detects Coastal Storm Water And Sewage Runoff." EOS 82(50).

46. Taniguchi, M. and Y. Fukuo (1993). "Continuous Measurements Of Ground-Water Seepage Using An Automatic Seepage Meter." Ground Water 31(4): 675-679.

47. USEPA (1998). New Hampshire List of Impaired Waters for 1998, http://www.epa.gov/OWOW/tmdl/states/nhtmdltables.html, United States Environmental Protection Agency, Office of Water, Washington DC.

48. USEPA (2000). National Water Quality Inventory: 1998 Report to Congress, US. Environmental Protection Agency, Office of Water,, Washington, D.C.

49. US Geological Survey (2002). National Water Information System, http://water.usgs.gov/usa/nwis/help/?redirect=nwis_w_redirect.

50. Valiela, I., J. M. Teal, S. Volkmann, D. Shafer and E. J. Carpenter (1978). "Nutrient Particulate Fluxes in a Salt Marsh Ecosystem: Tidal Exchanges and Inputs by Precipitation and Groundwater." Limnology and Oceanography **23**: 798-812.

51. Webb, K. (1980). Personal communication with Johannes 1980.

52. Weston, R. F. I. (1993). Pease Air Force Base Site 32/36 Feasibility Study Report. Revised Final Draft., HG Air Force Base Disposal Agency. Washington D.C.

53. Whittemore, R., G. Ice. 2001. "TMDL at the Crossroads". Environmental Science and Technology 35(11):249a-255a

54. Wu, J. and D. L. Nofziger (1999). "Incorporating Temperature Effects On Pesticide Degradation Into A Management Model." Journal of Environmental Quality **28**: 92-100.

APPENDIX A

MONITORING WELL DATABASE: PARTICIPANT HOMEOWNERS

#	Well#	First Name	Last Name	St# or Station ID	Road	Town
1	359	Alice	Drake	11	Bay View Rd	Dover
2	139	Susan	Blumenthal	63	Bay View Rd	Dover
3	1114	Terry	Shepperd	45	Drew Rd	Dover
4	1110	Katherine	Shea	65	Drew Rd	Dover
5	368	Elizabeth	Dunn	123	Drew Rd	Dover
6	1160	Sharon	Spickler	5	Gold Post Rd	Dover
7	1095	Robert	Schneider	314	Old Garrison Rd	Dover
8	478	Helen	Gingras	6	Piscataqua Rd	Dover
9	941	Michael	Patterson	14	Piscataqua Rd	Dover
10	755	Richard & Stephanie	Lund	38	Piscataqua Rd	Dover
11	309	Dorothy	Dagle	58	Piscataqua Rd	Dover
12	140	Paul	Bolduc	60	Piscataqua Rd	Dover
13	520	Francis	Hallhan	63	Piscataqua Rd	Dover
14	821	Kathleen	Mcshera	72	Piscataqua Rd	Dover
15	1063	Walter	Rous	64	Adams Point Rd	Durham
16	658	Kennett	Kendall	395	Bay Rd	Durham
17	404	Steven	Fellows	426	Bay Rd	Durham
18	429	Daniel	Ford	433	Bay Rd	Durham
19	162	Gerhard	Brand	561	Bay Rd	Durham
20	161	Frederick	Bramante Jr	587	Bay Rd	Durham
21	797	Paul & Marilyn	Mayewski	591	Bay Rd	Durham
22	797A	Paul & Marilyn	Mayewski	593	Bay Rd	Durham
23	452	Richard	Gallant	594	Bay Rd	Durham
24	1041	Lois	Roberts	6	Cedar Point Rd	Durham
25	1276	Stephen	Weglarz Jr	19	Cedar Point Rd	Durham
26	964	Arthur	Pierce	24	Colony Cove Rd	Durham
27	81	Christopher	Auty	32	Colony Cove Rd	Durham
28	583	Lee	Hodsdon	114	Dame Rd	Durham
29	946	Michael	Pazobn	163	Dame Rd	Durham
30	1073	Barry	Ryan	321	Dame Rd	Durham
31	820A	Pamela	Mcphee	340	Dame Rd	Durham
32	820	Pamela	Mcphee	342	Dame Rd	Durham
33	862	Gregory	Moore	343	Dame Rd	Durham
34	1094	Susan	Schettini	351	Dame Rd	Durham
35	978	Robert & Laura	Potter	1	Deer Meadow Rd	Durham
36	449	Barry	Fussell	3	Deer Meadow Rd	Durham
37	1158	Kathleen	Sparr	5	Deer Meadow Rd	Durham
38	1140	Edson	Smith	10	Deer Meadow Rd	Durham
39	116	Ray	Belles	14	Deer Meadow Rd	Durham
40	1237	Garrison	Valentine	17	Deer Meadow Rd	Durham
41	1268	K.	Warren	19	Deer Meadow Rd	Durham
42	1002	Stephen	Ransom	22	Deer Meadow Rd	Durham
43	504	Fred & Shirley	Greenberg	59	Durham Point Rd	Durham
44	1231	John	Tucker	139	Durham Point Rd	Durham
45	480	Philip	Ginsburg	151	Durham Point Rd	Durham

#	Well#	First Name	Last Name	St# or Station ID	Road	Town
46	346	Lewis	Ditommaso	255	Durham Point Rd	Durham
47	228	Malcolm	Chase	273	Durham Point Rd	Durham
48	1239	Ann	Valpey	277	Durham Point Rd	Durham
49	1400	Sheryl	Hoffman	300	Durham Point Rd	Durham
50	863	Kenneth	Moore	305	Durham Point Rd	Durham
51	352	Mark & Tracey	Donaldson	7	Edgerly Garrison Rd	Durham
52	264	Richard	Collopy	8	Frost Dr	Durham
53	775	Cordelia	Marche	13	Frost Dr	Durham
54	1169	Jane	Stark	66	Long Marsh Dr	Durham
55	1061	Gina	Ross	86	Long Marsh Dr	Durham
56	875	Basil	Mott	8	Mathes Cove Rd	Durham
57	1193	James	Swisher	9	Mathes Cove Rd	Durham
58	351	Donald	Mcnamara	16	Mathes Cove Rd	Durham
59	6	Paul	Blackardar	13	Morgan Way	Durham
60	710	David & Lori	Larson	6	Pinecrest Lane	Durham
61	793	Dale & Laura	Matheny	21	Pinecrest Lane	Durham
62	578	Bruce & Aggy	Hird	33	Pinecrest Lane	Durham
63	1189	Larry	Swanson	34	Pinecrest Lane	Durham
64	1221	Elizabeth	Towle	75	Piscataqua Rd	Durham
65	1204	George	Thomas	77	Piscataqua Rd	Durham
66	271	Timothy	Connifey	79	Piscataqua Rd	Durham
67	635	Philip	Johnson	190	Piscataqua Rd	Durham
68	382	Dale	Eichorn	196	Piscataqua Rd	Durham
69	206	Johonet	Carpenter	4	Riverview Court	Durham
70	355	Sean	Doody	1	Riverview Rd	Durham
71	177	Walter	Buckley	20	Riverview Rd	Durham
72	199	Lionel	Carbonneau	21	Riverview Rd	Durham
73	1134	Julius	Slutzky	23	Riverview Rd	Durham
74	505	Stephen	Greiner	2	Shearwater St	Durham
75	1192	Dan	Swift	17	Sunnyside Rd	Durham
76	718	Sandra	Leathe	3	Tirrell Place	Durham
77	528	Keith	Haney	4	Tirrell Place	Durham
78	789	Russell	Mason	7	Tirrell Place	Durham
79	194	Anne	Moher	15	Watson Rd	Durham
80	1340	Jamos	Zieggra	31	Watson Rd	Durham
81	1191	David	Swenson	3	Williams Way	Durham
82	1242	Johannes	Vanhoorn	4	Williams Way	Durham
83	416	Jay	Flanders	9	Williams Way	Durham
84	1401		Adams Point		WMR MW Well	Durham
85	154	Anthony	Brackett	4	Bay Ridge Rd	Greenland
86	1179	John	Strebel	12	Bay Ridge Rd	Greenland
87	196	Victoria	Canner	18	Bay Ridge Rd	Greenland
88	1250	Stephen	Vickery	24	Bay Ridge Rd	Greenland
89	433	Richard	Fralick	29	Bay Ridge Rd	Greenland
90	860	Roger	Mooers	10	Bay Shore Dr	Greenland

#	Well#	First Name	Last Name	St# or Station ID	Road	Town
91	1270	Mark	Weaver	12	Bay Shore Dr	Greenland
92	171	Ronald	Brouillette	17	Bay Shore Dr	Greenland
93	555	Nathan	Hazen	18	Bay Shore Dr	Greenland
94	1230	A-Ha	Trust	23	Bay Shore Dr	Greenland
95	1083	Lisa	Sanderson	33	Bayside Rd	Greenland
96	1283	Michael	Whalen	95	Bayside Rd	Greenland
97	550	George & Muriel	Hayden	121	Bayside Rd	Greenland
98	273	Mary	Connor	161	Bayside Rd	Greenland
99	774	Dennis	Marasco	292	Bayside Rd	Greenland
100	306	Jeffrey	Cutter	295	Bayside Rd	Greenland
101	796	Fredrick & Lisa	Mauer	4	Caswell Dr.	Greenland
102	1084	Carol	Sanderson	58	Caswell Dr.	Greenland
103	477	Richard	Gilstan	3	Cortland Dr	Greenland
104	665	Gerald	Keto	12	Cortland Dr	Greenland
105	652	David & Carrie	Kayarian	26	Dearborn Rd	Greenland
106	836	Barrt	Metcalf	250	Dearborn Rd	Greenland
107	1035	George	Rickley	24	Great Bay Dr East	Greenland
108	1206	Jo Ellen	Thomas	33	Great Bay Dr East	Greenland
109	1013	Thomas	Reilly	56	Great Bay Dr East	Greenland
110	517	David	Hagner	57	Great Bay Dr West	Greenland
111	957	Dennis & Beverly	Perriccio	126	Great Bay Rd	Greenland
112	338	Richard	Desrosiers	178	Great Bay Rd	Greenland
113	122	Louise	Bergeran	338	Great Bay Rd	Greenland
114	455	Robert	Garcia	408	Great Bay Rd	Greenland
115	812	Kenneth	Mcgillvary	8	Mcintosh Way	Greenland
116	294	Tabita	Cronin	17	Mcintosh Way	Greenland
117	1246	Dennis & Marilyn	Varney	8	Melloon Rd	Greenland
118	441	Rolff	French	1	Orchard Hill Rd	Greenland
119	1036	Judith	Lierna	3	Orchard Hill Rd	Greenland
120	716	John	Leach	10	Orchard Hill Rd	Greenland
121	723	Craig	Leffingwell	26	Orchard Hill Rd	Greenland
122	1262	Linda	Walsh	40	Orchard Hill Rd	Greenland
123	1200	Anne	Taylor	18	Tidewater Farm Rd	Greenland
124	45	T.	Adams	27	Tidewater Farm Rd	Greenland
125	598	June	Hulbert	31	Tidewater Farm Rd	Greenland
126	561	Peggy	Heidt	35	Tidewater Farm Rd	Greenland
127	660	James	Kenny	49	Tidewater Farm Rd	Greenland
128	1331	Kristine	Yanofsty	85	Tidewater Farm Rd	Greenland
129	1402	Bracketts Point				Greenland
130	159	William	Bragg	24	Main Street	Newfields
131	623	Tripp	Jean	3	Rte 108	Newfields
132				615	Pease AFB	Newington
133				6013	Pease AFB	Newington
134				603	Pease AFB	Newington
135				6034	Pease AFB	Newington

#	Well#	First Name	Last Name	St# or Station ID	Road	Town
136				6035	Pease AFB	Newington
137				6043	Pease AFB	Newington
138				6044	Pease AFB	Newington
139				6046	Pease AFB	Newington
140				6047	Pease AFB	Newington
141				6048	Pease AFB	Newington
142				6049	Pease AFB	Newington
143				6050	Pease AFB	Newington
144				6051	Pease AFB	Newington
145				6083	Pease AFB	Newington
146				6098	Pease AFB	Newington
147				6099	Pease AFB	Newington
148				610	Pease AFB	Newington
149				6103	Pease AFB	Newington
150				6106	Pease AFB	Newington
151				6107	Pease AFB	Newington
152				6108	Pease AFB	Newington
153				6109	Pease AFB	Newington
154				6110	Pease AFB	Newington
155				6111	Pease AFB	Newington
156				6112	Pease AFB	Newington
157				6113	Pease AFB	Newington
158				6114	Pease AFB	Newington
159				6121	Pease AFB	Newington
160				614	Pease AFB	Newington
161				615	Pease AFB	Newington
162				618	Pease AFB	Newington
163				620	Pease AFB	Newington
164				621	Pease AFB	Newington
165				6506	Pease AFB	Newington
166				6507	Pease AFB	Newington
167	1403	Fabyan Pt	Drilled Well			Newington
168	1404	Fabyan Pt	Dug Well			Newington
169	1405		NWR Well			Newington
170	298	Ronald	Crowley	165	Ash Swamp Rd	Newmarket
171	485	Robert	Godfrey Jr.	257	Ash Swamp Rd	Newmarket
172	1067	Theresa	Roy	74	Bay Rd	Newmarket
173	687	Joseph	Kruczek	110	Bay Rd	Newmarket
174	421	Alexsandra	Fleszar	113	Bay Rd	Newmarket
175	421A	Alexsandra	Fleszar	113	Bay Rd	Newmarket
176	1145	Dickson	Smith	211	Bay Rd	Newmarket
177	1157	Terrance	Spande	3	Cushing Rd	Newmarket
178	991	Alfred	Puchlopek	5	Cushing Rd	Newmarket
179	627	Lynn	Jennings	17	Cushing Rd	Newmarket
180	765	Marshall	Magee	3	Moody Point Dr	Newmarket

#	Well#	First Name	Last Name	St# or Station ID	Road	Town
181	1328	Daniel	Wright	5	Moody Point Rd	Newmarket
182	28	John	Sawyer	83	New Rd	Newmarket
183	278	David	Copestakes	85	New Rd	Newmarket
184	358	Robert	Downing	89	New Rd	Newmarket
185	525	Albert	Hamel	165	New Rd	Newmarket
186	312	Herbert	Dalaymple	179	New Rd	Newmarket
188	1247	Claudia	Vatcher	184	New Rd	Newmarket
187	1247	Claudia	Vatcher	184	New Rd	Newmarket
189	119	D.	Bender	10	Shady Ln	Newmarket
190	344	Paul	Dietterlb III	4	Smith Garrison	Newmarket
191	48	John	Ahlgren	50	Smith Garrison	Newmarket
192	902	Eugene	Novak	16	Smith Garrison Rd	Newmarket
193	356	William	Doucet	25	Smith Garrison Rd	Newmarket
194	1148	Sarah	Smith	31	Smith Garrison Rd	Newmarket
195	1055	William	Rogers	38	Smith Garrison Rd	Newmarket
196	134	David	Bird	42	Smith Garrison Rd	Newmarket
197	191	Robert	Calef	3	Benjamin Rd	Stratham
198	791	Joseph	Mastin	5	Benjamin Rd	Stratham
199	886	Thomas	Muse	15	Benjamin Rd	Stratham
200	1039	Judith	Rivais	17	Benjamin Rd	Stratham
201	986	Gary	Prince	19	Benjamin Rd	Stratham
202	1298	Roger	Wilkinson	22	Benjamin Rd	Stratham
203	558	Jeffery & Linda	Hebert	26	Benjamin Rd	Stratham
204	40	R.	Abounudja	38	College Rd	Stratham
205	1159	Gertrude	Spencer	8	Crestview Terr	Stratham
206	30	George	Miller	9	Crestview Terr	Stratham
207	803	Mark	Mccleary	11	Crestview Terr	Stratham
208	825	Donald	Meeves	18	Crestview Terr	Stratham
209	638	William	Johnstone	29	Crestview Terr	Stratham
210	940	David	Paterson	30	Crestview Terr	Stratham
211	244	William	Clapp	31	Crestview Terr	Stratham
212	816	Wendy	Mckeon	16	Depot Rd	Stratham
213	1009	Stephen & Anne	Reichert	18	Depot Rd	Stratham
214	265	William	Columbia	32	Depot Rd	Stratham
216	650	Robert	Kart	38	Depot Rd	Stratham
215	650	Robert	Kart	38	Depot Rd	Stratham
217	1011	Robert	Reid	53	Depot Rd	Stratham
218	470	Edward	Geppner	1	Dumbarton Oaks	Stratham
219	88	Richard	Ballantyne	12	Dumbarton Oaks	Stratham
220	643	Scott	Joy	14	Dumbarton Oaks	Stratham
221	591	Joanne	Odence-Flackett	21	Dumbarton Oaks	Stratham
222	59	Ray	Ames	54	Dumbarton Oaks	Stratham
223	636	Rogers	Johnson	55	Dumbarton Oaks	Stratham
224	523	Giles & Lissa	Ham	58	Dumbarton Oaks	Stratham
225	1267	Richard	Warren	60	Dumbarton Oaks	Stratham

#	Well#	First Name	Last Name	St# or Station ID	Road	Town
226	668	Jeffrey	Kimball	66	Dumbarton Oaks	Stratham
227	1064	Kenneth	Rowe	5	French Ln	Stratham
228	679	Ian	Know	16	Sandy Point Rd	Stratham
229	1076	John	Sable	11	Squamscott Rd	Stratham
230	1336	Scott	Zeller	91	Tidewater Farm Rd	Stratham
231	955	Mr./Ms.	Peplinski	93	Tidewater Farm Rd	Stratham
232	1341	Douglas	Zimmerman	95	Tidewater Farm Rd	Stratham
233	1259	James	Walker	112	Tidewater Farm Rd	Stratham
234	918	Theresa	O'Neil	1	Winding Brook	Stratham
235	310	Michael	Daigle	5	Winding Brook	Stratham

APPENDIX B

MONITORING WELL DATABASE: COORDINATE DATA

#	Well#	Easting/X (NH State Plane, NAD83, feet)	Northing/Y (NH State Plane, NAD83, feet)	ELTOC (ft)	WSEL (ft) 6/00 Event	DTW (ft)
1	359	1198456	234338.3	117.10	91.18	25.92
2	139	1199745	234430.3	48.04	40.16	7.88
3	1114	1194915	240046.3	79.23	74.12	5.11
4	1110	1194833	239615.9	70.40	57.41	12.99
5	368	1193771	238739.8	83.77	74.28	9.49
6	1160	1194057	238527.2	87.95	74.65	13.30
7	1095	1197888	236666	100.61	69.58	31.03
8	478	1205664	248583.6	121.88	85.78	36.10
9	941	1195741	239520.1	118.30	88.26	30.04
10	755	1196137	238247.8	148.00	113.04	34.96
11	309	1197008	236193.9	97.31	78.16	19.15
12	140	1197522	235936.6	87.21	56.72	30.49
13	520	1197027	235940	90.77	81.49	9.28
14	821	1198064	234610.3	129.96	97.85	32.11
15	1063	1194845	219183.4	64.00	22.96	41.04
16	658	1194855	217280.6	43.66	11.76	31.90
17	404	1192915	216149.6	47.56	34.52	13.04
18	429	1194847	215975.7	21.65	7.15	14.50
19	162	1192961	214540.6	51.00	29.01	21.99
20	161	1192175	214646.5	47.64	28.81	18.83
21	797	1191959	213720.2	44.67	27.78	16.89
22	797A	1191775	213559.3	23.76	14.63	9.13
23	452	1191269	213725	33.77	15.15	18.62
24	1041	1200014	230082	10.65	3.38	7.27
25	1276	1200438	230315.7	17.34	3.89	13.45
26	964	1197301	224555.6	22.04	11.92	10.12
27	81	1197480	224718.4	23.70	7.96	15.74
28	583	1184421	215982.4	76.00	63.59	12.41
29	946	1185516	217527.2	78.62	58.70	19.92
30	1073	1190111	222644.3	58.36	51.11	7.25
31	820A	1192819	221540.8	81.62	51.67	29.95
32	820	1191758	221880.2	75.05	47.43	27.62
33	862	1188679.3	221820.3	72.08	55.17	16.91
34	1094	1192358	221906	80.46	58.55	21.91
35	978	1191039	227401.9	46.83	27.31	19.52
36	449	1191222	227687.1	32.67	24.19	8.48
37	1158	1191307	228032.2	32.43	17.22	15.21
38	1140	1193021	228122.5	21.11	8.26	12.85
39	116	1193310	228191.6	30.40	8.15	22.25
40	1237	1192830	229433.4	22.51	3.59	18.92
41	1268	1192480	229551.7	13.83	4.26	9.57
42	1002	1192617	230008.6	19.34	-14.60	33.94
43	504	1186993	231598.9	18.37	8.76	9.61
44	1231	1190475	227557.1	55.26	50.00	5.26
45	480	1191449	229215.3	14.71	5.03	9.68
46	346	1195534	224618.3	52.24	46.60	5.64
47	228	1196736	223705.7	17.11	0.36	16.75
48	1239	1195323	223301.3	57.63	42.01	15.62
49	1400	1194448	222858.8	61.62	49.14	12.48

#	Well#	Easting/X (NH State Plane, NAD83, feet)	Northing/Y (NH State Plane, NAD83, feet)	ELTOC (ft)	WSEL (ft) 6/00 Event	DTW (ft)
50	863	1194629	222700.6	53.61	36.08	17.53
51	352	1196042	225009.2	68.33	47.87	20.46
52	264	1185529	226950.9	77.96	38.16	39.80
53	775	1185582	226319.4	53.04	38.28	14.76
54	1169	1185681	223533.8	82.43	61.73	20.70
55	1061	1186570	223838.7	86.58	67.25	19.33
56	875	1193475	226928.6	75.14	49.43	25.71
57	1193	1193535	226937.6	57.39	39.82	17.57
58	351	1193746	227240	52.59	47.07	5.52
59	6	1193855	232419.8	89.39	54.14	35.25
60	710	1185121	228041.1	85.47	53.79	31.68
61	793	1186445	228554.7	112.68	82.00	30.68
62	578	1186930	228670.6	105.29	53.48	51.81
63	1189	1186711	228607.7	115.64	83.41	32.23
64	1221	1189925	233223.7	33.64	15.59	18.05
65	1204	1190195	232979	31.25	26.01	5.24
66	271	1190194	232974.6	31.44	27.11	4.33
67	635	1198119	230050.4	33.13	30.42	2.71
68	382	1198547	230297.5	25.06	23.10	1.96
69	206	1190118	231605.5	10.28	-4.00	14.28
70	355	1190872	232584.5	25.41	22.96	2.45
71	177	1191146	230298.7	28.32	8.48	19.84
72	199	1191094	231827.1	33.97	19.63	14.34
73	1134	1190921	232088.8	33.15	13.35	19.80
74	505	1191080	232976.3	44.51	25.29	19.22
75	1192	1184942	227949.8	48.34	42.14	6.20
76	718	1194096	231996.8	75.28	44.35	30.93
77	528	1193873	232075.7	79.41	52.70	26.71
78	789	1194069	231723.2	66.29	42.02	24.27
79	194	1197269	232118	70.20	32.01	38.19
80	1340	1197111	232329.1	63.36	37.34	26.02
81	1191	1193088	231977.3	51.73	34.83	16.90
82	1242	1193101	232190	78.94	42.81	36.13
83	416	1192695	232330.6	41.00	13.02	27.98
84	1401	1198085	216539	15.00	11.00	4.00
85	154	1195425	203006.7	79.95	65.92	14.03
86	1179	1195284	203733.6	59.32	44.94	14.38
87	196	1195664	203986.6	65.69	36.82	28.87
88	1250	1195466	204549.9	57.14	49.99	7.15
89	433	1195180	204242.5	60.81	49.93	10.88
90	860	1204550	199450.8	18.95	8.22	10.73
91	1270	1204706	199764.2	15.88	9.21	6.67
92	171	1204416	199883.5	22.06	13.65	8.41
93	555	1204438	200215	22.53	11.32	11.21
94	1230	1204271	199572.1	28.69	12.77	15.92
95	1083	1202936	196915.1	28.97	6.38	22.59
96	1283	1196539	200613.1	18.51	7.76	10.75
97	550	1202182	197889	25.59	7.38	18.21
98	273	1196566	197887	20.49	6.96	13.53

#	Well#	Easting/X (NH State Plane, NAD83, feet)	Northing/Y (NH State Plane, NAD83, feet)	ELTOC (ft)	WSEL (ft) 6/00 Event	DTW (ft)
99	774	1199943	198802	84.82	42.43	42.39
100	306	1199451	198916.5	66.72	54.15	12.57
101	796	1203434	197497.2	17.79	5.60	12.19
102	1084	1203430	197495.5	16.87	7.05	9.82
103	477	1197749	198833.6	92.72	68.49	24.23
104	665	1197404	198442.5	99.41	70.87	28.54
105	652	1195710	201368.5	89.87	76.25	13.62
106	836	1194263	203611.3	52.55	44.43	8.12
107	1035	1194411	204310.4	31.63	24.29	7.34
108	1206	1194562	204651.5	20.56	16.39	4.17
109	1013	1194635	204529.7	25.92	7.56	18.36
110	517	1193232	204850.8	20.97	3.88	17.09
111	957	1197987	198759	86.77	66.84	19.93
112	338	1197896	199742.8	58.47	55.66	2.81
113	122	1196539	200613.1	89.98	80.02	9.96
114	455	1196847	200983	78.83	64.68	14.15
115	812	1198598	197530.1	60.34	56.32	4.02
116	294	1198890	197771.7	66.67	55.40	11.27
117	1246	1200347	201124.9	20.48	1.76	18.72
118	441	1193872	203342.8	64.25	44.72	19.53
119	1036	1193531	203189.4	79.07	62.66	16.41
120	716	1193866	203052.8	71.08	55.85	15.23
121	723	1193138	202911.3	65.57	53.89	11.68
122	1262	1192745	202741.4	60.57	56.47	4.10
123	1200	1191665	202182.9	61.49	55.14	6.35
124	45	1192179	202560.2	66.46	55.34	11.12
125	598	1200434	194842.5	29.87	26.15	3.72
126	561	1192337	202573.6	64.93	57.38	7.55
127	660	1193308	201846.6	94.34	86.49	7.85
128	1331	1192158	201577.9	98.64	92.79	5.85
129	1402	1196391	205122.4	21.00	12.95	8.05
130	159	1179781	197935.2	45.89	37.32	8.57
131	623	1181382	197532.2	19.59	4.43	15.16
132	PAFB615	1206856	214060		76.95	
133	PAFB6013	1213257	211858.2		49.55	
134	PAFB603	1205312	214762		39.88	
135	PAFB6034	1206026	218458.2		57.76	
136	PAFB6035	1205710	218011.7		51.95	
137	PAFB6043	1206102	218945.7		61.69	
138	PAFB6044	1206721	218808		83.43	
139	PAFB6046	1206280	219377		61.61	
140	PAFB6047	1206506	214193.6		77.06	
141	PAFB6048	1207324	213909		79.67	
142	PAFB6049	1207231	212901		76.33	
143	PAFB6050	1205840	215006		63.09	
144	PAFB6051	1205728	215336		51.91	
145	PAFB6083	1207096	217618		92.35	
146	PAFB6098	1208054	213678		79.82	
147	PAFB6099	1206960	214372		77.08	

#	Well#	Easting/X (NH State Plane, NAD83, feet)	Northing/Y (NH State Plane, NAD83, feet)	ELTOC (ft)	WSEL (ft) 6/00 Event	DTW (ft)
148	PAFB610	1206525	214929		75.68	
149	PAFB6103	1206409	213945		77.45	
150	PAFB6106	1204765	214386		31.10	
151	PAFB6107	1206968	214372		77.98	
152	PAFB6108	1207041	213552		77.40	
153	PAFB6109	1206767	215197		77.41	
154	PAFB6110	1207153	214862		79.27	
155	PAFB6111	1207129	214846		78.14	
156	PAFB6112	1206799	215185		77.79	
157	PAFB6113	1207801	214004		78.11	
158	PAFB6114	1206244	213288		69.67	
159	PAFB6121	1206523	212374		61.58	
160	PAFB614	1207275	214678		77.22	
161	PAFB615	1206856	214060		78.91	
162	PAFB618	1205724	218215.7		53.92	
163	PAFB620	1206990	217788		87.37	
164	PAFB621	1207174	217468		93.22	
165	PAFB6506	1210125	211592		64.01	
166	PAFB6507	1211905	208736		57.34	
167	1403	1205147	209039.7	28.00	23.27	4.73
168	1404	1204943	209089.4	28.00	24.12	3.88
169	1405	1201938	215883.8	26.18	22.48	3.70
170	298	1261844	204951.9	113.48	97.11	16.37
171	485	1169557	206755.9	1.77	-11.37	13.13
172	1067	1182565	211891.7	76.85	33.81	43.04
173	687	1184105	211513.4	26.76	15.38	11.38
174	421	1184885	211449.5	34.48	12.10	22.38
175	421A	1184885	211449.5	34.86	22.18	12.68
176	1145	1188574	213072.5	86.72	38.63	48.09
177	1157	1182614	211449.6	60.27	34.25	26.02
178	991	1182941	211485	49.61	32.98	16.63
179	627	1184481	210448.2	18.53	7.08	11.45
180	765	1185214	208718.7	49.22	29.48	19.74
181	1328	1185363	208103.5	18.97	8.04	10.93
182	28	1183116	207235.6	67.45	51.60	15.85
183	278	1182739	207371.5	66.12	56.33	9.79
184	358	1183121	207243.3	61.71	57.41	4.30
185	525	1182643	203254.4	43.05	21.53	21.52
186	312	1182830	202604.6	60.62	47.41	13.21
188	1247	1181821	202873.1	30.51	30.51	0.00
187	1247	1181767	202806.3	30.51	22.87	7.64
189	119	1170941	207648.6	106.00	97.09	8.91
190	344	1181713	211755.5	41.04	35.02	6.02
191	48	1184070	209094.2	40.45	22.09	18.36
192	902	1181753	210591.5	54.82	8.42	46.40
193	356	1182671	209859	33.56	20.74	12.82
194	1148	1182925	209896.7	60.66	29.83	30.83
195	1055	1183227	209053.3	28.96	11.16	17.80
196	134	1183351	209481.7	45.76	37.07	8.69

#	Well#	Easting/X (NH State Plane, NAD83, feet)	Northing/Y (NH State Plane, NAD83, feet)	ELTOC (ft)	WSEL (ft) 6/00 Event	DTW (ft)
197	191	1187822	198326.9	100.96	74.59	26.37
198	791	1187727	198174	93.26	70.83	22.43
199	886	1187059	198592.9	77.22	72.64	4.58
200	1039	1186914	198734.4	74.29	69.16	5.13
201	986	1186969	199054.9	73.15	64.21	8.94
202	1298	1187316	198762.6	85.29	78.91	6.38
203	558	1187661	198318.5	92.76	70.96	21.80
204	40	1183878	194252.2	29.06	8.04	21.02
205	1159	1188812	196505.7	130.59	123.59	7.00
206	30	1184841	196335.1	131.24	122.38	8.86
207	803	1189307	196320.8	128.76	122.12	6.64
208	825	1189412	196161.4	124.53	120.80	3.73
209	638	1190472	199115.2	123.08	121.44	1.64
210	940	1190518	195598.1	132.33	127.82	4.51
211	244	1190151	196145.9	117.78	116.01	1.77
212	816	1189884	199011.2	138.88	125.82	13.06
213	1009	1189930	199167.3	113.64	105.19	8.45
214	265	1190388	200087.4	108.81	100.48	8.33
216	650	1190536	200666.4	99.65	94.74	4.91
215	650	1190522	200648.3	100.10	92.60	7.50
217	1011	1190010	201935.1	119.55	106.80	12.75
218	470	1189461	201565.1	84.22	75.88	8.34
219	88	1189844	202521.7	39.50	24.20	15.30
220	643	1189644	202600.1	42.20	28.99	13.21
221	591	1189045	202359.4	46.91	35.64	11.27
222	59	1188564	201780	32.29	24.54	7.75
223	636	1188467	202127.6	63.23	52.88	10.35
224	523	1188848	201538.8	55.74	44.00	11.74
225	1267	1189057	201534	74.15	65.35	8.80
226	668	1189397	201423	83.53	76.00	7.53
227	1064	1183713	192913.1	23.71	9.35	14.36
228	679	1190207	199461.1	125.87	108.80	17.07
229	1076	1187712	197001.8	69.52	65.13	4.39
230	1336	1191785	201657.4	98.20	81.30	16.90
231	955	1191587	201321.1	100.18	90.93	9.25
232	1341	1191386	196529.3	95.16	90.14	5.02
233	1259	1191117	201639.8	69.46	61.61	7.85
234	918	1184176	190005.6	101.19	70.84	30.35
235	310	1184065	190089.6	88.44	70.59	17.85

APPENDIX C

MONITORING WELL DATABASE: WELL WATER QUALITY FROM SUMMER 2001 SAMPLING EVENT

Well#	mg NO3-N/L
6	0.00
28	0.00
30	1.73
40	0.17
45	0.00
48	0.22
59	0.00
81	0.03
88	0.26
116	0.04
119	1.06
122	0.01
134	2.52
139	2.52
140	0.15
154	0.05
159	0.71
161	1.90
171	0.02
177	0.57
191	1.08
194	0.06
196	0.00
199	1.79
206	0.09
228	0.33
244	0.00
265	0.24
271	0.54
273	0.00
278	0.01
294	0.00
298	2.67
306	0.00
309	0.00
310	0.02
338	0.01
344	0.00
346	0.36
351	0.03
352	1.22
355	2.63

Well#	mg NO3-N/L
356	1.29
358	1.73
359	1.42
368	1.75
382	0.05
404	0.14
416	1.15
429	2.19
433	0.31
441	0.13
449	2.39
455	0.01
455	0.01
470	0.00
477	0.01
478	0.68
480	0.00
485	1.55
504	0.00
517	0.15
520	0.00
523	1.15
525	0.06
528	3.84
550	0.79
555	0.00
558	0.01
561	0.07
578	3.33
583	0.06
591	2.95
598	0.01
623	2.23
627	1.04
635	1.05
636	0.01
638	0.00
643	0.02
650	0.00
652	0.00
658	0.21

Well#	mg NO3-N/L
660	0.04
665	0.00
679	0.00
687	1.40
710	2.13
716	0.00
718	0.01
723	0.16
755	0.16
765	0.56
775	1.59
789	2.59
791	0.02
793	3.38
796	0.00
797	0.97
803	0.01
812	0.00
820	0.43
825	0.00
836	0.86
860	0.04
875	4.94
886	0.00
902	0.01
918	1.07
940	0.01
941	0.66
946	5.10
957	0.01
964	0.29
978	0.36
986	0.73
991	1.79
1002	0.14
1011	2.12
1013	0.00
1035	1.95
1036	3.16
1039	0.05
1041	0.36

Well#	mg NO3-N/L
1055	0.05
1061	1.49
1063	0.45
1064	0.00
1067	1.39
1073	0.77
1076	5.18
1083	0.00
1084	0.00
1094	0.48
1095	0.30
1110	0.87
1114	1.96
1134	1.13
1140	2.15
1145	0.62
1148	2.70
1157	0.01
1158	0.74

Well#	mg NO3-N/L
1159	0.01
1160	10.20
1179	0.00
1189	0.95
1191	1.56
1192	5.03
1193	4.80
1200	0.02
1204	0.01
1206	3.30
1221	0.42
1230	0.07
1231	0.08
1237	0.23
1239	0.00
1242	0.90
1246	0.00
1247	1.69
1250	0.00

Well#	mg NO3-N/L
1259	1.36
1262	0.01
1267	0.04
1268	0.21
1270	0.00
1276	1.24
1283	0.06
1298	1.70
1328	0.15
1331	0.01
1336	0.01
1340	0.53
1341	0.01
1400	1.19
797A	0.06
820A	3.02

APPENDIX D

GROUNDWATER DISCHARGE ZONE DATABASE: CLASSIFICATION AND COORDINATES FROM APRIL 2000 SURVEY

#	SGD ID	SIZE	TYPE	INTENSITY	Easting, NH State Plane feet	Northing, NH State Plane Feet
1	4.1.1	Medium	linear	Medium/low	1184296.6861	232958.7615
2	7.1.1	Small	linear	Medium/low	1191216.6687	230610.6636
3	8.1.1	Small	diffuse	low	1193122.7717	230016.7329
4	8.2.1	Small	diffuse	low	1193343.7691	229850.9849
5	9.1.1	Small	diffuse	low	1200774.8083	232226.7074
6	9.2.1	Small	point	Medium/high	1201865.9832	233041.6355
7	16.1.1	Small	point	high	1198316.2117	229768.1108
8	17.1.1	medium	diffuse	medium	1196990.2270	228745.9976
9	17.3.1	Medium/Large	dendritic	Medium/high	1196423.9210	228773.6223
10	18.1.1	Medium/Large	dendritic	Medium/low	1195318.9338	228953.1827
11	18.2.1	small/medium	dendritic	Medium/low	1195097.9363	229270.8666
12	19.2.1	Small	point	low	1193910.0751	228649.3112
13	19.3.1	small	diffuse	low	1193509.5172	229422.8023
14	19.4.1	Small	diffuse	low	1193357.5814	229795.7355
15	20.4.1	Small	point	low	1196230.5483	227199.0155
16	21.1.1	Small	point	low	1197169.7874	226991.8304
17	21.2.1	Small/Medium	dendritic	Medium/low	1197404.5972	226342.6504
18	28.1.1	Small	linear	low	1209338.4594	224809.4806
19	28.2.1	Small	point	low	1209407.5211	224975.2287
20	29.2.1	Medium/Large	diffuse	low	1204752.7623	224270.7993
21	29.3.1	Small/Medium	diffuse	low	1204490.3279	224298.424
22	29.4.1	Small/Medium	linear	high	1203841.1479	224284.6116
23	29.5.1	Small/Medium	linear	Medium/low	1203744.4615	224450.3597
24	29.6.1	Small	point	Medium/low	1203523.4640	224740.4189
25	30.2.1	Small	point	low	1203122.9061	225859.2185
26	30.3.1	Small	point	low	1203095.2815	225997.3419
27	30.4.1	Small	point	low	1203067.6568	226149.2776
28	31.1.1	Small/Medium	point	Medium	1201644.9857	225527.7223
29	31.3.1	Small	dendritic	Medium/high	1201327.3019	226411.7121
30	31.4.1	Medium/Large	dendritic	high	1201589.7364	226011.1542
31	32.1.1	Small	point	low	1197280.2861	224077.4265
32	32.2.1	Small	point	low	1197169.7874	223828.8044
33	32.3.1	Small	point	low	1197556.5329	224754.2312
34	32.4.1	Small	point	low	1197045.4763	225486.2853
35	32.5.1	Small	point	low	1196783.0419	225555.347
36	32.6.1	medium	diffuse	low	1197211.2244	223676.8687
37	34.1.1	Small/Medium	dendritic	Medium/low	1201258.2402	223538.7453
38	34.2.1	Small/Medium	dendritic	Medium/low	1201299.6772	223317.7478
39	34.3.1	Small/Medium	point	medium	1201216.8032	223414.4342
40	35.1.1	Medium/Large	diffuse	low	1201313.4895	221273.5214
41	36.1.1	Small	diffuse	low	1196934.9776	221605.0176
42	36.2.1	Medium	diffuse	low	1197142.1627	220872.9636
43	36.3.1	Small	diffuse	low	1196907.3529	223055.3133
44	37.1.1	Small	diffuse	low	1197653.2193	219975.1614

#	SGD ID	SIZE	TYPE	INTENSITY	Easting, NH State Plane feet	Northing, NH State Plane Feet
45	38.1.1	Medium	diffuse	Medium/low	1197805.1551	219685.1023
46	38.2.1	medium	diffuse	low	1201672.6104	220513.8427
47	39.1.1	Medium	linear	low	1201783.1091	220361.907
48	39.2.1	small	linear	Medium/low	1201548.2993	219961.3491
49	39.3.1	Small	point	low	1197653.2193	219436.4801
50	40.1.1	Medium/Large	diffuse	low	1201441.1842	217147.3005
51	40.2.1	Small	point	low	1201836.4692	216955.8994
52	40.3.1	medium	diffuse	medium	1202036.1921	217396.9542
53	40.4.1	Medium	linear	high	1201994.5832	217130.657
54	44.1.1	Small	linear	low	1194492.4011	215021.3639
55	44.2.1	Small	diffuse	low	1194386.7534	215297.6733
56	44.3.1	Small	linear	low	1194646.8093	215752.7711
57	44.4.1	Small/Medium	diffuse	low	1194825.5978	215842.1653
58	44.5.1	Large	diffuse	medium	1194793.0908	216207.8689
59	44.6.1	Large	diffuse	low	1194988.1327	216549.1923
60	48.1.1	Small	point	Medium/low	1196418.4402	218296.4429
61	48.2.1	Small/Medium	linear	Medium/low	1196776.0170	218215.1754
62	48.3.1	Small	point	low	1196841.0310	218174.5417
63	48.4.1	Small	linear	low	1196938.5520	218117.6544
64	48.5.1	Small	point	low	1197044.1997	218003.88
65	48.6.1	Small	linear	low	1197117.3404	218052.6405
66	48.7.1	Small	linear	low	1197157.9741	218012.0067
67	48.8.1	Small	point	Medium/low	1197174.2276	217971.373
68	48.9.1	Small/Medium	diffuse	low	1197174.2276	217906.359
69	48.10.1	Small/Medium	diffuse	low	1197157.9741	217849.4718
70	48.11.1	Large	diffuse	low	1195955.2156	218150.1614
71	48.12.1	X- Large	diffuse	low	1196662.2426	217321.2332
72	49.1.1	Small	linear	low	1202643.5283	210803.5822
73	49.2.1	Small	diffuse	low	1202749.1760	210844.216
74	49.3.1	Small	point	Medium/low	1202830.4434	210974.2439
75	49.4.1	Small	diffuse	low	1202854.8237	211088.0184
76	49.5.1	Small	point	Medium/high	1203651.2449	210949.8637
77	49.6.1	Small	point	Medium/high	1203724.3856	210876.723
78	49.7.1	Small	point	Medium/low	1203805.6531	210827.9625
79	49.8.1	Small	diffuse	Medium/low	1203927.5543	210779.202
80	52.1.1	Large	diffuse	low	1191387.9838	212705.241
81	52.2.1	small	linear	medium	1191396.1106	213404.1412
82	52.3.1	Large	diffuse	medium	1191769.9409	213379.761
83	52.4.1	Large	diffuse	medium	1191339.2234	213420.3947
84	53.1.1	Small	linear	low	1189375.4762	211827.5523
85	53.2.1	Small	linear	low	1189370.2751	211988.787
86	53.3.1	Small	linear	Medium	1189245.4483	212238.4407
87	53.4.1	Small	linear	Medium	1189255.8505	212306.0552
88	53.5.1	Small	point	Medium	1189380.6774	212566.1111

#	SGD ID	SIZE	TYPE	INTENSITY	Easting, NH State Plane feet	Northing, NH State Plane Feet
89	53.6.1	Small	linear	low	1189885.1858	212774.1558
90	53.7.1	Medium	linear	Medium/low	1189796.7668	212992.6028
91	53.8.1	Small/Medium	diffuse	low	1189874.7836	213055.0162
92	53.9.1	Small	point	low	1190010.0126	213049.8151
93	53.10.1	Small	point	low	1190634.1468	213081.0218
94	53.11.1	Large	diffuse	low	1189619.9288	212633.7256
95	53.12.1	Large	diffuse	low	1189458.6941	211609.1054
96	54.1.1	Small	diffuse	Medium/low	1189120.6215	210397.2449
97	54.2.1	Small	linear	low	1188865.7667	210386.8427
98	54.3.1	Large	diffuse	low	1189068.6103	210584.4851
99	54.4.1	Large	diffuse	low	1189354.6718	211208.6193
100	54.5.1	Large	diffuse	low	1189510.7053	211432.2674
101	56.8.1	X- Large	diffuse	Medium/low	1190332.4820	213060.2173
102	58.1.1	Small	linear	Medium	1204822.7967	208753.6916
103	58.3.1	Small	point	high	1204900.8135	208649.6692
104	58.4.1	Medium	dendritic	Medium/low	1204484.7240	209424.6358
105	58.5.1	Medium	dendritic	Medium/low	1204484.7240	209606.675
106	58.6.1	Small	point	low	1204874.8079	208072.3451
107	58.7.1	Small	point	low	1204744.7799	208067.144
108	58.8.1	Small	point	low	1204599.1486	208025.5351
109	58.9.1	Small	point	Medium/high	1204157.0536	208077.5463
110	58.10.1	Small	point	Medium/low	1203850.1876	208269.9876
111	64.1.1	X- Large	diffuse	low	1185318.6042	206548.4176
112	64.2.1	X- Large	diffuse	low	1185240.5874	207427.4065
113	64.3.1	X- Large	diffuse	low	1186015.5540	207547.0322
114	66.1.1	Small/Medium	point	high	1205628.9700	208108.753
115	66.2.1	Small	point	Medium	1205446.9309	208259.5854
116	66.3.1	Small	point	Medium	1205389.7186	208223.1776
117	66.4.1	X- Large	diffuse	low	1205155.6683	208228.3787
118	67.1.1	Small	point	Medium/low	1206809.6238	204363.948
119	67.2.1	Large	diffuse	Medium/high	1206689.9981	205523.7973
120	67.3.1	Small	point	low	1206518.3612	205799.4566
121	67.4.1	Small	point	low	1206523.5623	205939.8868
122	67.5.1	Small	point	low	1206393.5344	206069.9147
123	67.6.1	Small	point	Medium/low	1206424.7411	206210.3449
124	67.7.1	X- Large	diffuse	low	1206991.6629	204858.0542
125	67.8.1	medium	diffuse	low	1206778.4171	203911.4507
126	69.1.1	Small	diffuse	low	1198253.7847	204571.9927
127	69.3.1	Large	linear	Medium/low	1197848.0975	204889.2609
128	69.4.1	Small	diffuse	Medium/low	1197759.6785	204837.2497
129	70.1.1	Small/Medium	linear	Medium/high	1195049.8960	204603.1994
130	70.2.1	Small	linear	Medium	1195564.8067	204670.814
131	70.3.1	Small	diffuse	low	1195835.2648	204764.4341
132	70.4.1	Small	diffuse	low	1195341.1586	204644.8084

#	SGD ID	SIZE	TYPE	INTENSITY	Easting, NH State Plane feet	Northing, NH State Plane Feet
133	70.5.1	Small	diffuse	medium	1194971.8792	204722.8251
134	71.1.1	Small	diffuse	low	1193447.9516	204530.3838
135	71.2.1	Small	point	low	1193598.7841	204415.9592
136	71.3.1	Small	diffuse	low	1194680.6166	205086.9034
137	73.1.1	Small	point	Medium	1191138.6552	203386.1378
138	73.2.1	Medium	linear	Medium	1191559.9458	203464.1546
139	73.3.1	Small	point	Medium/low	1192038.4487	203656.596
140	74.2.1	Small	diffuse	low	1189027.0013	203640.9926
141	74.5.1	medium	diffuse	low	1188704.5320	203750.2161
142	74.6.1	medium	diffuse	low	1189905.9903	203620.1881
143	75.1.1	X- Large	diffuse	low	1185994.7495	205820.261
144	77.1.1	Small	diffuse	low	1185443.4310	204551.1883
145	77.2.1	Large	diffuse	low	1185729.4925	205081.7023
146	78.1.1	Small	linear	low	1186811.3251	202715.1936
147	80.1.1	Small	diffuse	low	1199382.4273	204171.5066
148	80.2.1	Small/Medium	linear	Medium/low	1199502.0530	203765.8194
149	80.3.1	Small	point	low	1199751.7067	203505.7635
150	80.4.1	Small	point	low	1199866.1313	203573.3781
151	80.5.1	Small	point	Medium/low	1199928.5447	203745.015
152	80.6.1	Small	diffuse	low	1200453.8576	203422.5456
153	80.7.1	Small	linear	low	1200427.8520	203276.9143
154	81.1.1	Medium/Large	diffuse	low	1200542.2766	202314.7075
155	81.2.1	Small/Medium	diffuse	low	1200713.9135	201940.227
156	81.3.1	Large	diffuse	low	1201832.1539	201700.9756
157	82.1.1	Small/Medium	point	Medium/high	1203699.3552	202678.7858
158	83.1.1	Small	diffuse	low	1205030.8414	202278.2997
159	83.2.1	Small/Medium	linear	Medium/high	1204833.1990	202257.4952
160	84.1.1	Large	diffuse	Medium/low	1206762.8137	204166.3055
161	84.2.1	X- Large	dendritic	Medium/low	1206887.6406	203604.5848
162	84.3.1	Small/Medium	dendritic	low	1206866.8361	203152.0875
163	84.4.1	Small	diffuse	Medium/low	1206747.2104	202741.1992
164	84.5.1	Small	diffuse	Medium/low	1206689.9981	202538.3556
165	84.6.1	Small	linear	low	1206622.3835	202356.3165

APPENDIX E

GROUNDWATER DISCHARGE ZONE DATABASE: WATER QUALITY OF SGD ZONES

SGD ID	mg NO3-N/L	Northing NH State Plane, NAD83, feet	Easting NH State Plane, NAD83, feet
17.3.1	0.35	228773.6	1196423.9
18.1.1	0.15	228953.2	1195318.9
18.2.1	0.23	229270.9	1195097.9
19.2.1	0.57	228595.8	1194105.2
19.3.1	1.51	229402.3	1193726.8
19.4.1	1.55	229805.2	1193500.5
21.2.1	2.59	226401.0	1197538.0
31.4.1	1.14	226036.0	1201695.0
34.1.1	0.03	223641.0	1201305.0
35.1.1	0.09	221275.4	1201519.0
39.2.1	0.17	220367.2	1201824.6
39.3.1	2.73	219960.8	1201680.2
53.3.1	0.03	212186.0	1189273.0
53.5.1	0.02	212556.0	1189506.0
64.1.1	0.01	206504.4	1185049.8
69.3.1	1.45	204866.3	1197772.3
69.4.1	1.01	204837.2	1197759.7
73.1.1	0.24	203385.7	1191145.5
73.2.1	2.08	203454.6	1191559.1
73.3.1	0.29	203661.4	1192041.6
Average=	0.84		
Median=	0.29		
Stdev=	0.91		
Max	2.73		
Min	0.01		
N	19.00		

APPENDIX F

GROUNDWATER DISCHARGE ZONE DATABASE: FLOW EXPRESSION MATRIX

SGD ID	Size	Type	Intensity	Seepage Face Surface Area (Ft2)	Specific Discharge (GPD/Ft2)	Type Coefficient	SGD Flow (GPD)
4.1.1	Medium	linear	Medium/low	7266	17	1.0	76020
7.1.1	Small	linear	Medium/low	2066	17	1.0	21617
8.1.1	Small	diffuse	low	2066	9	0.3	3253
8.2.1	Small	diffuse	low	2066	9	0.3	3253
9.1.1	Small	diffuse	low	2066	9	0.3	3253
9.2.1	Small	point	Medium/high	2066	35	1.0	43167
16.1.1	Small	point	high	2066	44	1.0	53942
17.1.1	medium	diffuse	medium	7266	26	0.3	34174
17.3.1	Medium/Large	dendritic	Medium/high	9865	35	1.0	206119
18.1.1	Medium/Large	dendritic	Medium/low	9865	17	1.0	103219
18.2.1	small/medium	dendritic	Medium/low	4666	17	1.0	48821
19.2.1	Small	point	low	2066	9	1.0	10842
19.3.1	small	diffuse	low	2066	9	0.3	3253
19.4.1	Small	diffuse	low	2066	9	0.3	3253
20.4.1	Small	point	low	2066	9	1.0	10842
21.1.1	Small	point	low	2066	9	1.0	10842
21.2.1	Small/Medium	dendritic	Medium/low	4666	17	1.0	48821
28.1.1	Small	linear	low	2066	9	1.0	10842
28.2.1	Small	point	low	2066	9	1.0	10842
29.2.1	Medium/Large	diffuse	low	9865	9	0.3	15531
29.3.1	Small/Medium	diffuse	low	4666	9	0.3	7346
29.4.1	Small/Medium	linear	high	4666	44	1.0	121827
29.5.1	Small/Medium	linear	Medium/low	4666	17	1.0	48821
29.6.1	Small	point	Medium/low	2066	17	1.0	21617
30.2.1	Small	point	low	2066	9	1.0	10842
30.3.1	Small	point	low	2066	9	1.0	10842
30.4.1	Small	point	low	2066	9	1.0	10842
31.1.1	Small/Medium	point	Medium	4666	26	1.0	73156
31.3.1	Small	dendritic	Medium/high	2066	35	1.0	43167
31.4.1	Medium/Large	dendritic	high	9865	44	1.0	257570
32.1.1	Small	point	low	2066	9	1.0	10842
32.2.1	Small	point	low	2066	9	1.0	10842
32.3.1	Small	point	low	2066	9	1.0	10842
32.4.1	Small	point	low	2066	9	1.0	10842
32.5.1	Small	point	low	2066	9	1.0	10842
32.6.1	medium	diffuse	low	7266	9	0.3	11438
34.1.1	Small/Medium	dendritic	Medium/low	4666	17	1.0	48821
34.2.1	Small/Medium	dendritic	Medium/low	4666	17	1.0	48821
34.3.1	Small/Medium	point	medium	4666	26	1.0	73156
35.1.1	Medium/Large	diffuse	low	9865	9	0.3	15531
36.1.1	Small	diffuse	low	2066	9	0.3	3253
36.2.1	Medium	diffuse	low	7266	9	0.3	11438
36.3.1	Small	diffuse	low	2066	9	0.3	3253
37.1.1	Small	diffuse	low	2066	9	0.3	3253

SGD ID	Size	Type	Intensity	Seepage Face Surface Area (Ft2)	Specific Discharge (GPD/Ft2)	Type Coefficient	SGD Flow (GPD)
38.1.1	Medium	diffuse	Medium/low	7266	17	0.3	22806
38.2.1	medium	diffuse	low	7266	9	0.3	11438
39.1.1	Medium	linear	low	7266	9	1.0	38127
39.2.1	small	linear	Medium/low	2066	17	1.0	21617
39.3.1	Small	point	low	2066	9	1.0	10842
40.1.1	Medium/Large	diffuse	low	9865	9	0.3	15531
40.2.1	Small	point	low	2066	9	1.0	10842
40.3.1	medium	diffuse	medium	7266	26	0.3	34174
40.4.1	Medium	linear	high	7266	44	1.0	189698
44.1.1	Small	linear	low	2066	9	1.0	10842
44.2.1	Small	diffuse	low	2066	9	0.3	3253
44.3.1	Small	linear	low	2066	9	1.0	10842
44.4.1	Small/Medium	diffuse	low	4666	9	0.3	7346
44.5.1	Large	diffuse	medium	12465	26	0.3	58630
44.6.1	Large	diffuse	low	12465	9	0.3	19624
48.1.1	Small	point	Medium/low	2066	17	1.0	21617
48.2.1	Small/Medium	linear	Medium/low	4666	17	1.0	48821
48.3.1	Small	point	low	2066	9	1.0	10842
48.4.1	Small	linear	low	2066	9	1.0	10842
48.5.1	Small	point	low	2066	9	1.0	10842
48.6.1	Small	linear	low	2066	9	1.0	10842
48.7.1	Small	linear	low	2066	9	1.0	10842
48.8.1	Small	point	Medium/low	2066	17	1.0	21617
48.9.1	Small/Medium	diffuse	low	4666	9	0.3	7346
48.10.1	Small/Medium	diffuse	low	4666	9	0.3	7346
48.11.1	Large	diffuse	low	12465	9	0.3	19624
48.12.1	X- Large	diffuse	low	15065	9	0.3	23717
49.1.1	Small	linear	low	2066	9	1.0	10842
49.2.1	Small	diffuse	low	2066	9	0.3	3253
49.3.1	Small	point	Medium/low	2066	17	1.0	21617
49.4.1	Small	diffuse	low	2066	9	0.3	3253
49.5.1	Small	point	Medium/high	2066	35	1.0	43167
49.6.1	Small	point	Medium/high	2066	35	1.0	43167
49.7.1	Small	point	Medium/low	2066	17	1.0	21617
49.8.1	Small	diffuse	Medium/low	2066	17	0.3	6485
52.1.1	Large	diffuse	low	12465	9	0.3	19624
52.2.1	small	linear	medium	2066	26	1.0	32392
52.3.1	Large	diffuse	medium	12465	26	0.3	58630
52.4.1	Large	diffuse	medium	12465	26	0.3	58630
53.1.1	Small	linear	low	2066	9	1.0	10842
53.2.1	Small	linear	low	2066	9	1.0	10842
53.3.1	Small	linear	Medium	2066	26	1.0	32392
53.4.1	Small	linear	Medium	2066	26	1.0	32392
53.5.1	Small	point	Medium	2066	26	1.0	32392

SGD ID	Size	Type	Intensity	Seepage Face Surface Area (Ft2)	Specific Discharge (GPD/Ft2)	Type Coefficient	SGD Flow (GPD)
53.6.1	Small	linear	low	2066	9	1.0	10842
53.7.1	Medium	linear	Medium/low	7266	17	1.0	76020
53.8.1	Small/Medium	diffuse	low	4666	9	0.3	7346
53.9.1	Small	point	low	2066	9	1.0	10842
53.10.1	Small	point	low	2066	9	1.0	10842
53.11.1	Large	diffuse	low	12465	9	0.3	19624
53.12.1	Large	diffuse	low	12465	9	0.3	19624
54.1.1	Small	diffuse	Medium/low	2066	17	0.3	6485
54.2.1	Small	linear	low	2066	9	1.0	10842
54.3.1	Large	diffuse	low	12465	9	0.3	19624
54.4.1	Large	diffuse	low	12465	9	0.3	19624
54.5.1	Large	diffuse	low	12465	9	0.3	19624
56.8.1	X- Large	diffuse	Medium/low	15065	17	0.3	47288
58.1.1	Small	linear	Medium	2066	26	1.0	32392
58.3.1	Small	point	high	2066	44	1.0	53942
58.4.1	Medium	dendritic	Medium/low	7266	17	1.0	76020
58.5.1	Medium	dendritic	Medium/low	7266	17	1.0	76020
58.6.1	Small	point	low	2066	9	1.0	10842
58.7.1	Small	point	low	2066	9	1.0	10842
58.8.1	Small	point	low	2066	9	1.0	10842
58.9.1	Small	point	Medium/high	2066	35	1.0	43167
58.10.1	Small	point	Medium/low	2066	17	1.0	21617
64.1.1	X- Large	diffuse	low	15065	9	0.3	23717
64.2.1	X- Large	diffuse	low	15065	9	0.3	23717
64.3.1	X- Large	diffuse	low	15065	9	0.3	23717
66.1.1	Small/Medium	point	high	4666	44	1.0	121827
66.2.1	Small	point	Medium	2066	26	1.0	32392
66.3.1	Small	point	Medium	2066	26	1.0	32392
66.4.1	X- Large	diffuse	low	15065	9	0.3	23717
67.1.1	Small	point	Medium/low	2066	17	1.0	21617
67.2.1	Large	diffuse	Medium/high	12465	35	0.3	78133
67.3.1	Small	point	low	2066	9	1.0	10842
67.4.1	Small	point	low	2066	9	1.0	10842
67.5.1	Small	point	low	2066	9	1.0	10842
67.6.1	Small	point	Medium/low	2066	17	1.0	21617
67.7.1	X- Large	diffuse	low	15065	9	0.3	23717
67.8.1	medium	diffuse	low	7266	9	0.3	11438
69.1.1	Small	diffuse	low	2066	9	0.3	3253
69.3.1	Large	linear	Medium/low	12465	17	1.0	130423
69.4.1	Small	diffuse	Medium/low	2066	17	0.3	6485
70.1.1	Small/Medium	linear	Medium/high	4666	35	1.0	97491
70.2.1	Small	linear	Medium	2066	26	1.0	32392
70.3.1	Small	diffuse	low	2066	9	0.3	3253
70.4.1	Small	diffuse	low	2066	9	0.3	3253

SGD ID	Size	Type	Intensity	Seepage Face Surface Area (Ft2)	Specific Discharge (GPD/Ft2)	Type Coefficient	SGD Flow (GPD)
70.5.1	Small	diffuse	medium	2066	26	0.3	9718
71.1.1	Small	diffuse	low	2066	9	0.3	3253
71.2.1	Small	point	low	2066	9	1.0	10842
71.3.1	Small	diffuse	low	2066	9	0.3	3253
73.1.1	Small	point	Medium	2066	26	1.0	32392
73.2.1	Medium	linear	Medium	7266	26	1.0	113913
73.3.1	Small	point	Medium/low	2066	17	1.0	21617
74.2.1	Small	diffuse	low	2066	9	0.3	3253
74.5.1	medium	diffuse	low	7266	9	0.3	11438
74.6.1	medium	diffuse	low	7266	9	0.3	11438
75.1.1	X- Large	diffuse	low	15065	9	0.3	23717
77.1.1	Small	diffuse	low	2066	9	0.3	3253
77.2.1	Large	diffuse	low	12465	9	0.3	19624
78.1.1	Small	linear	low	2066	9	1.0	10842
80.1.1	Small	diffuse	low	2066	9	0.3	3253
80.2.1	Small/Medium	linear	Medium/low	4666	17	1.0	48821
80.3.1	Small	point	low	2066	9	1.0	10842
80.4.1	Small	point	low	2066	9	1.0	10842
80.5.1	Small	point	Medium/low	2066	17	1.0	21617
80.6.1	Small	diffuse	low	2066	9	0.3	3253
80.7.1	Small	linear	low	2066	9	1.0	10842
81.1.1	Medium/Large	diffuse	low	9865	9	0.3	15531
81.2.1	Small/Medium	diffuse	low	4666	9	0.3	7346
81.3.1	Large	diffuse	low	12465	9	0.3	19624
82.1.1	Small/Medium	point	Medium/high	4666	35	1.0	97491
83.1.1	Small	diffuse	low	2066	9	0.3	3253
83.2.1	Small/Medium	linear	Medium/high	4666	35	1.0	97491
84.1.1	Large	diffuse	Medium/low	12465	17	0.3	39127
84.2.1	X- Large	dendritic	Medium/low	15065	17	1.0	157627
84.3.1	Small/Medium	dendritic	low	4666	9	1.0	24486
84.4.1	Small	diffuse	Medium/low	2066	17	0.3	6485
84.5.1	Small	diffuse	Medium/low	2066	17	0.3	6485
84.6.1	Small	linear	low	2066	9	1.0	10842

TIR	Total SGD (GPD)		4,930,406
TIR	Total SGD (cfs)		7.63
TIR	Total SGD (MGD)		4.93
TIR	Average (GPD)		30,248
	stdev (GPD)		38,506
	max (GPD)		257,570
	min (GPD)		3,253

APPENDIX G

GROUNDWATER DISCHARGE ZONE DATABASE: THERMAL INFRARED IMAGES FOR APRIL 2000 SURVEY

KEYS TO SGD LOCATIONS

Following are 5 keys to SGD locations around the bay: the Little Bay, the Oyster River, lower Little Bay and Upper Great Bay, Western Great Bay, and Eastern Great Bay. Most of the SGDs are located in the keys. The exceptions are high-density populations of discharge zones, in which overlapping labels are excluded. In all cases, SGDs can be located by coordinates and nearby labels.

Little Bay SGD Labels

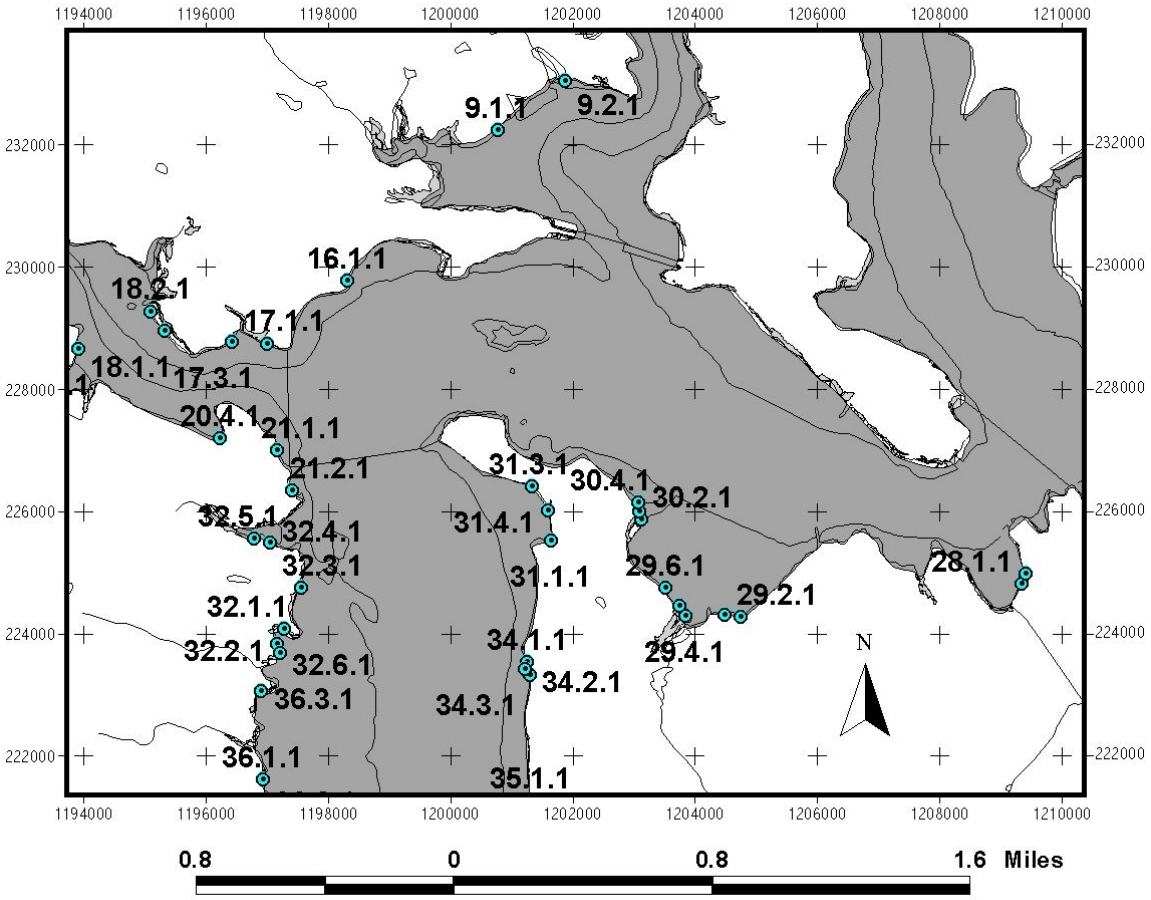

Oyster River SGD Labels

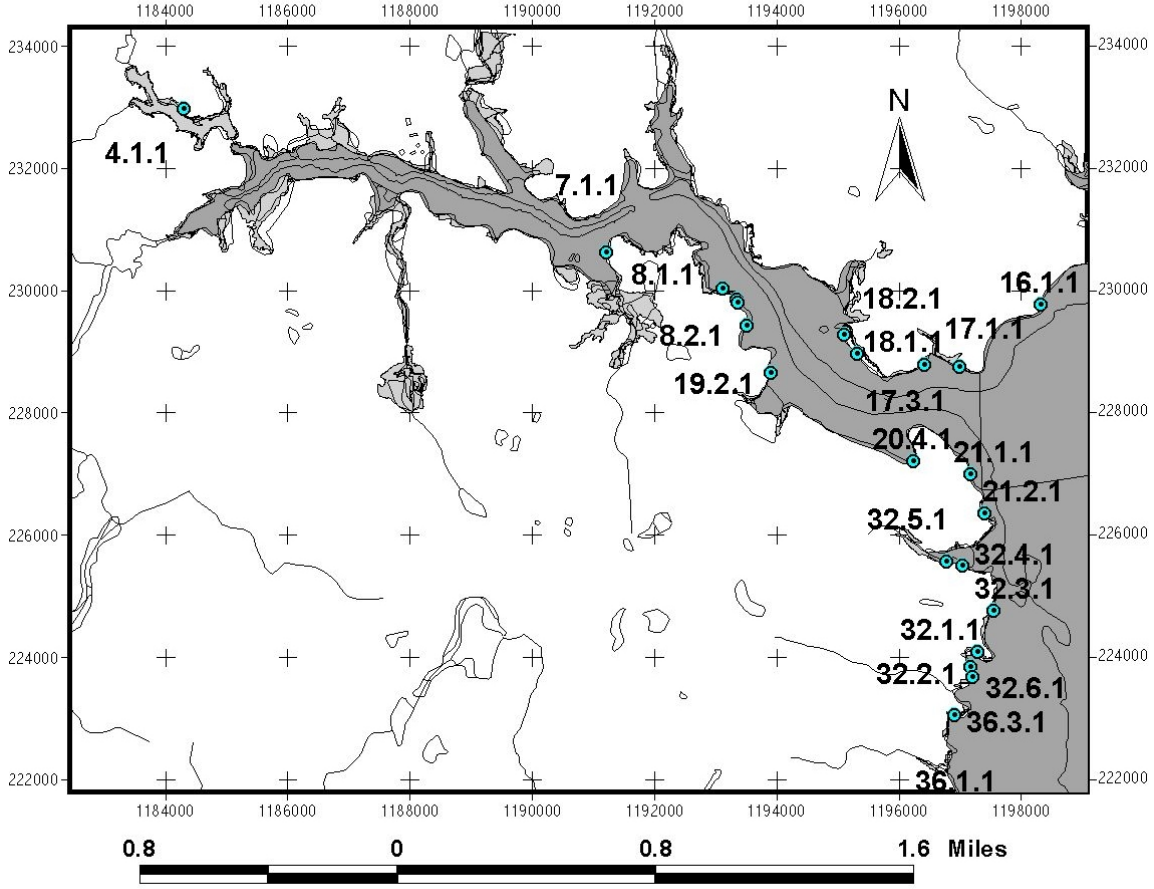

Lower Little Bay Upper Great Bay

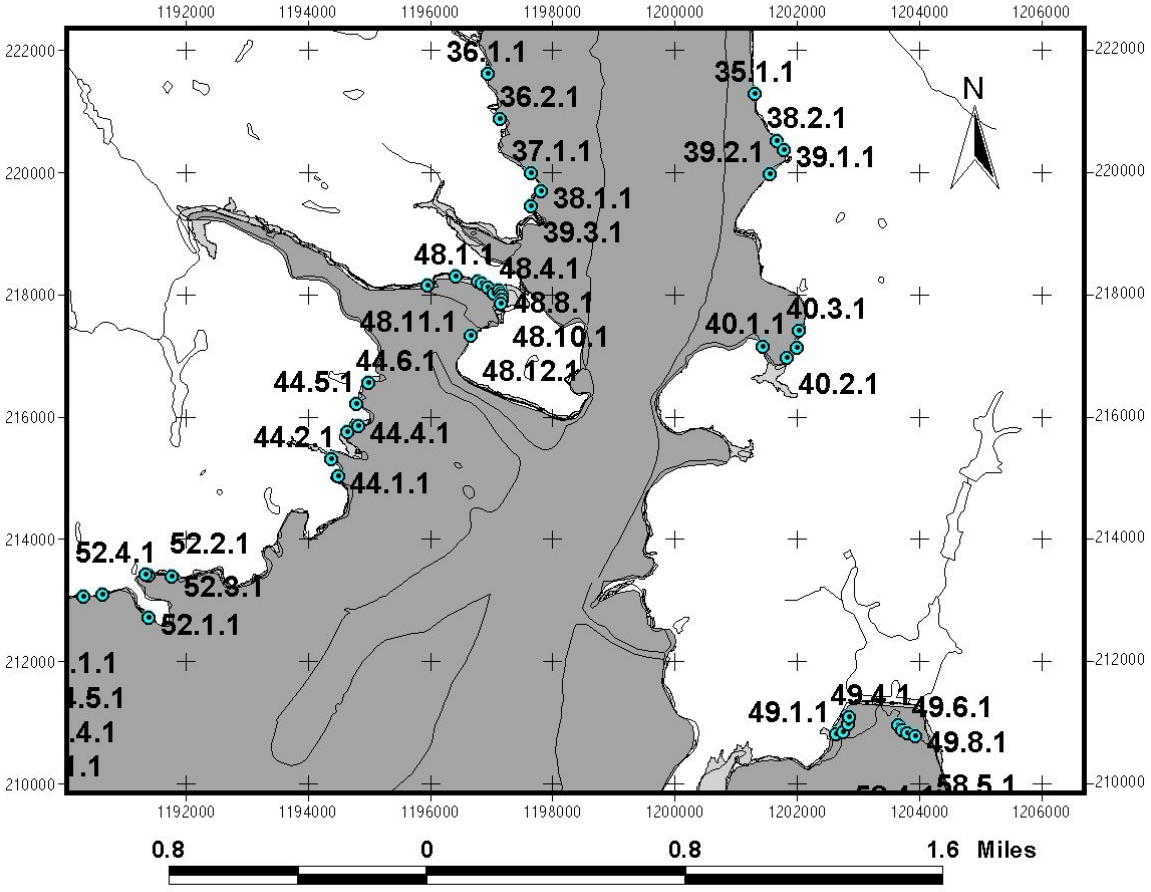

Western Great Bay

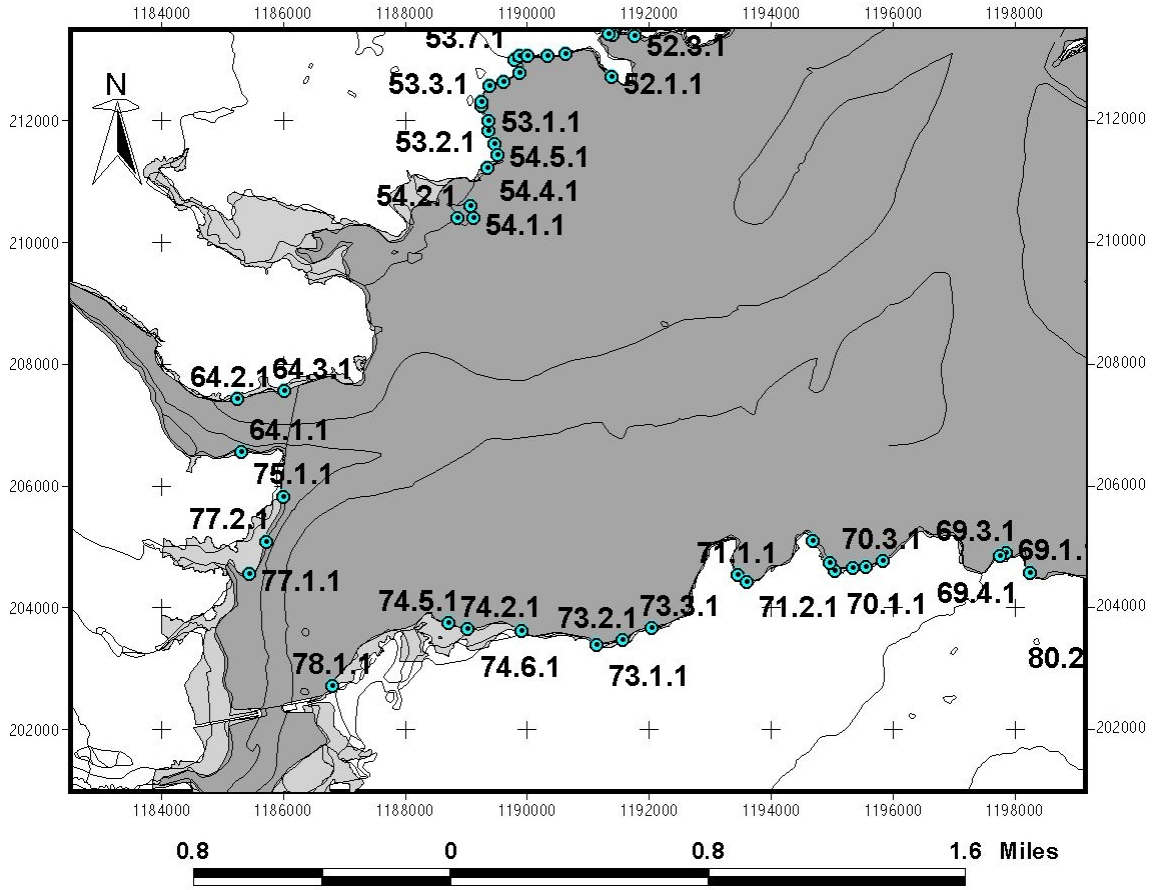

Eastern Great Bay

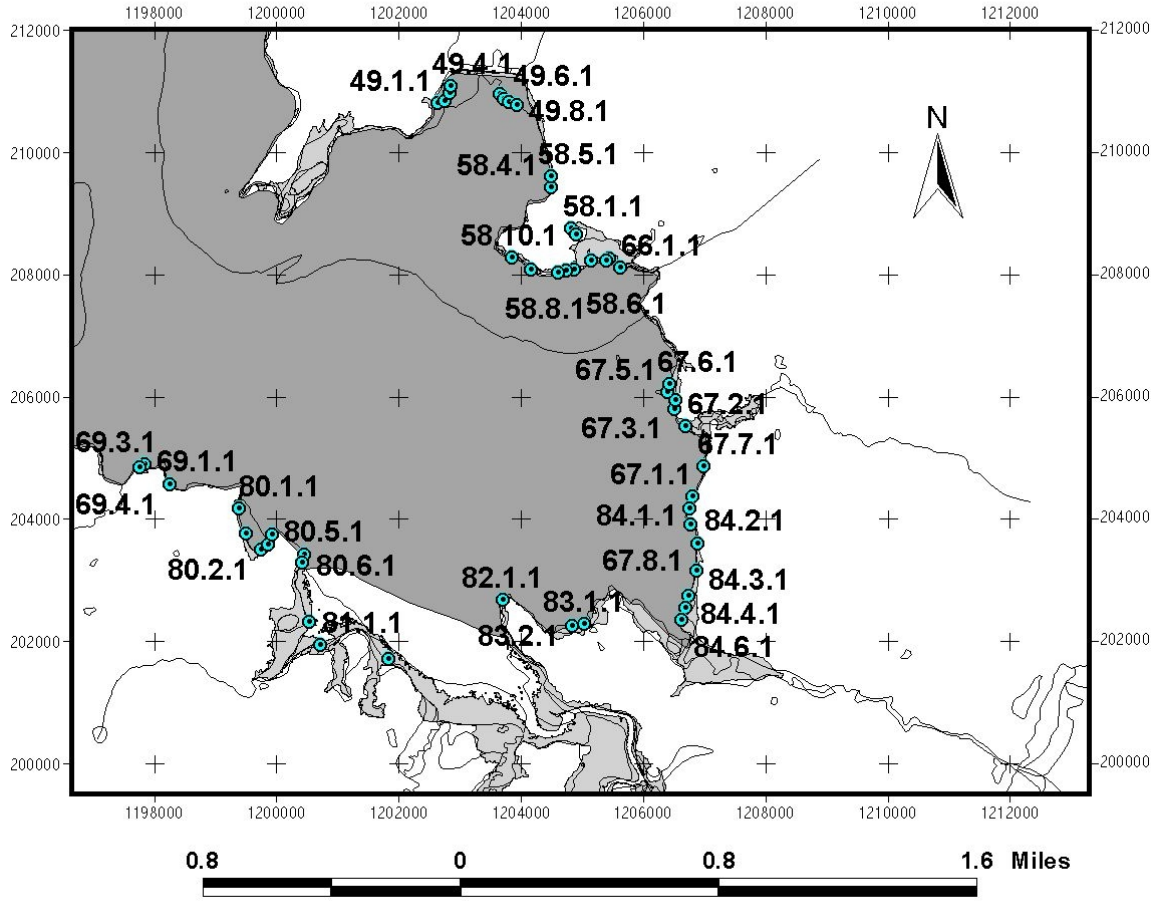

IMAGE FOUR

IMAGE SEVEN

IMAGE EIGHT

IMAGE NINE

IMAGE SIXTEEN

IMAGE SEVENTEEN

IMAGE EIGHTEEN

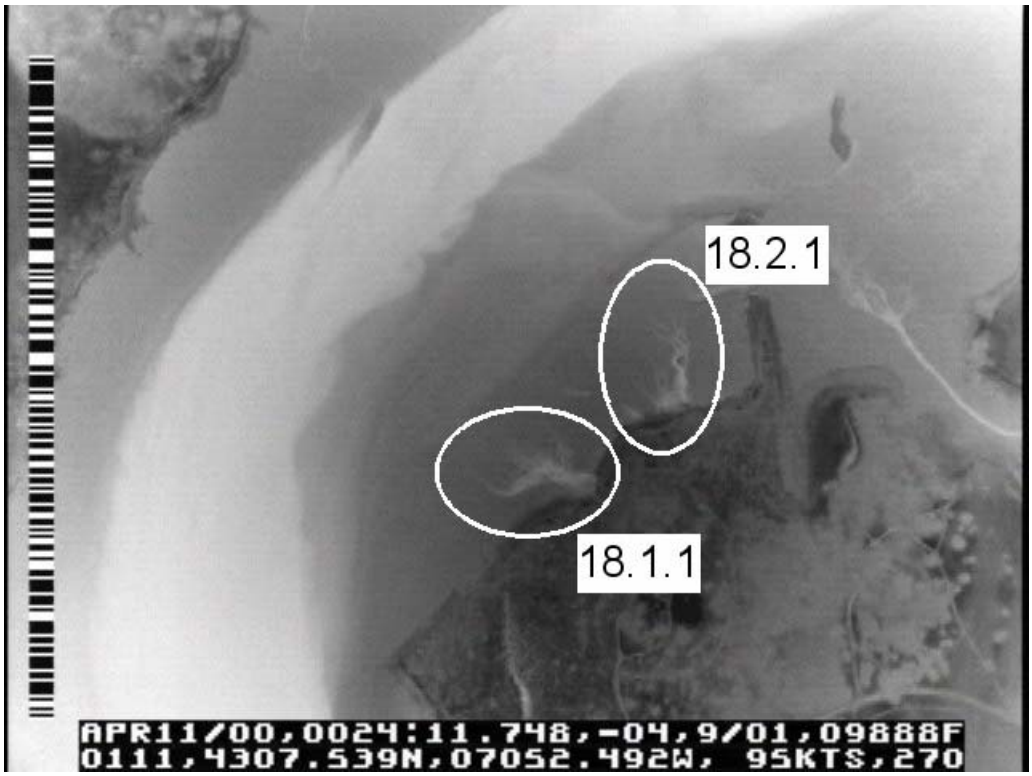

IMAGE NINETEEN

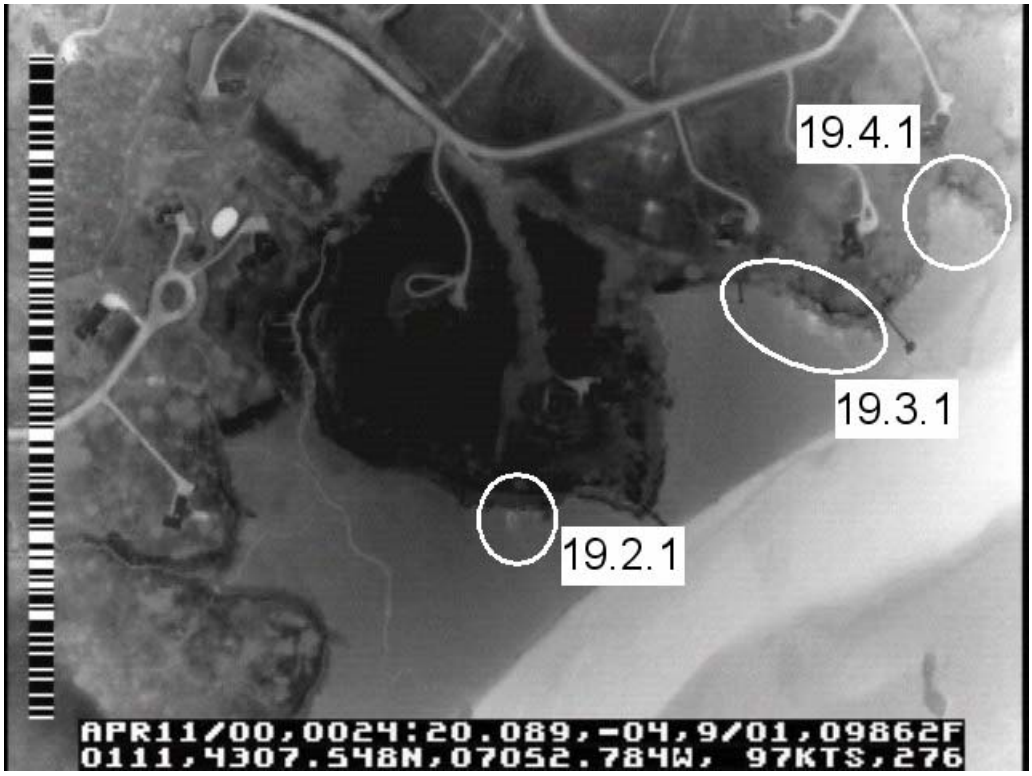

IMAGE TWENTY

IMAGE TWENTY-ONE

IMAGE TWENTY-EIGHT

IMAGE TWENTY-NINE

IMAGE THIRTY

IMAGE THIRTY-ONE

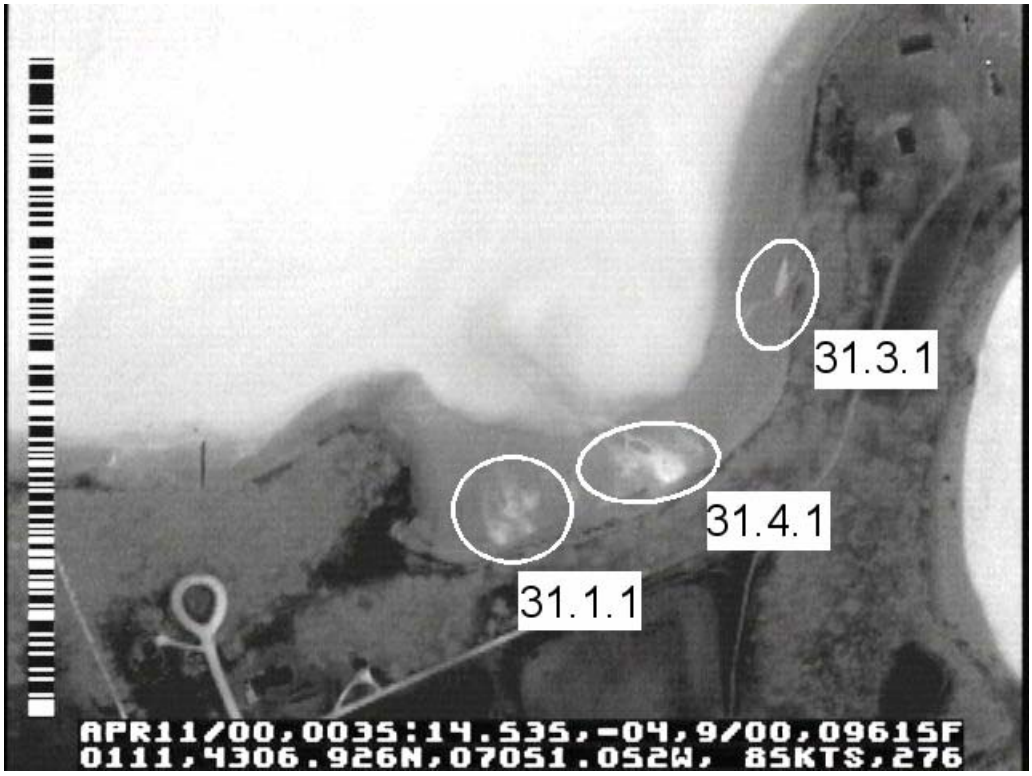

IMAGE THIRTY-TWO

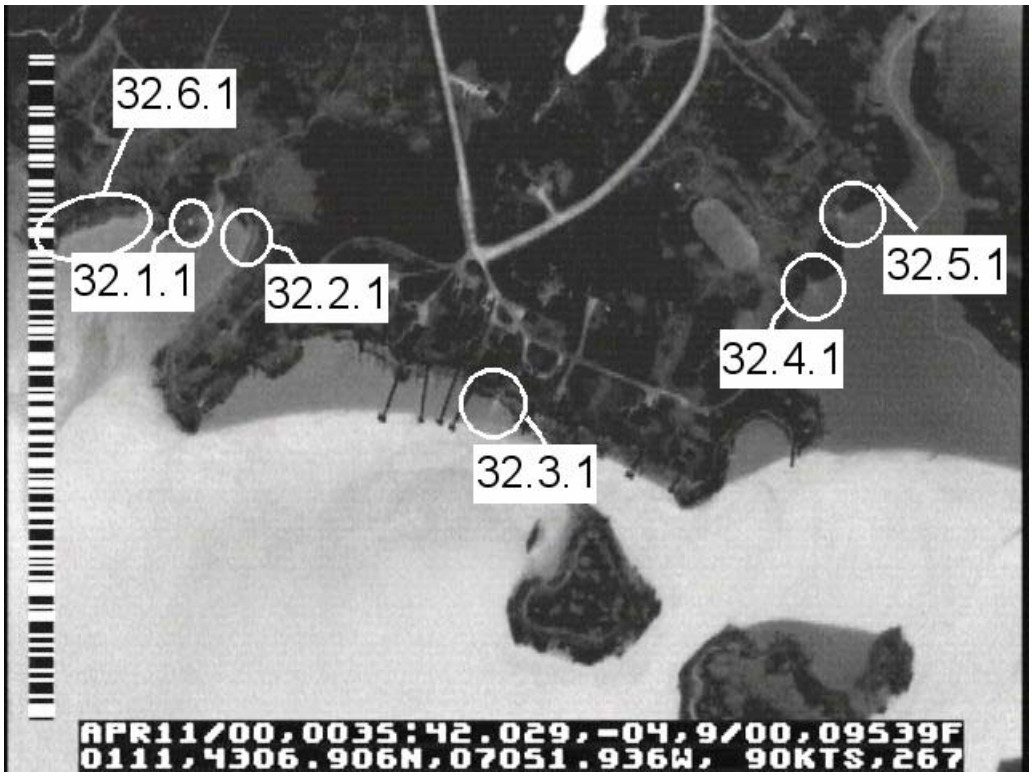

IMAGE THIRTY-THREE

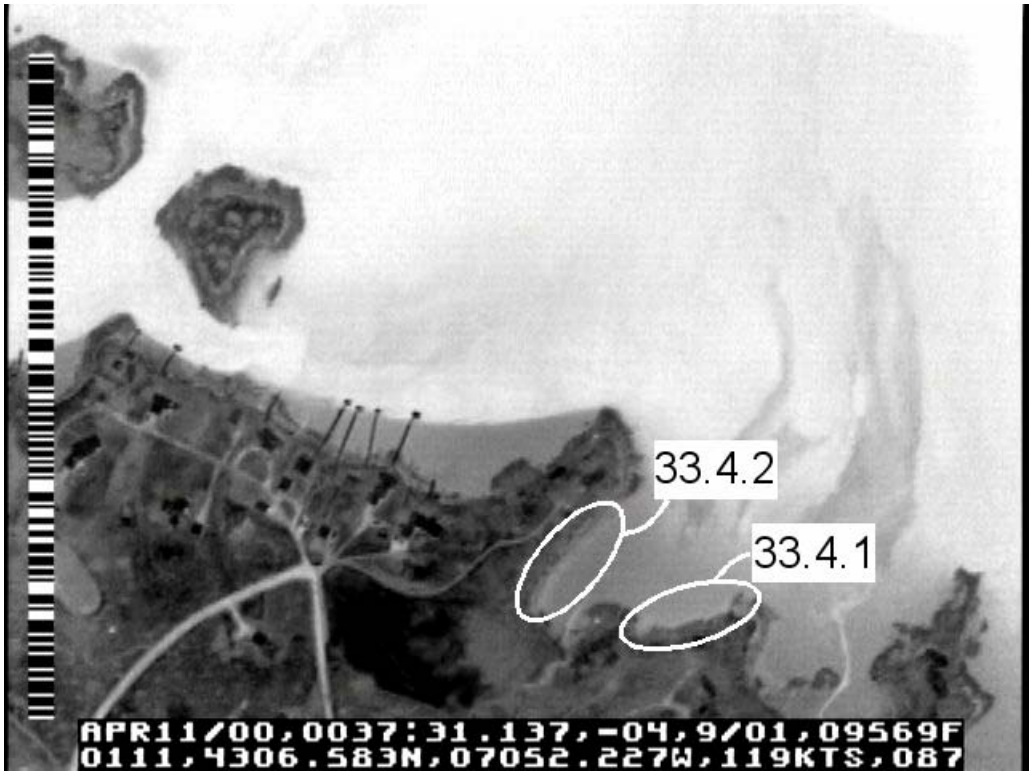

IMAGE THIRTY-FOUR

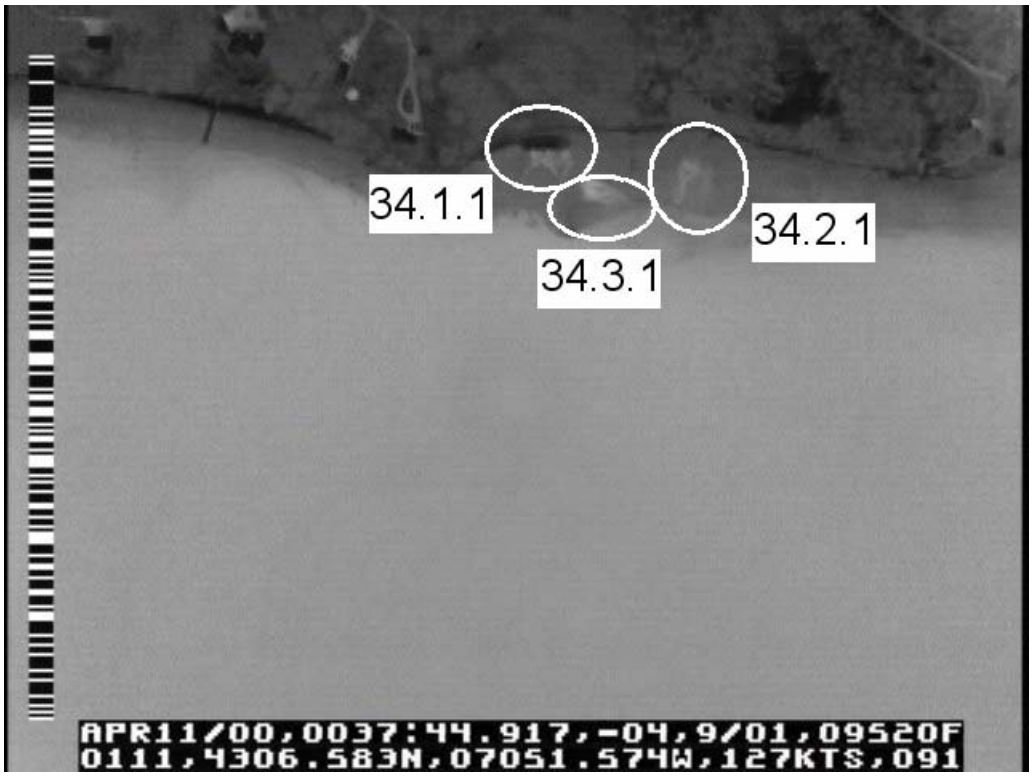

IMAGE THIRTY-FIVE

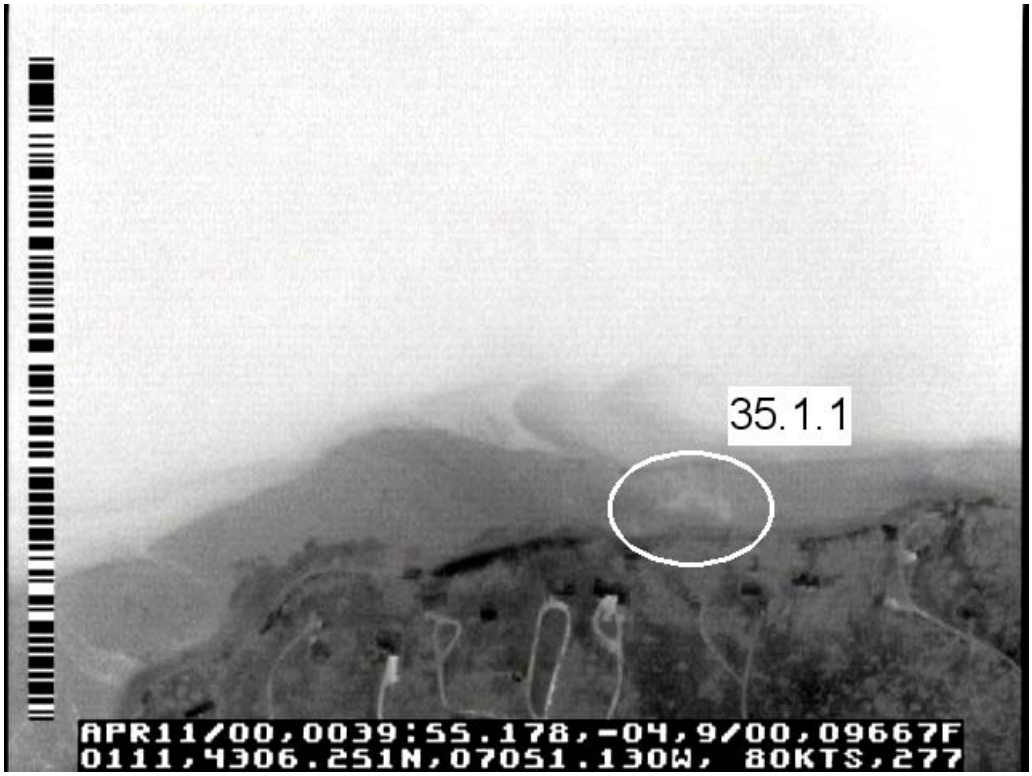

IMAGE THIRTY-SIX

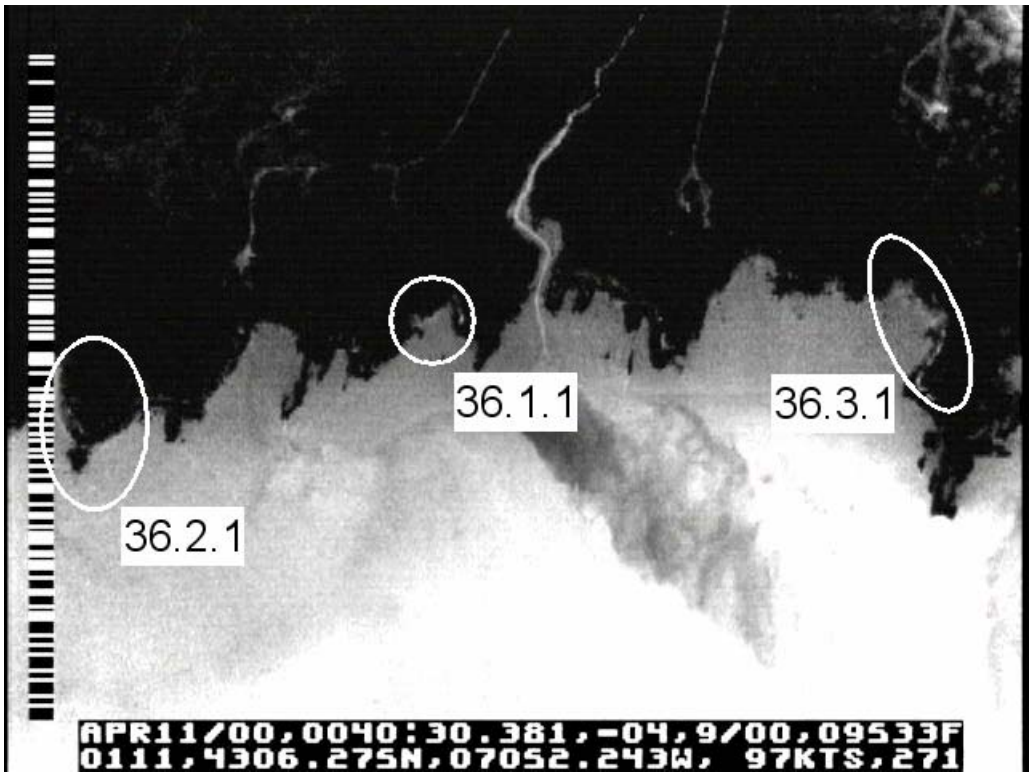

IMAGE THIRTY-SEVEN

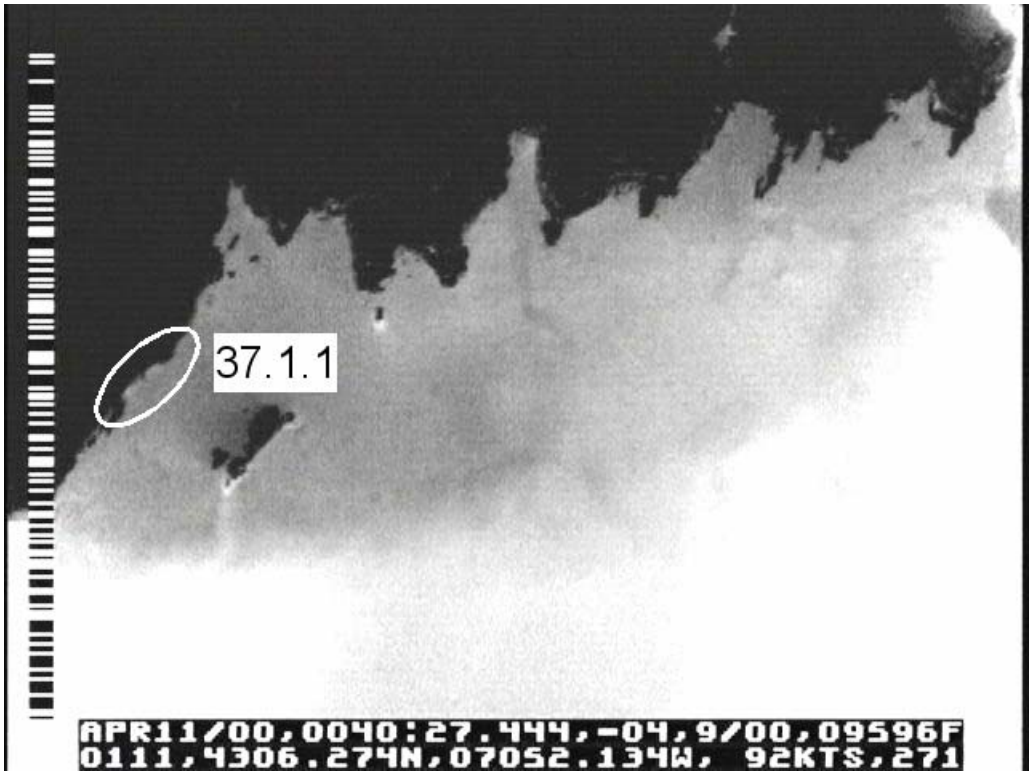

IMAGE THIRTY-EIGHT

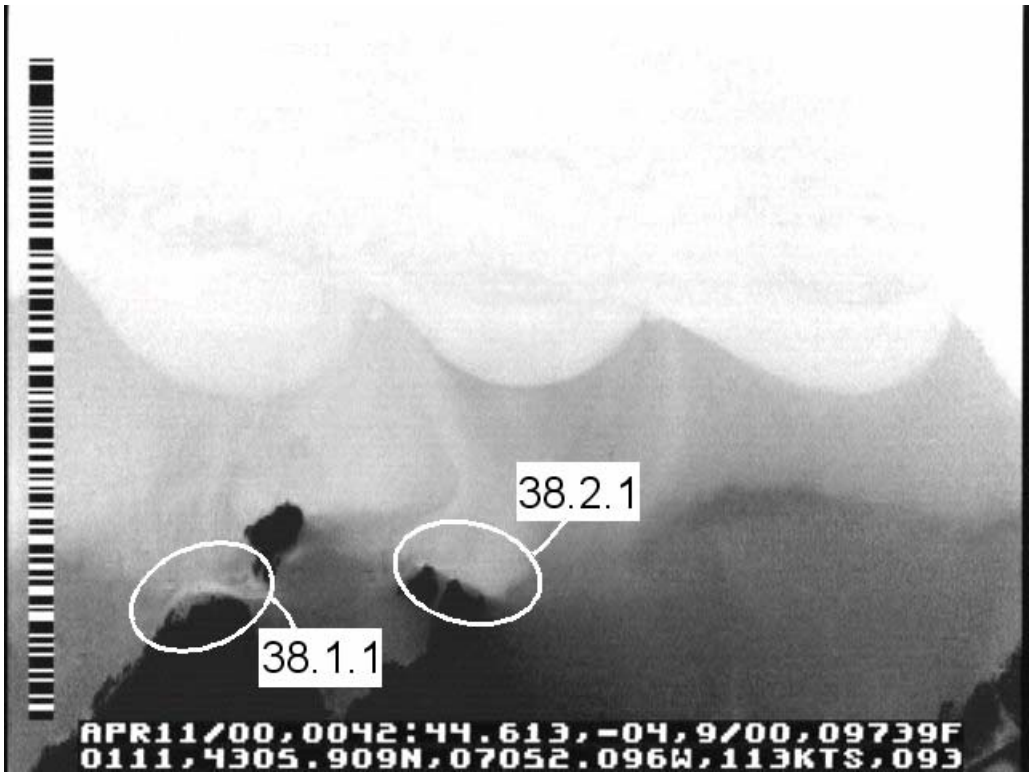

IMAGE THIRTY-NINE

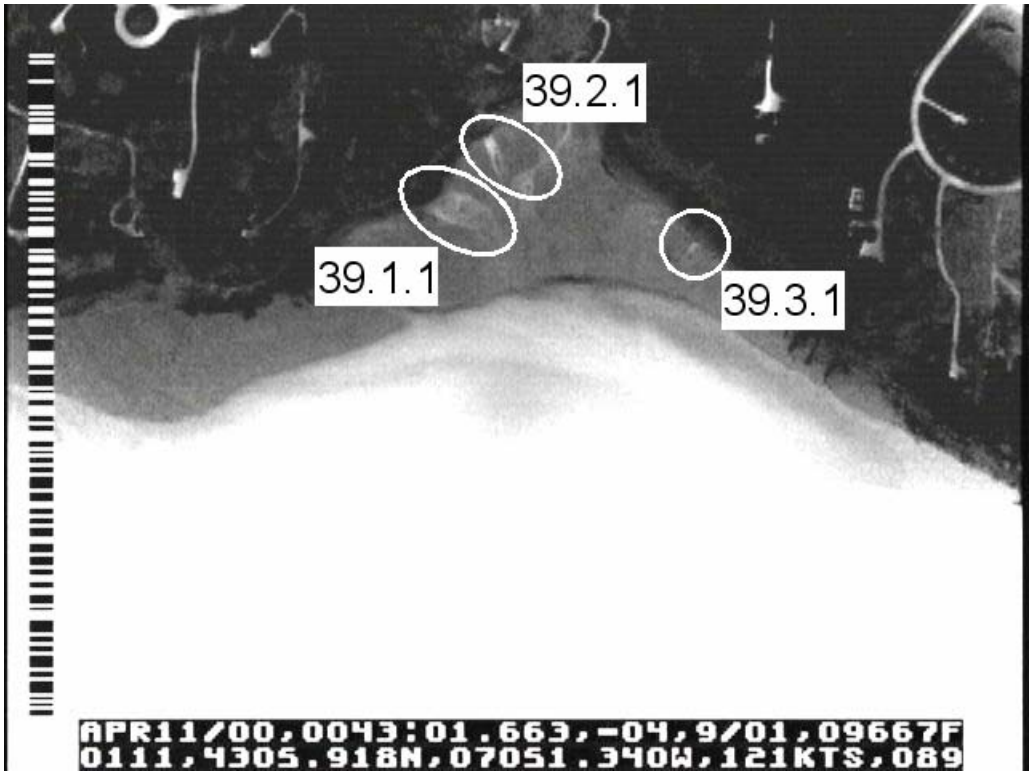

IMAGE FORTY

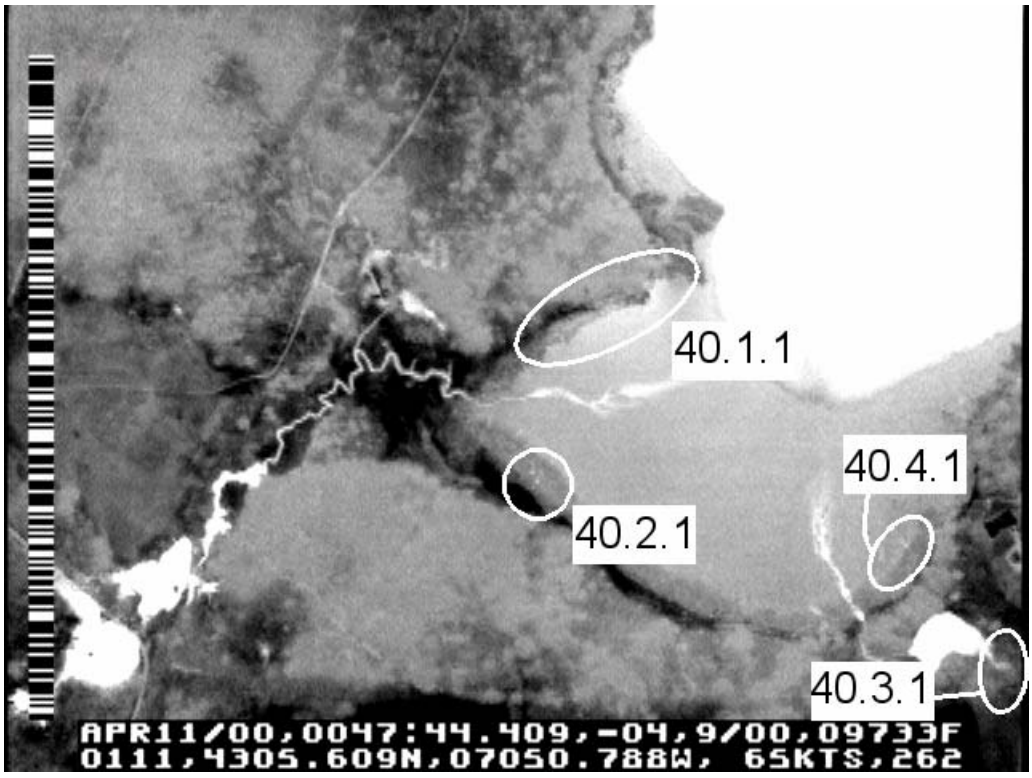

IMAGE FORTY-FOUR

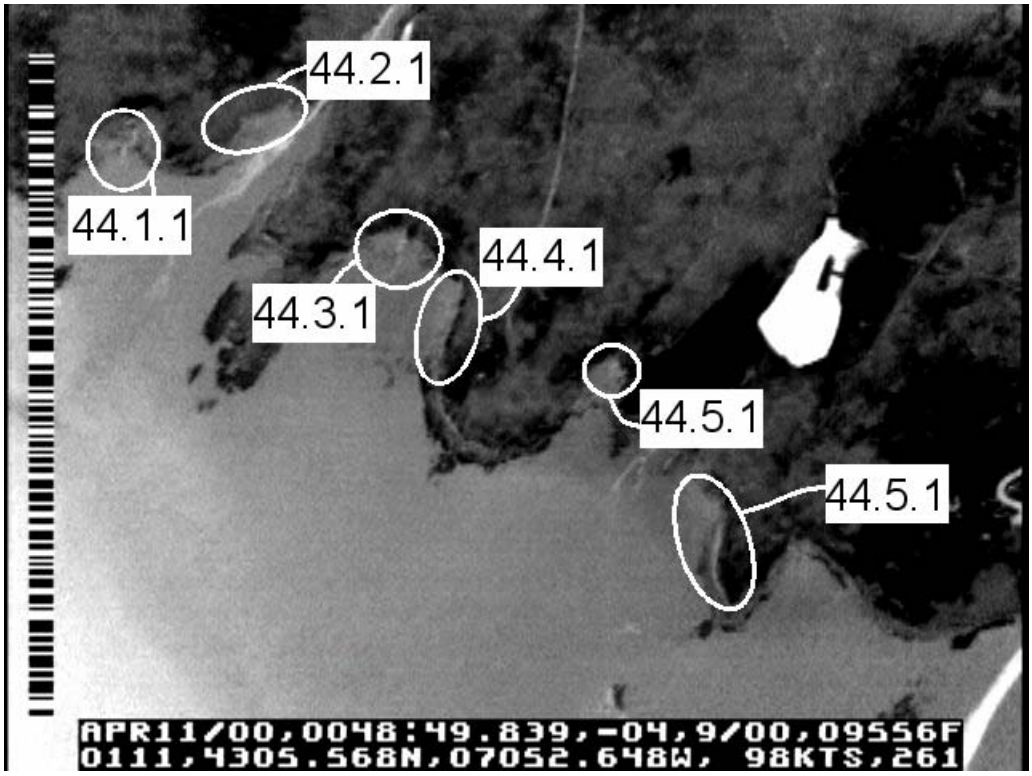

IMAGE FORTY-EIGHT

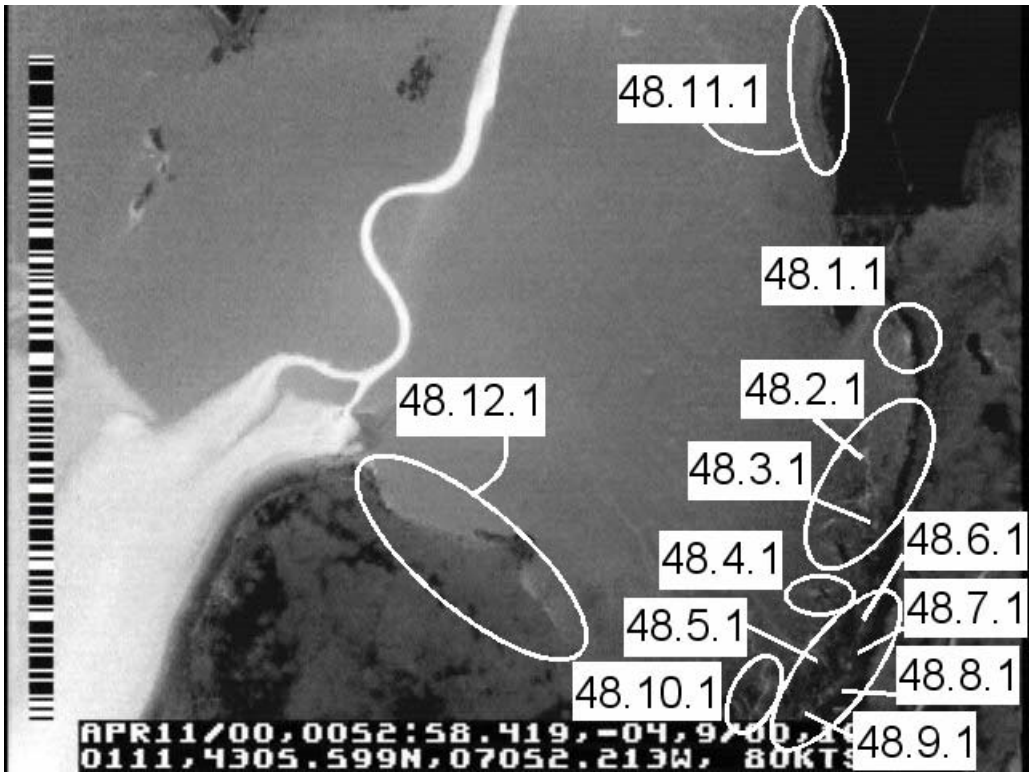

IMAGE FORTY-NINE

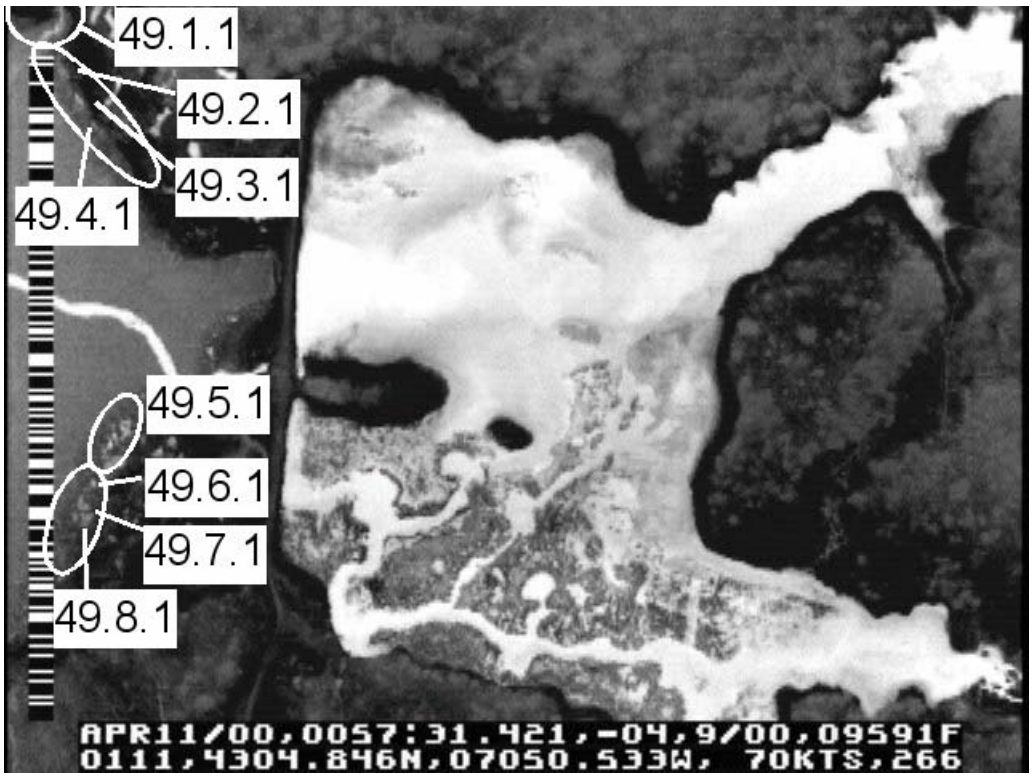

IMAGE FIFTY-TWO

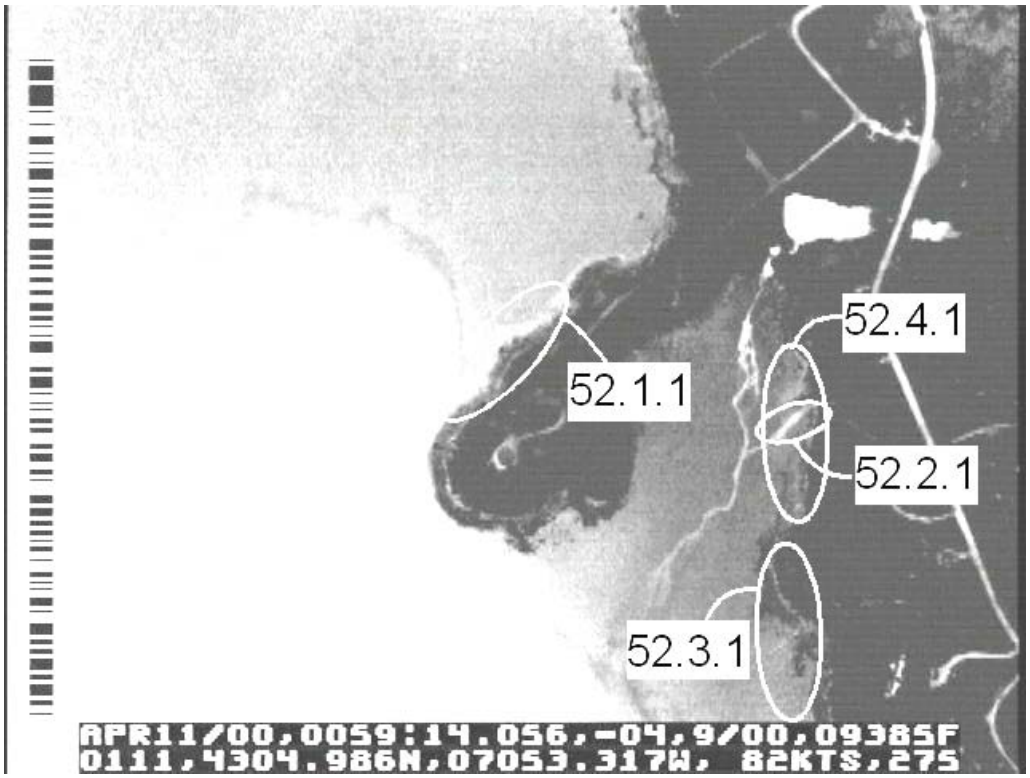

IMAGE FIFTY-THREE

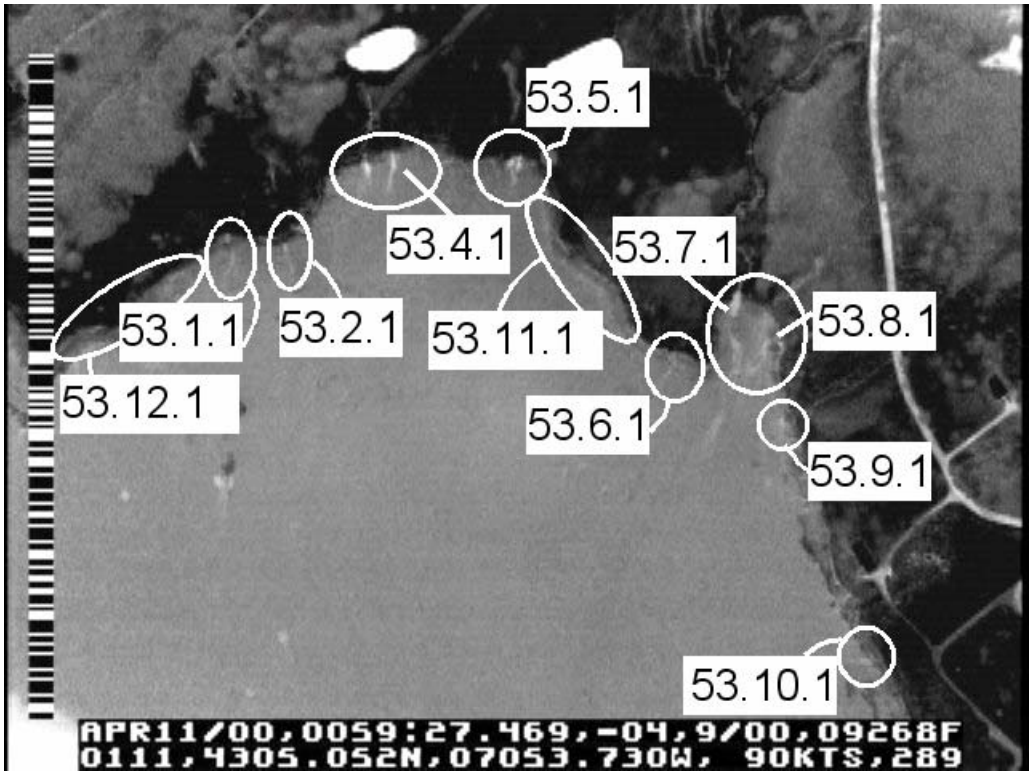

IMAGE FIFTY-FOUR

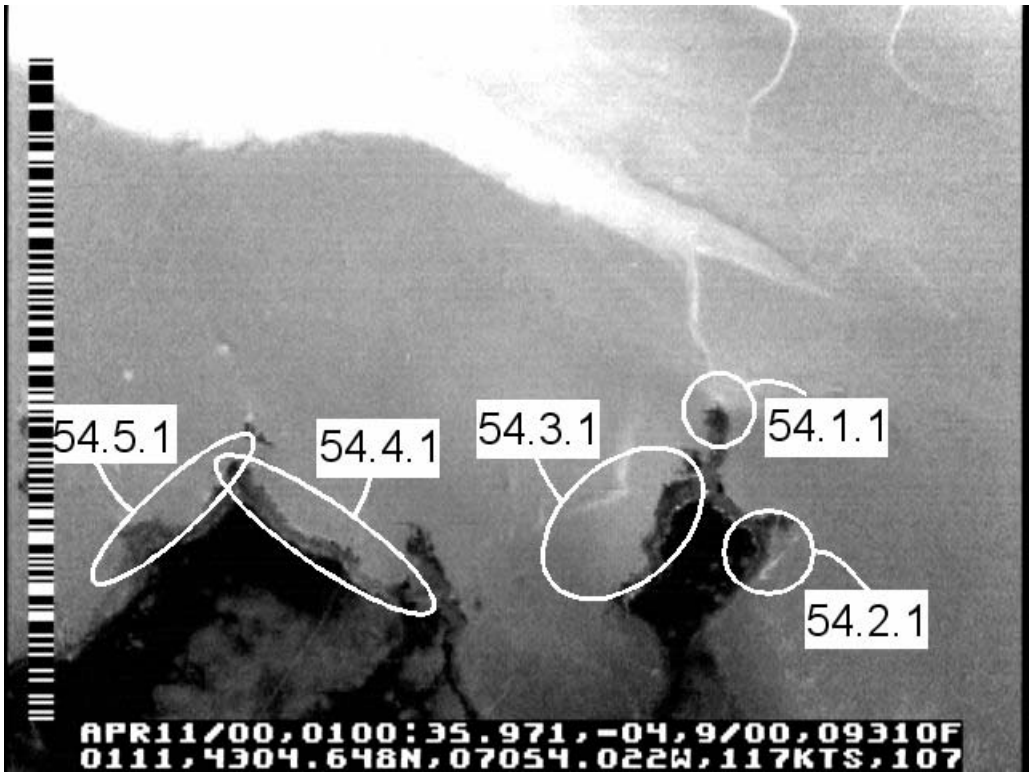

IMAGE FIFTY-SIX

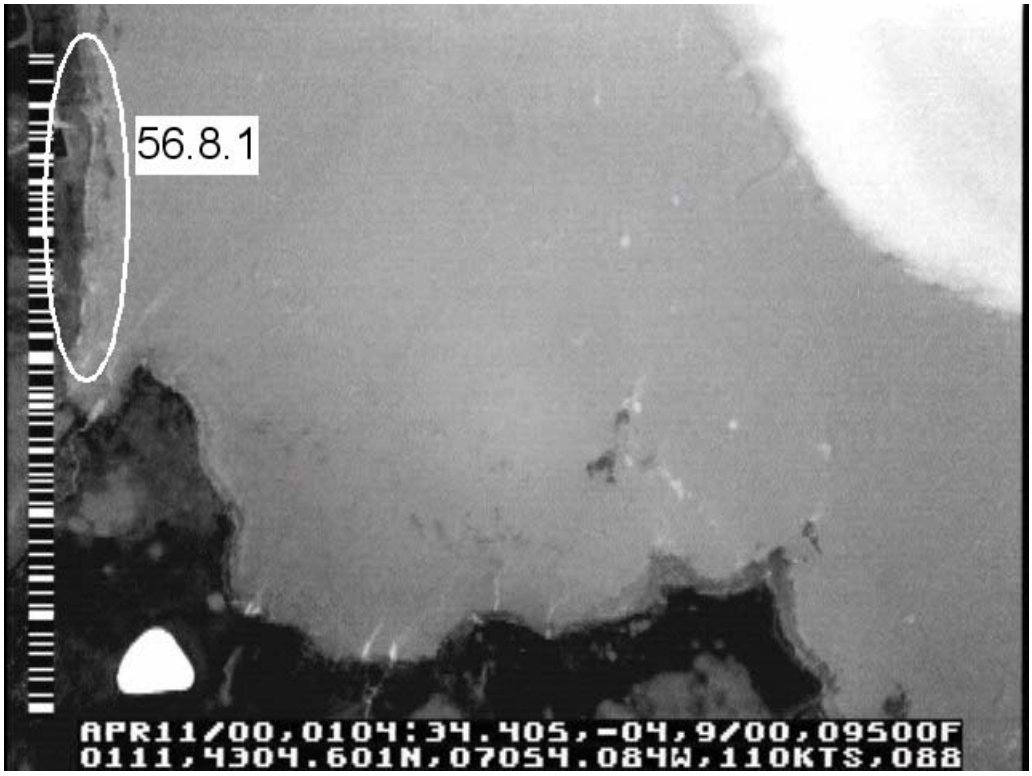

IMAGE FIFTY-EIGHT

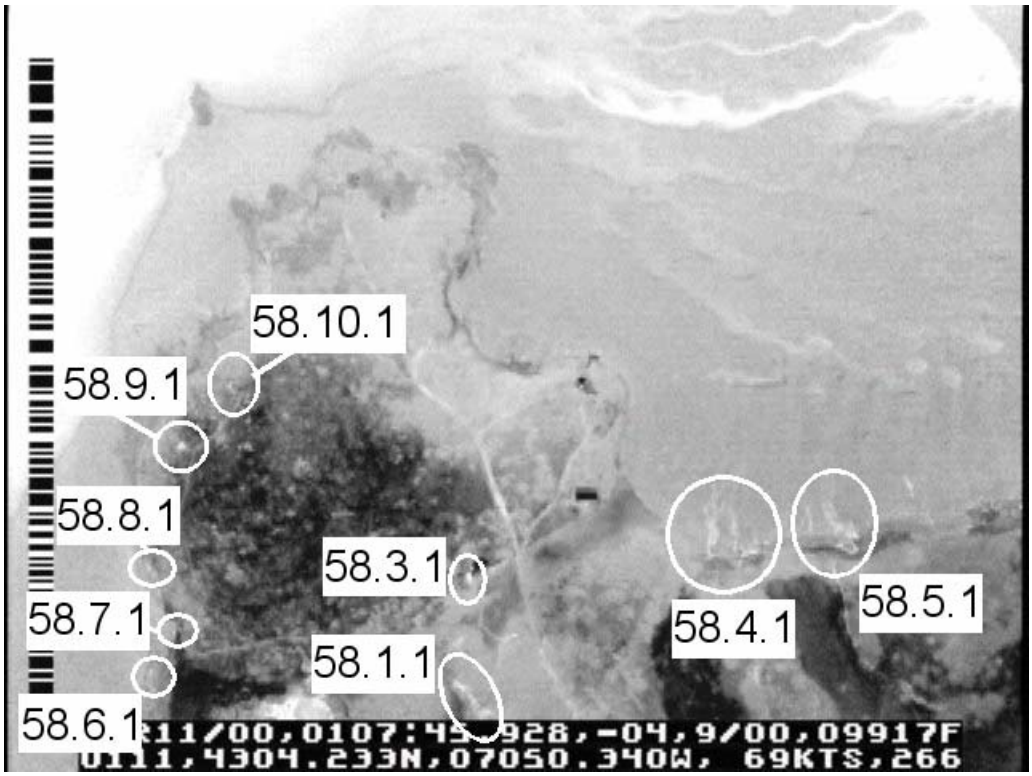

IMAGE SIXTY-FOUR

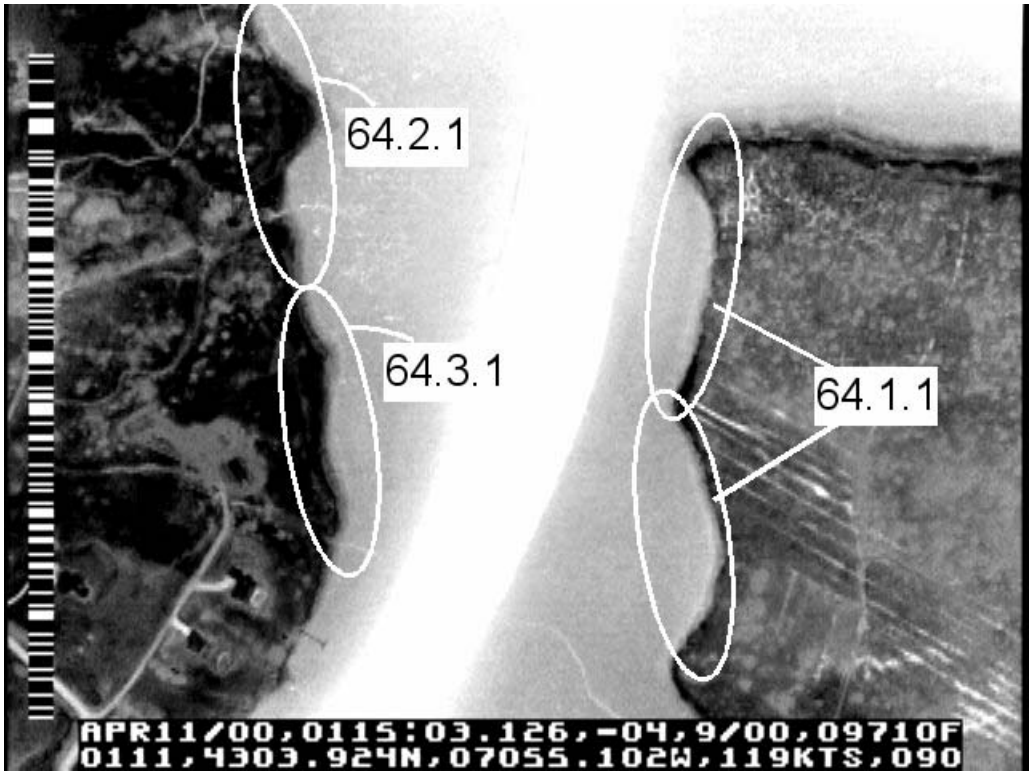

IMAGE SIXTY-SIX

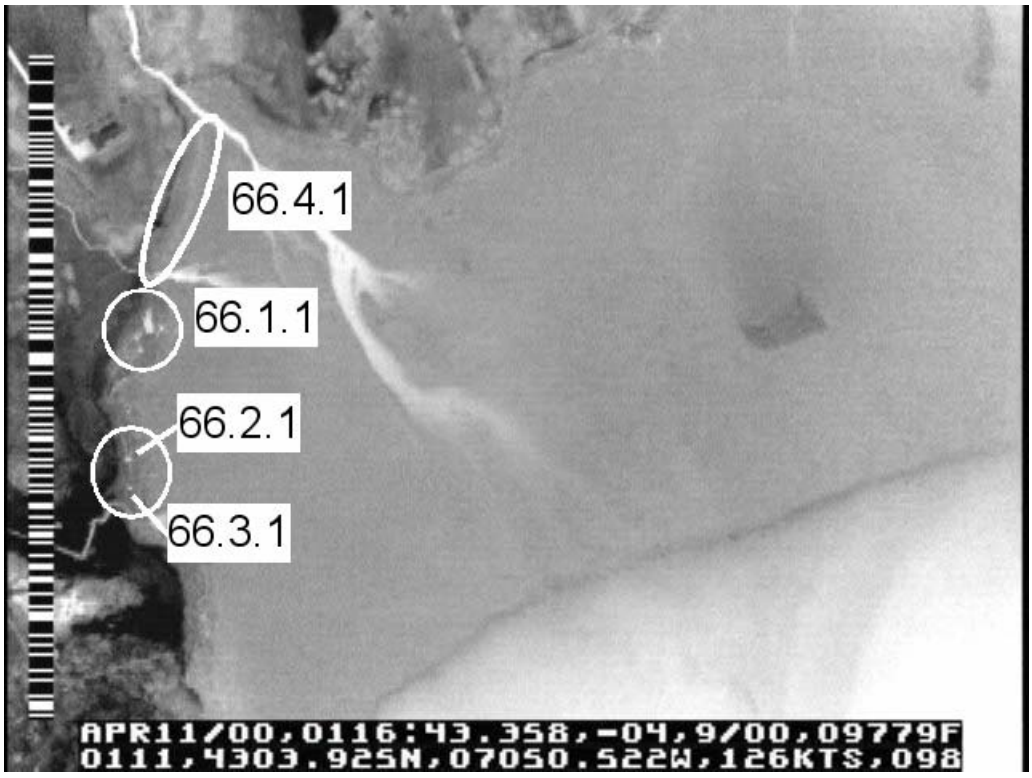

IMAGE SIXTY-SEVEN

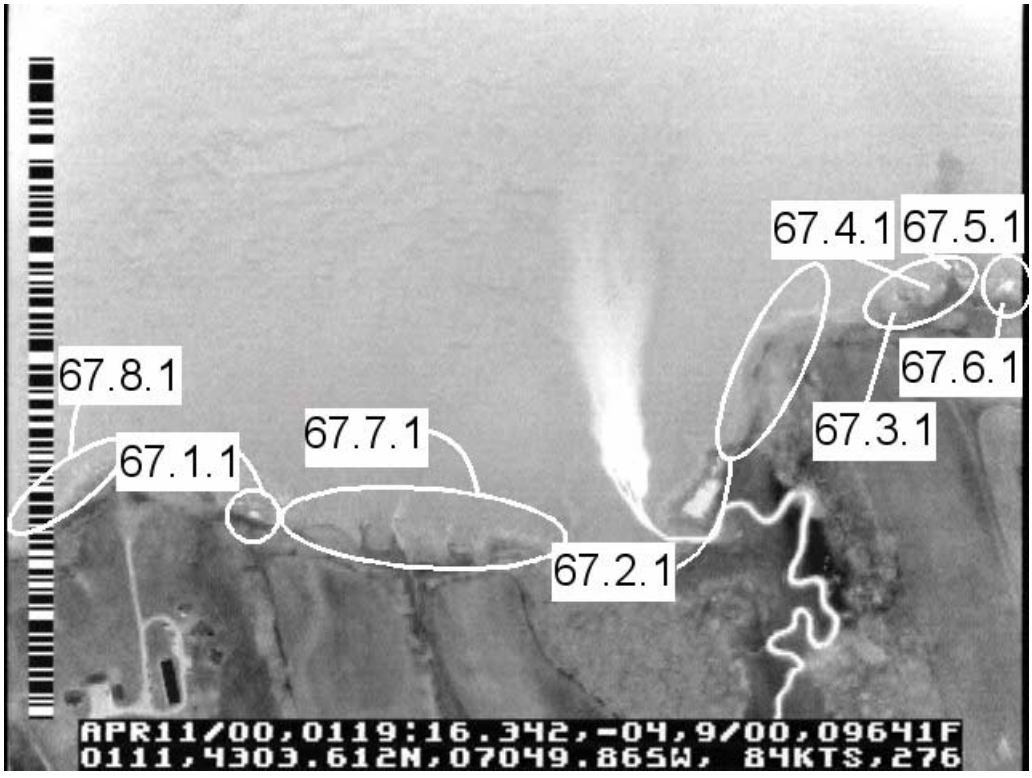

IMAGE SIXTY-NINE

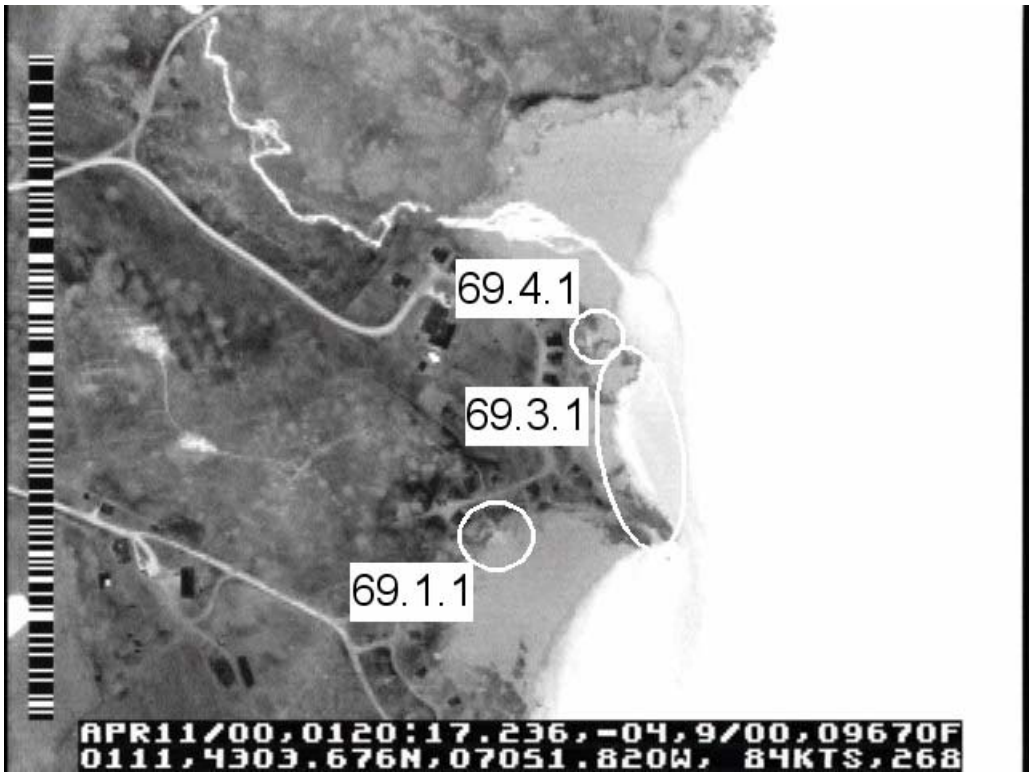

IMAGE SEVENTY

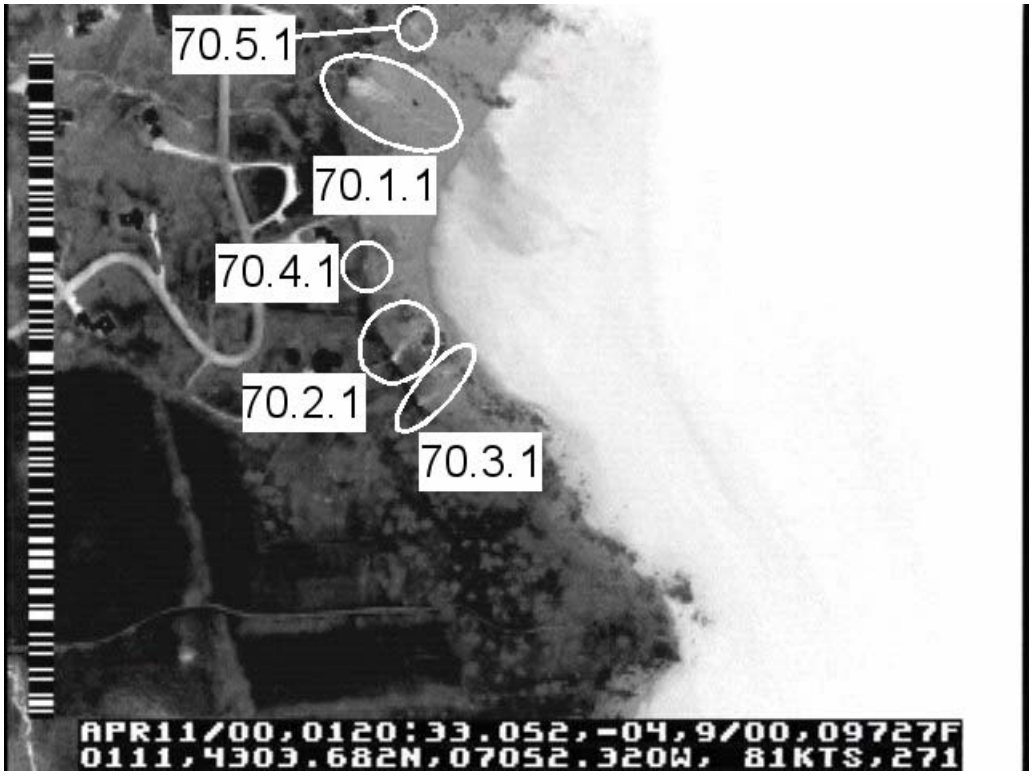

IMAGE SEVENTY-ONE

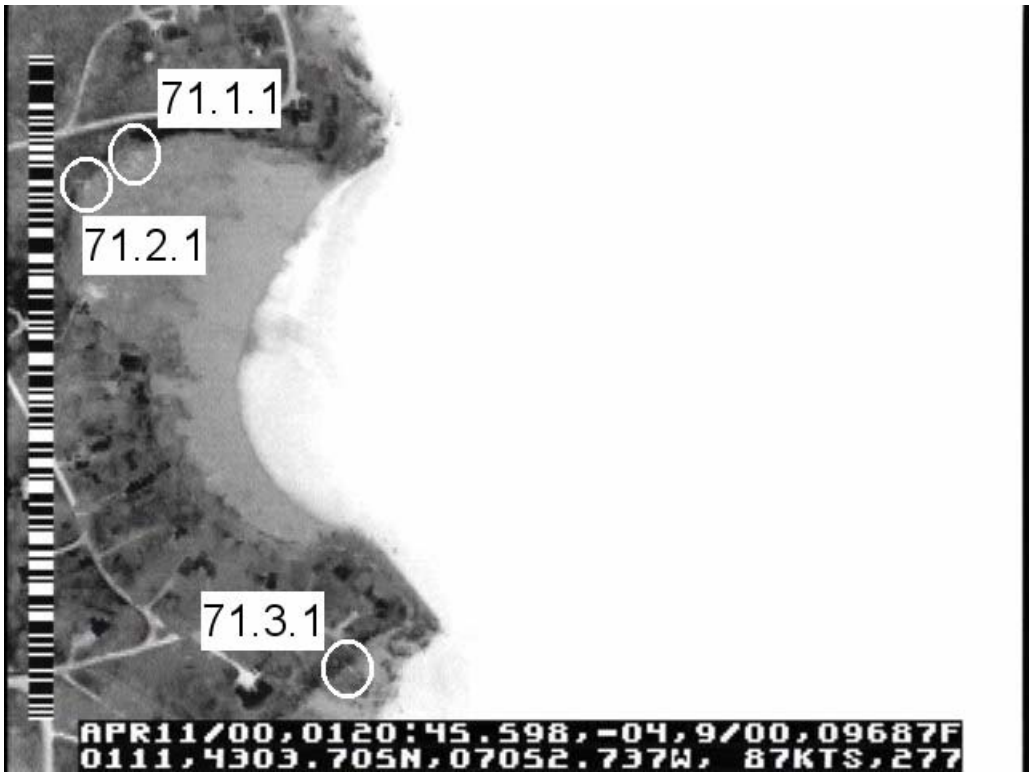

IMAGE SEVENTY-THREE

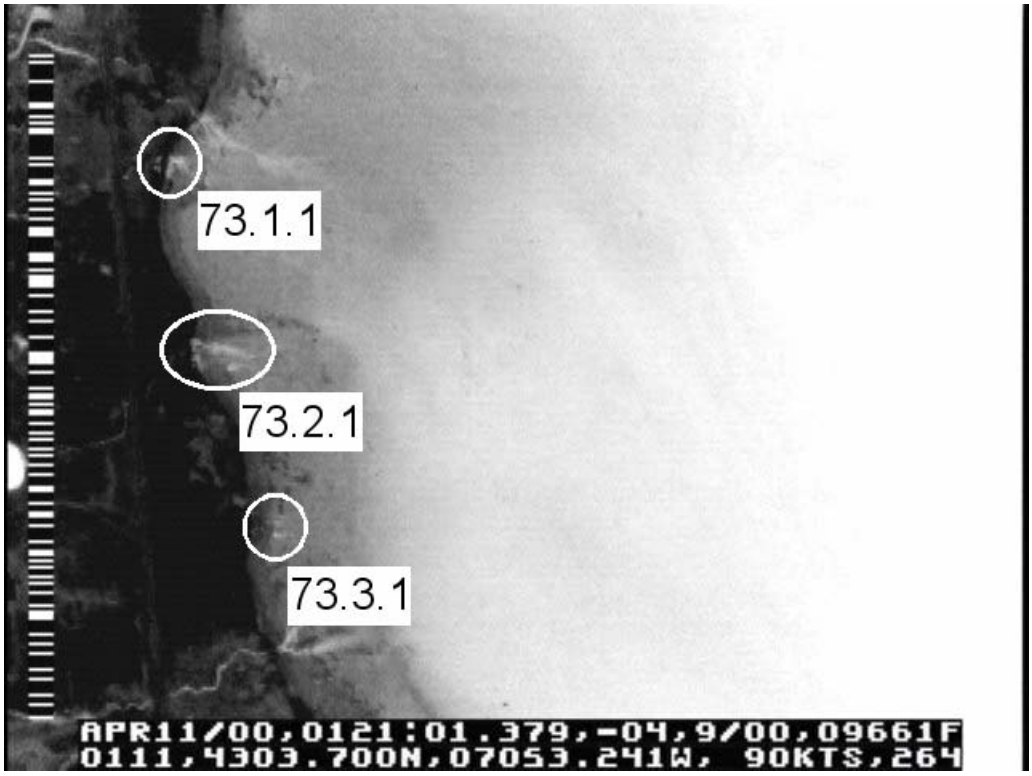

IMAGE SEVENTY-FOUR

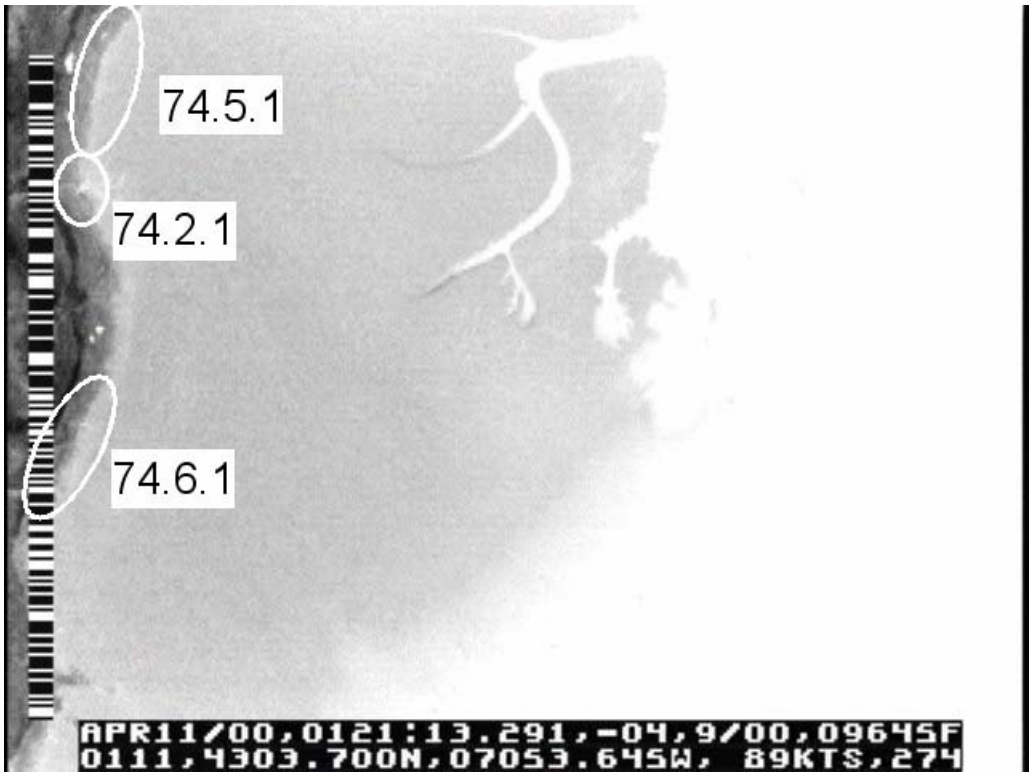

IMAGE SEVENTY-FIVE

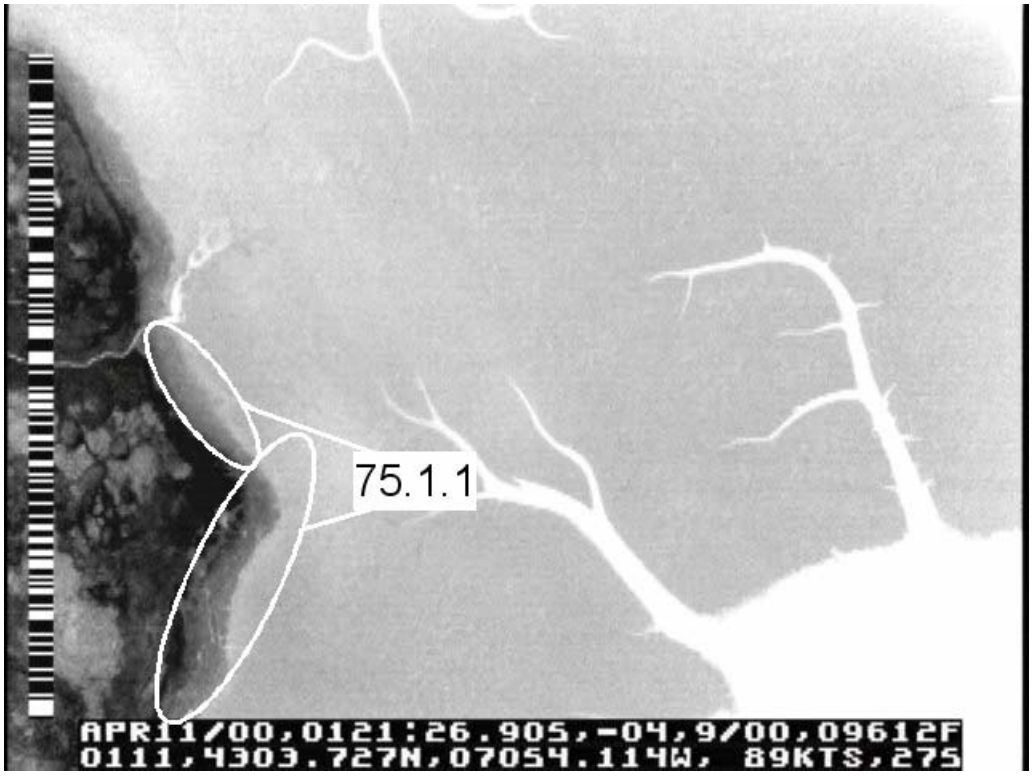

IMAGE SEVENTY-SEVEN

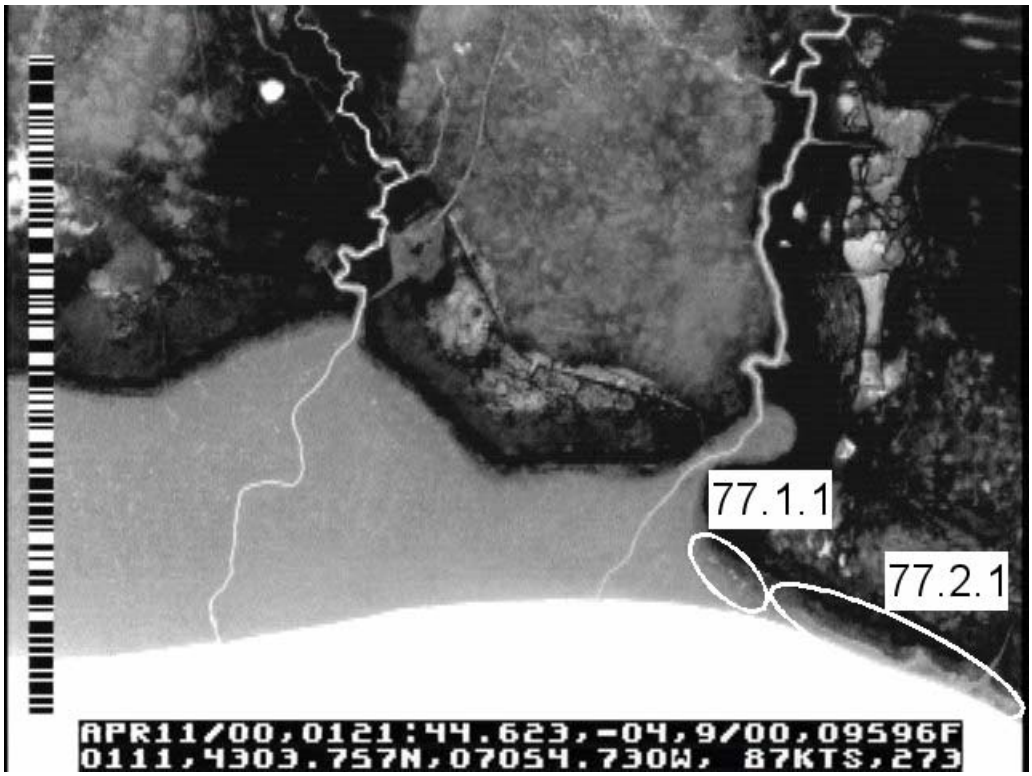

IMAGE SEVENTY-EIGHT

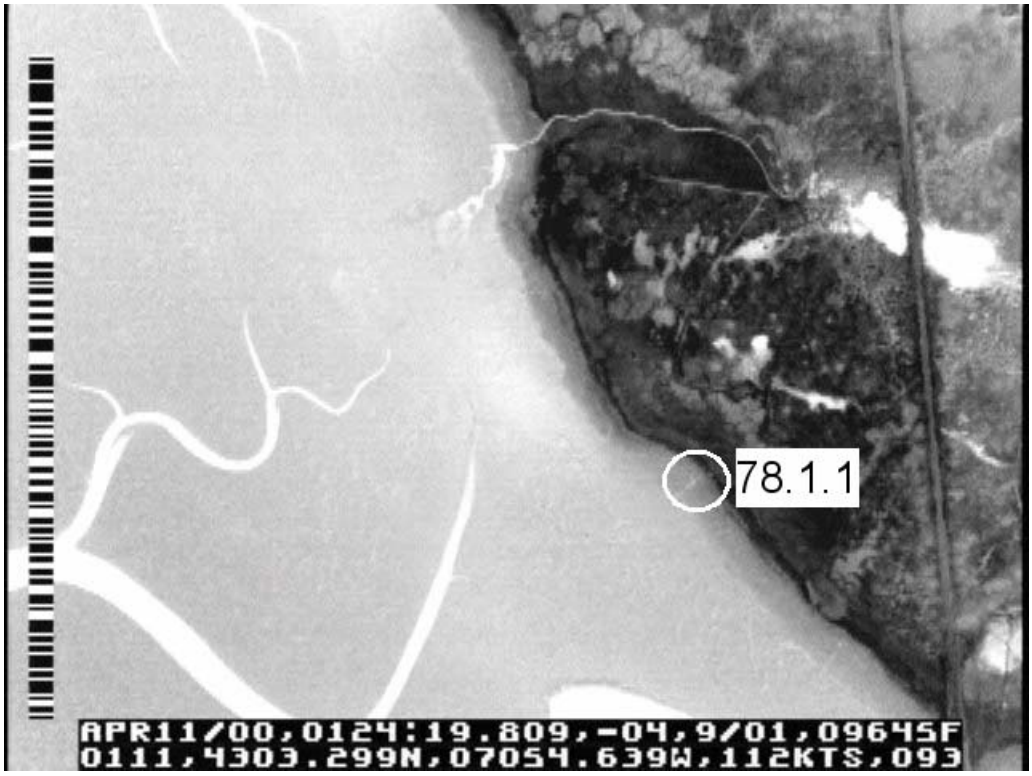

IMAGE EIGHTY

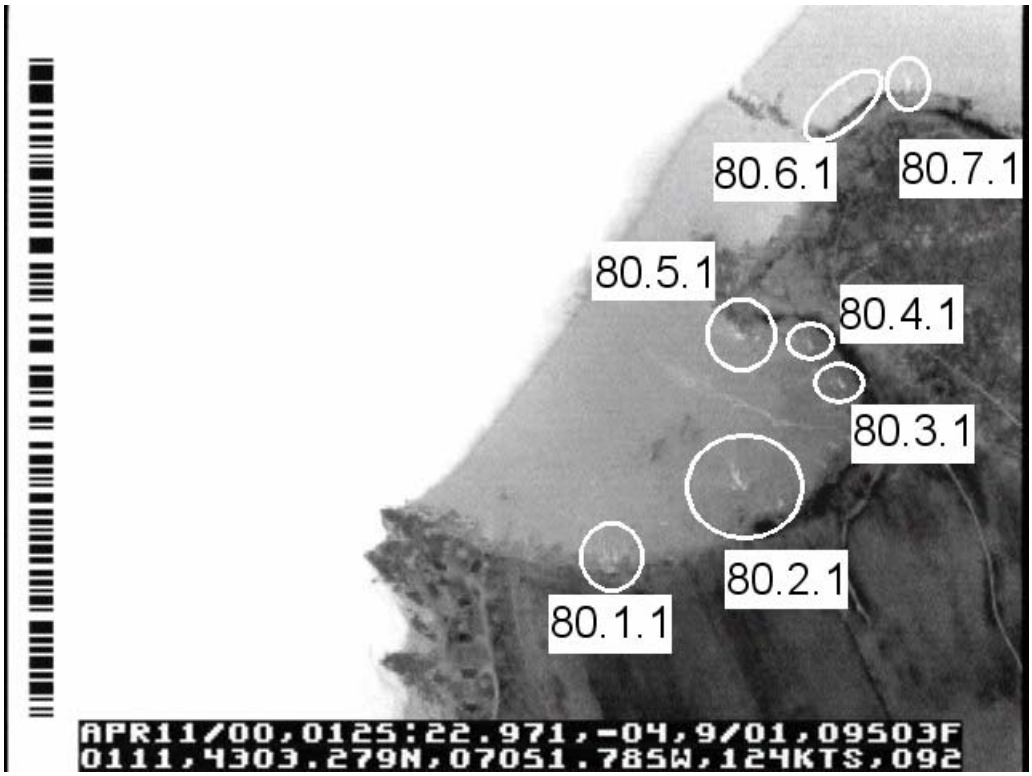

IMAGE EIGHTY-ONE

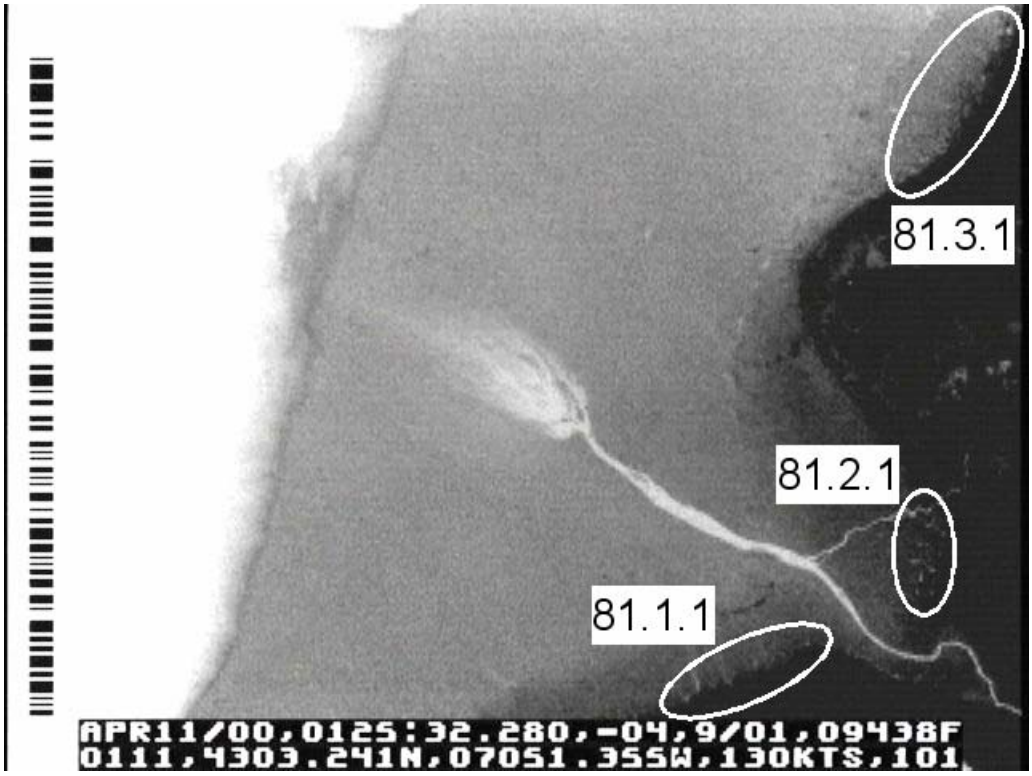

IMAGE EIGHTY-TWO

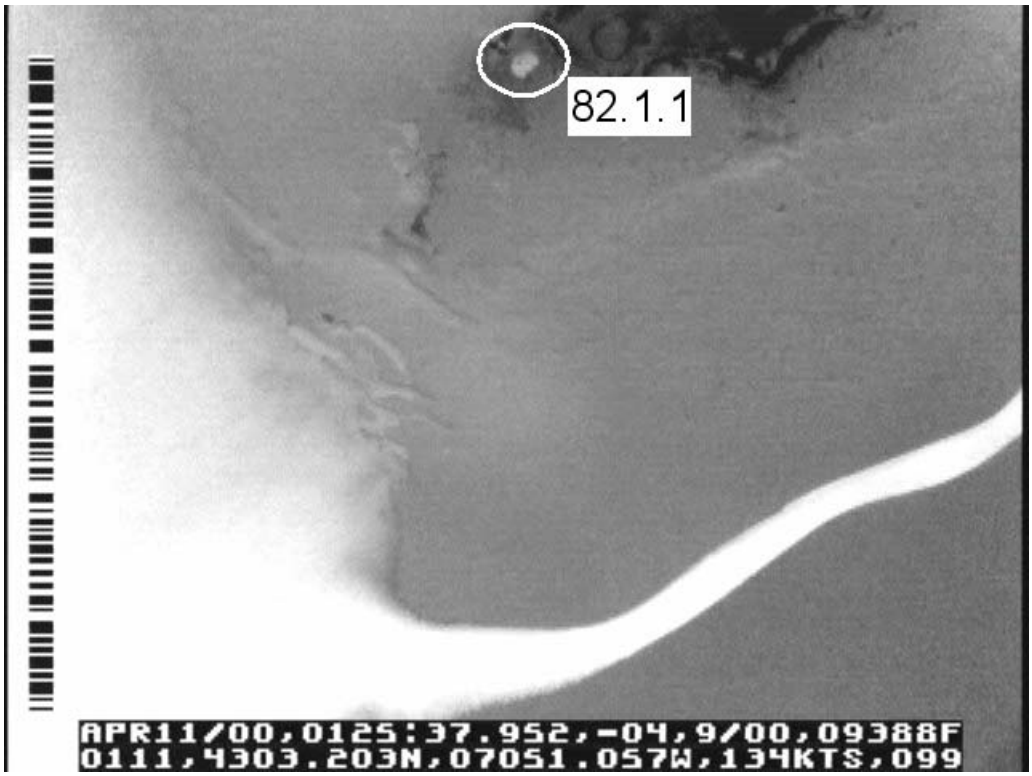

IMAGE EIGHTY-THREE

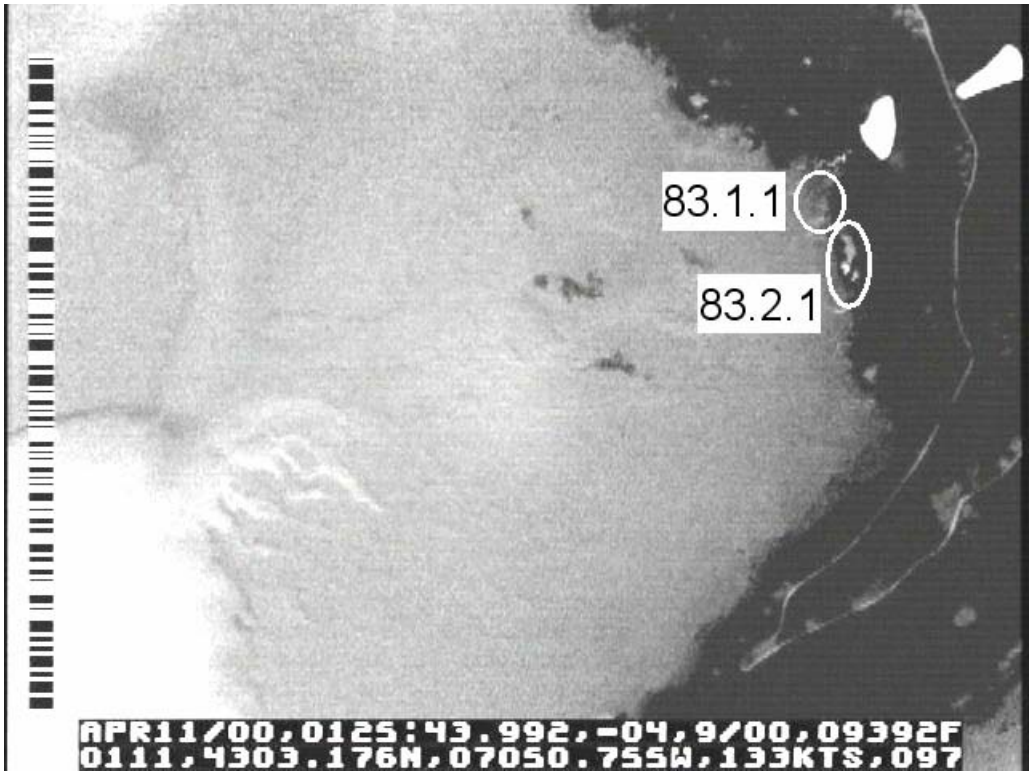

IMAGE EIGHTY-FOUR